DESIGN OF A THERMOELECTRIC GENERATOR FOR HARVESTING BRAKE HEAT ENERGY FOR A RAIL VEHICLE

By

Lubaale Solomon Azarius

A thesis presented to

African Railway Center of Excellence

Addis Ababa Institute of Technology

Addis Ababa University

In partial fulfillment

of the Requirements for the Degree of Master of Science

Railway Engineering-Rolling Stock

Supervised by;

Kamil Dino Adem (PhD)

Tollossa Deberie (Mr)

June 2019

Approved by Board of Examiners

……. ……

Chairman Graduate Committe

Kamil Dino Adem (PhD) ……

Supervisor

Tollosa Deberie (Mr) ……

Co-supervisor

Yilma Tadesse Birhane (PhD) ……

Internal Examiner

Ing. Demiss Alemu Ambie (PhD) ……

External Examiner

Declaration

I hereby declare that the work which is presented in this thesis entitled "Design of a Thermoelectric Generator for Harvesting Brake Heat Energy for a Rail Vehicle" is an original piece of work of my own, has not been presented for a degree in any other university; and that all the sources of the material used for the thesis have been duly acknowledged.

Lubaale Solomon Azarius _____ _____

Candidate Signature Date

This is to certify that the above declaration made by the candidate is correct to the best of my knowledge.

Kamil Dino Adem (PhD) _____ _____

Advisor Signature Date

Tollossa Deberie (Mr) _____ _____

Co-advisor Signature Date

Abstract

We live in an era where energy needs are increasing daily, fossil fuels are reducing and yet also renewable energy source development still has a long way to go. Systems that run on energy do not use the available energy as efficiently as we would want to. Despite the continued efforts to improve system energy efficiencies, too much energy is still being lost in different forms especially in the form of heat. During the vehicle braking process, all the energy is converted into heat energy at the brake disc. This wasted energy presents a problem to be tackled in order to improve resource efficiency. This thesis investigates the use of thermoelectric generators (TEGs) as a means of recovering this energy. A TEG, working on the principle of Seebeck effect converts heat energy into electrical energy directly. Heat simulations were done for a brake disc using temperature as the input gave an input temperature of 160 ^{0}C and also heat flux in the case of repeated braking which gave an average input temperature of 261.5 ^{0}C. A model of a TEG was developed in 3D by SOLIDWORKS and applied to a brake disc of a railway vehicle to use the brake heat to generate power. Furthermore, by simulation using ANSYS, a parametric study was performed on the influence of voltage increase, the number of legs and the size of the legs. Based on the data acquired, the effects of changing voltage, current, leg size as parameters were noted and discussed. Here, heat absorbed at the hot junction and the energy generated were considered. Based on this data the TEG's system efficiency and TEG's recovery efficiency are calculated and discussed. From the design made, a device recovery efficiency of 2.94% of heat lost per second was achieved which amounts to 67 kW per vehicle per braking. In the case of repeated braking, a 5% recovery efficiency was achieved. The results obtained in this thesis allow the drawing of essential conclusions with regards to the overall TEG system performance which are essential to further studies.

Keywords; **Braking, Disc brake, Thermoelectricity, Thermoelectric generator, Waste heat energy, Energy harvesting**

Acknowledgment

I would like to thank my advisors Kamil Dino Adem (PhD) and Tollosa Deberie (Mr) for giving me an opportunity to work under their guidance to the accomplishment of this thesis by sharing their knowledge and experience with me. I am grateful to the World Bank Group in conjunction with Addis Ababa University for providing me with the scholarship for my MSc study. Without them, this work would not have been possible.

Special thanks go to the Addis Ababa University and African Railway center of excellence lecturers for all the help rendered for the accomplishment of this MSc and this research in particular.

I would also like to express my gratitude to my course mates and friends that have aided me in this research from time to time discussions that have opened my mind to understand the subject matter. My friends back home with family, their support, spiritually meant a lot to me and helped me to concentrate on the tasks at hand.

Table of Contents

List of figures

List of tables

Nomenclature

Variables

A: Cross section area (m^2)
I: Electrical current (A)
k: Thermal conductivity ($Wm^{-1}K^{-1}$)
L: Length of legs (m)
P_e: Output electrical power (W)
Q: Heat power (W)
R: Electrical resistance (Ω)
T: Temperature (K)
W: Work output (W)
Z: Figure of merit (FOM) (K^{-1})
ZT: Dimensionless figure of merit.

Greek Symbols

α: Seebeck coefficient (VK^{-1})
η: Efficiency
η_c: Carnot efficiency
η_r: Reduced efficiency
γ: Thomson coefficient (VK^{-1})
π: Peltier coefficient (V)
ρ: Electrical resistivity (Ω·m).

Scripts

c: Cold source
h: Hot source
n: n-leg
p: p-leg

1. CHAPTER ONE

1.0 Introduction

Human activities all over the world are closely dependent on the usage of several forms and sources of energy to perform work. Energy is the potential that allows movement and/or the modification of matter[1]. Energy is one of the world's biggest needs, and yet there is still a bottleneck since harvesting most of the renewable energy forms is still tricky[2]. Not only is this energy needed domestically, but also in the manufacturing industry and transport sector. The total energy available is not enough and yet much of the energy is lost to the environment and atmosphere during processes especially those involving heat. More than half of the energy attained from burning fuel is lost as waste heat. Waste heat is the unused heat given to the surrounding environment; in the form of thermal energy by a hot body in a thermodynamic process in which it converts heat to useful work. Close to 30% of the energy generated by the combustion of fuel in the engine is converted by the cylinder piston motion into the brake force of vehicles. But about 70% of this energy does not do mechanical work as it is dissipated to the environment as waste heat[3]. Most of the energy is lost through the exhaust and the rest lost during the deceleration of the vehicles. Reclaiming just a small portion of what is lost as heat, would have a significant impact on energy use. During the train braking process, the kinetic energy possessed by the moving train is all converted into heat energy at the brakes through friction. The heat energy is later lost to the environment. Efforts have been made to recover part of this energy by replacing the friction brakes with regenerative brakes but there is a limitation to using the motors in vehicles, especially since even in regenerative braking in trains, the motors act as generators up to the momentum that can be handled by the friction brakes. This loss of heat is, therefore, ineluctable but it can be reduced by harvesting some of it using thermoelectric generators and producing electricity out of the heat directly. By this, the efficiency of the system is improved and the amount of fuel used in the system reduces in due process. Thermoelectric generators show promising improvement in combustion vehicles, with overall efficiency increase from 33% to 57%, with an increase of 6% in the available power in automobiles[4]. [5]shows all the progress in the automotive industry to try to harness the heat

lost from the vehicle by exhaust and engine cooling. From experiments, the progress is promising and also vehicle manufacturers have started adopting it. Efforts have been made to recover some of the energy lost to the atmosphere by using the exhaust flue gases that are released to the atmosphere by first using its heat to generate energy using thermoelectric generators. Even though the vehicle industry is so receptive to the concept, rail vehicle manufacturers have not yet embraced the idea. The harvesting of that heat energy lost to the atmosphere is so integral to the boosting of the energy efficiency and effectiveness in the transport world. This would improve the efficiency of the systems by up to 30% for a mere small portion reclaimed. Even though a series of studies have been done to recover some of the heat lost to the atmosphere in the transport business, little studies have been done on the heat lost in the brakes, at the contact of the friction plate and the pads. Efforts have to be made to make sure that at least part of the brake heat energy is also recovered. Herein, a novel design is jotted to propose a way of harvesting brake heat energy with the aim of improving the system's energy efficiency.

1.1 Problem statement

Transportation is one of the largest energy consuming sectors in the world as it stands today. The trend of energy use in transportation is positive; the energy increases by the day as the need for transportation increases. The vehicles used in transportation are not yet fuel efficient enough as a great portion of the provided energy is not put to use, rather, it is wasted as heat. Although there are numerous efforts that have been made to boost vehicle energy efficiency so as to reduce fossil fuels burnt, lots of other losses occur. During braking, all the energy of the vehicle at that point is converted into heat at the brakes through friction. All this energy is later dissipated to the atmosphere. A massive 800 to 5000 kW of energy is lost during single braking with most of it being converted into heat. Reclaiming a portion of this lost energy would have a significant impact on energy use, improve the systems fuel efficiency and boost the energy sources since energy has become a very rare invaluable resource. This suggests that a major interest of research in order to develop a competitive and reliable key technology to recover this energy be pursued. However, finding an energy harvesting technology at a scale of our braking system may be problematic, since most of them as power cycles have scalability problems[6]. A thermoelectric generator (TEG), might match the problem. The compactness,

lack of moving parts, noise free, low maintenance and a simple working principle of temperature gradient could be adopted for a braking system[7]. One economic challenge to thermoelectrically recover waste heat is to do it in such a way that it is competitive with utility generated power [8].

1.2 Objectives

Main Objectives

To design and simulate a thermoelectric generator for harvesting brake heat energy for a rail vehicle.

Specific objectives

1. To develop a computational model for the thermoelectric generator relating the brake disk temperature with the generator performance
2. To design a TEG module for a brake disk
3. To simulate the designed generator to check power output and also compare with the mathematical model results

1.3 Delimitation

This study is aimed at understanding how thermoelectric generators can be incorporated into a brake disc so as to harvest a portion of the brake heat energy that is always lost to the atmosphere. The research helps in increasing the energy efficiencies of rail vehicles that use friction brakes as a braking system. It is limited to thermoelectric generator design to suit a brake disc and analyzing performance to check for the energy harvest in percentage to that lost per braking process. It also covers the specific TEG model leg choice by simulating to check which size is optimum and gives the highest power output. The study does not cover the building and testing of a prototype as well as TEG material tests.

1.4 Thesis outline

With chapter 1 introducing the subject, the problem at hand, as well as the aims and objectives of the study, chapter 2 highlights the subject of waste heat in industries, thermoelectric device

theory and literature review about brake heat waste energy and as well as the use of TEGs for waste heat recovery. Chapter 3 talks about the theoretical steps of design and modeling of engineering systems. Chapter 4 in detail shows the methodologies used in this study, SOLIDWORKS and ANSYS modeling and simulations, calculations and empirical formulae that are used in the study of TEGs. In chapter 5 is documented the results and their analyses with a series of graphs that are used to explain certain factors as well as recovered energy from the design. Chapter 6 concludes the thesis, showing the achievements and the scientific contribution as it also gives some recommendations for future works.

In the next chapter, we delve into the understanding of waste heat, followed by the science of thermoelectricity, and will close in the literature review.

2. CHAPTER TWO

2.0 Thermoelectric device fundamentals

This chapter is about waste heat, where it comes from, the way we can capture and use it, so as to improve the overall efficiency of the systems.

2.1 Waste heat recovery

Waste heat is heat energy generated without being put to practical use. Sources of waste heat include hot combustion gases discharged to the atmosphere, heated products exiting industrial processes, the heat generated from surfaces in relative motion (friction) and heat transfer from hot equipment surfaces. Waste thermal energy (heat), is usually generated in a process of fuel combustion or chemical reaction, friction between surfaces and then dissipated (lost) into the environment. A strategy of how to recover this heat depends on the temperature of the waste heat and the economics involved. The waste heat temperature is a key factor determining waste heat recovery feasibility. Waste heat temperatures can vary significantly, with cooling water returns having low temperatures around 40-90 °C, glass melting furnaces having flue temperatures above 1,320 °C and brake disk heat that ranges from 240-540 ^{0}C. Waste heat is one of the largest sources of inexpensive, clean, and fuel-free energy available. In order to enable heat transfer and recovery, it is necessary that the waste heat source temperature is higher than the heat sink temperature (ambient temperature). Moreover, the magnitude of the temperature difference between the heat source and sink is an important determinant of waste heat quality. The source and sink temperature difference influences;

- the rate at which heat is transferred per unit surface area of the heat exchanger
- the maximum theoretical efficiency of converting thermal from the heat source to another form of energy (i.e. mechanical or electrical).

Also, the temperature range has important implications for the selection of materials in heat exchanger designs.

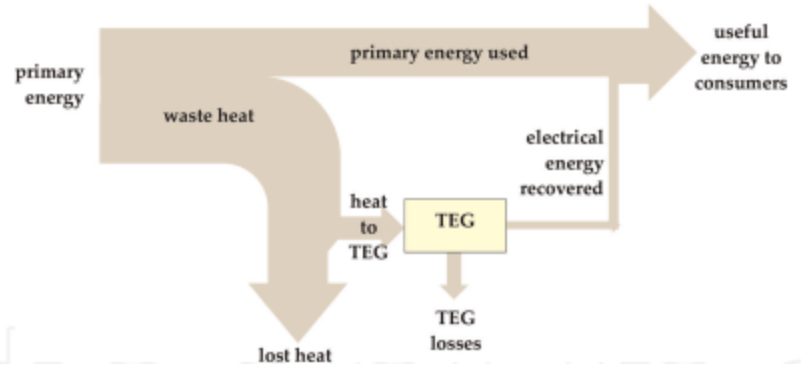

Figure 1: Electrical energy recovered from waste heat [9]

2.1.1 Factors Affecting Waste Heat Recovery Feasibility

Evaluating the feasibility of waste heat recovery requires characterizing the waste heat source and the stream to which the heat will be transferred. Important waste stream parameters that must be determined include:

- ✓ heat quantity,
- ✓ heat temperature/quality,
- ✓ composition,
- ✓ minimum allowed temperature, and
- ✓ operating schedules, availability

These parameters allow for analysis of the quality and quantity of the stream and also provide insight into possible materials/design limitations. For example, corrosion of heat transfer media is of considerable concern in waste heat recovery, even when the quality and quantity of the stream is acceptable.

An overview of important concepts to consider and determine waste heat recovery feasibility.

Heat Quantity

The quantity or content of heat is a measure of how much energy is contained in waste heat, while quality is a measure of the usefulness of the waste heat. The quantity of waste heat contained in a body or fluid is a function of the temperature and the rate at which the heat is produced. Although the quantity of waste heat available is an important parameter, it is not alone an effective measure of waste heat recovery opportunity. It is also important to specify the waste heat quality, as determined by its temperature.

Waste Heat Temperature/Quality

Waste heat temperature is a key factor in determining waste heat recovery feasibility. These temperatures can vary significantly depending on the kind of process that is losing the heat; ranging from as low as 40 ºC to as high as 1,320 °C. In order to enable heat transfer and recovery, it is necessary that the waste heat source temperature is higher than the heat sink temperature. Also, the magnitude of the temperature difference between the heat source and sink is an important determinant of waste heat quality. The source and sink temperature difference influences;

- ✓ the rate at which heat is transferred per unit surface area of the heat exchanger
- ✓ the maximum theoretical efficiency of converting thermal from the heat source to another form of energy (i.e., mechanical or electrical).

Finally, the temperature range has very important implications for the selection of materials in heat exchanger designs.

Waste heat recovery opportunities are categorized in this report by dividing temperature ranges into low, medium, and high quality of waste heat sources as follows:

- ✓ High: 650 ºC and higher
- ✓ Medium: 232 ºC to 650 ºC
- ✓ Low: 232 ºC and lower

Possible ways of recovering energy in these temperature ranges

Table 1: Different waste heat and possible recovery methods [10]

Temp Range	Example Sources	Temp (°C)	Advantages	Disadvantages/ Barriers	Typical Recovery Methods/Technologies
High > 650°C	Nickel refining furnace Steel electric arc furnace Basic oxygen furnace	1,370--1,650 1,370-1,650 1,200 1,100-1,200	High-quality energy, available for a diverse range of end uses with	High temperature creates increased thermal stresses on heat exchange materials	Combustion air preheat Steam generation for process heating or for mechanical/

	Aluminum reverberatory furnace Copper refining furnace Steel heating furnace Copper reverberatory furnace Hydrogen plants Fume incinerators Glass melting furnace Coke Oven Iron cupola	760-820 930-1,040 900--1,090 650-980 650-1,430 1,300--1,540 650--1,000 820--980	varying temperature requirements High-efficiency power Generation High heat transfer rate per unit area	Increased chemical activity/corrosion	electrical work Furnace load preheating Transfer to mid-low temperature processes
Medium 230-650°C	Steam boiler exhaust Steam boiler exhaust Reciprocating engine exhaust Heat treating furnace Drying & baking ovens Cement Kiln	230--480 370--540 320--590 430-650 230--590 450-620	More compatible with heat exchanger materials Practical for power generation		Combustion air preheat Steam/ power generation Organic Rankine cycle for power generation Furnace load preheating, feedwater preheating Transfer to low-temperature processes
Low <230°C	Exhaust gases exiting recovery devices in gas-fired boilers,	70-230 50-90	Large quantities of low temperature	Few end-uses for low temperature heat	Space heating Domestic water heating

	ethylene furnaces, etc. Process steam condensate Cooling water from: • furnace doors • annealing furnaces • air compressors • IC engines • AC condensers Drying, baking, and curing ovens Hot processed liquids/solids	30-50 70-230 30-50 70-120 30-40 90-230 30-230	heat contained in numerous product streams	Low-efficiency power generation For combustion exhausts, low-temperature heat recovery is impractical due to acidic condensation and heat exchanger corrosion	Upgrading via a heat pump to increase temp for end use Organic Rankine cycle

The vast amount of heat that is discharged into the atmosphere every day is one of the best sources of clean, fuel-free, and inexpensive energy. According to the US Department of Energy (DOE), up to 50% of all fuels burned in the US goes unused into the atmosphere as waste heat is released to the atmosphere. Research indicates that the energy currently wasted by the industrial facilities in the U.S. could produce as much as 20 % of the total US electrical output with the associated 20% reduction in greenhouse gas emissions[11]. Among the waste heat that has been directly discharged into the atmosphere, much of it is at temperatures which are too low to recover by using the conventional electrical power generators. Thermoelectric power

generation has as a technology given a ray of hope in the direct conversion of low-grade thermal energy. Recent development indicates that it can be used in more cases, like in cogeneration systems, to improve overall efficiencies of energy conversion systems by converting waste heat energy into electrical power[12]. In this chapter, we provide a summary of the progress in thermoelectricity as a potential technique to harvest waste thermal energy.

Waste heat to power (WHP) is the process of capturing heat discarded by an existing process and using that heat to generate power. Energy-intensive processes such as those occurring at refineries, steel mills, glass furnaces, cement kilns, and the braking process all release waste heat that can be harnessed with well-established technologies to generate electricity. The recovery of waste heat for power is a largely untapped type of combined heat and power (CHP), which is the use of a single fuel source to generate both thermal energy (heating or cooling) and electricity.

Today, we face some significant environmental and energy problems such as global warming, urban heat island, and the precarious balance of world oil supply and demand. However, a satisfactory solution to these problems has not been found yet. Waste heat recovery is considered to be one of the best solutions because it can improve energy efficiency by converting heat exhausted from plants, moving vehicles and machinery to electric power. This technology would also prevent atmospheric temperature increases caused by waste heat, and decrease fossil fuel consumption by recovering heat energy, thus also reducing carbon dioxide (CO_2) emissions [9].

Thus far, today's electrical energy production is mostly realized by generators, based on electromagnetic induction. Reciprocating steam engines, internal combustion engines, and steam and gas turbines have been coupled with such generators in utilizing chemical heat sources such as oil, coal and natural gas and nuclear heat for the production of electrical energy. Renewable energy sources like geothermal, solar and biomass energy are also being added to the list of heat sources used in modern electric power plants. Furthermore, solar energy provides hydropower indirectly. All these power plants have, however, a common disadvantage; the conversion of thermal energy into electric energy is accomplished by the utilization of moving and wear-subjected machine equipment.

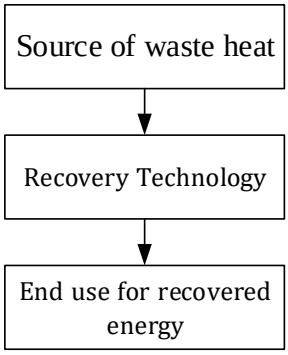

Figure 2: Waste heat recovery flowchart

The system proposed for this study is to generate electric power by providing waste heat or unharnessed thermal energy to built-in thermoelectric modules that can convert heat into electric power. The main advantages are the low maintenance requirement, the high modularity and the possibility of utilizing heat sources over a wide range of temperature.

2.2 Brake disc temperature build up during braking

During braking, the friction caused by applying brake force on the calipers to cause contact between the pad and rotor causes an increase in temperature. The temperature continues to build up until the braking force is released. Even if the brake disc is being cooled convectionally by the wind at ambient temperature, the rate at which the temperature builds up is a lot higher than the rate at which the cooling occurs. This causes the temperature to build up in the brake disc friction plates.

In a study carried out by Kumella [13] about the brake disc performance on Addis Ababa light rail transit (AALRT), the brake disc surface temperature build-up is high in cases of emergency braking of about 480 ^{0}C relative to the 250 ^{0}C in normal braking. The normal braking temperature is low temperature but can still be used in thermoelectric power generation.

In a study [14] done by Zhizong Wang et al., (2019), a detailed temperature build up with time is shown and a temperature of up to 430 ^{0}C in just 5 seconds of braking is achieved. This gives a high heat flux that can be used to give off even more power in a thermoelectric power generation.

Wu, Zuo, & Wu, (2012) [15] did the same study but calculated the temperatures numerically and did experiments too. The results of the temperatures got were around 510 and 530 ^{0}C respectively. This was like this (a gap between results) because of the approximations that are made during numerical analysis. This temperature is high, high heat flux drawn from it and higher power in thermoelectric power generation.

2.3 Thermoelectricity

Thermoelectricity is the direct conversion of temperature differences into electric voltage and vice versa. Thermoelectric devices create a voltage when there is a different temperature applied on each side. Likewise, when a voltage is applied to these devices, it creates a temperature difference. An applied temperature gradient causes charge carriers in the material to diffuse from the hot side to the cold side and thereby inducing a thermal current [16]. This effect can be used to generate electricity, measure temperature, or change the temperature of objects. Because the direction of heating and cooling is determined by the polarity of the applied voltage, thermoelectric devices are also efficient temperature controllers. Thermoelectric effect encompasses three effects: Seebeck effect, Peltier effect, and Thomson effect. As well as joule heating. This section introduces the thermoelectric effects and principles of thermoelectric module construction. Thermoelectric phenomena have been known for over a century, and are widely used for cooling, temperature measurements, and power generation. This thesis solely focuses on thermoelectric power generator modules. Having a good understanding of underlying thermoelectric effects is of crucial importance for thermoelectric system designers. This section describes the thermoelectric effects, TEG module structure, and module characteristic principles.

2.3.1 Seebeck Effect

This is the effect that facilitates the power generation in TEGs. It is the conversion of temperature differences directly into electricity. In 1821, Seebeck discovered that a compass needle was deflected by a closed loop formed by two metals joined in two places if there was a temperature difference between the junctions. This is because the metals respond differently to the temperature difference, creating a current loop and a magnetic field. Seebeck never recognized that there was an electric current involved but later Hans Christian Orsted rectified the mistake and coined the term thermoelectricity. The voltage created by this effect is of the

order of several microvolts per kelvin (μV/K) difference. The voltage V developed can be derived by using the following equation:

$$V = \int_{T1}^{T2} [S_B(T) - S_A(T)]dT \qquad (1)$$

where S_A and S_B are the thermo-powers (Seebeck coefficients) of metals A and B as a function of temperature, while T_1 and T_2 are the temperatures of the two junctions. The Seebeck coefficients are nonlinear as a function of temperature and depend on the absolute temperature of the conductors, as well as properties of the materials. If the Seebeck coefficients are independent of temperature in the measured temperature range, the above formula can be approximated as:

$$V = (S_B - S_A)(T_2 - T_1) \qquad (2)$$

The Seebeck effect can be used in a thermocouple to measure a temperature difference. It also can be used to measure absolute temperature if the temperature of one end is known. A metal of unknown composition can be classified by its thermoelectric effect if a metallic probe of known composition, kept at a constant temperature, is held in contact with it. Because the voltage induced over each individual couple could be very small, it is necessary to use thermocouples connected in series to form a thermopile, in order to increase the overall output voltage. Thermoelectric generators are used for creating power from these heat differentials.

2.2.2 Peltier Effect

Peltier effect is the presence of heat at an electrified junction of two different metals. It was discovered by Jean–Charles Peltier in 1834. When current flows through a junction of two different materials, A and B, heat is generated at the upper junction at T_2 and absorbed at the lower junction at T_1. The Peltier heat, Q, absorbed by the lower junction per unit time is equal to:

$$Q = \pi_{AB} I = (\pi_B - \pi_A) I \qquad (3)$$

where Π_{AB} is the Peltier coefficient for the thermocouple composed of materials A and B, while π_A and π_B are the Peltier coefficients of materials A and B. π varies with temperature and is determined by the specific composition of the materials. The Peltier coefficients represent the amount of heat current that is carried per unit charge through a material. Because charge current

must be continuous across a junction, the associated heat flow develops a discontinuity, if π_A and π_B are different. Depending on the magnitude of the current, heat must accumulate or deplete at the junction, due to a nonzero divergence caused by the carriers attempting to return to the equilibrium that exists before the current is applied by transferring energy from one connector to another. Individual couples can be connected in series to enhance the effect. This phenomenon has been used in either thermoelectric heat pumps or cooling devices such as refrigerators.

2.2.3 Thomson Effect

This effect was observed by Lord Kelvin in 1851. It describes the heating or cooling of a current-carrying conductor with a temperature gradient. Any current-carrying conductor, except for a superconductor, with a temperature difference between two points, either absorbs or emits heat, depending on the properties of the materials. If a current density, J, is passed through a homogeneous conductor, the heat production, q, per unit volume is given by:

$$q = \rho J^2 - \mu J \frac{dT}{dx} \qquad (4)$$

where q is the resistivity of the material, $\frac{dT}{dx}$ is the temperature gradient along the wire m and μ is the Thomson coefficient. The first term is Joule heating, which does not change in sign, while the second term is the Thomson heating, which changes sign following J.

In some metals, whose temperature is directly proportional to their potential, when current moves from the hotter to the colder end, there is a generation of heat and positive Thomson effect is observed. Likewise, in other metals, whose temperature is inversely proportional to their potential, when current moves from the hotter to the colder end, there is an absorption of heat and negative Thomson effect takes place. If the Thomson coefficient of a material is measured over a wide range of temperature, it can be integrated by using the Thomson relations to determine the absolute values for the Peltier and Seebeck coefficients. This needs to be done only for a single material since the values of others can be determined by measuring pairwise Seebeck coefficients in thermocouples containing the reference material and then adding back the absolute thermo-power of the reference material.

2.2.4 Thomson Relations

Thomson coefficient is unique among the three main thermoelectric coefficients because it is the only one directly measurable for individual materials. Since both Peltier and Seebeck coefficients can only be determined for pairs of materials, no direct methods are available to determine absolute Seebeck or Peltier coefficients for an individual material. In 1854, Lord Kelvin found relationships among the three coefficients, implying that only one could be considered unique. The first Thomson relation is

$$\mu = T\frac{dS}{dT} \qquad (5)$$

where T is the absolute temperature, μ is the Thomson coefficient, and S is the Seebeck coefficient. The second Thomson relation is:

$$\pi = S.T \qquad (6)$$

where; π is the Peltier coefficient.

2.3 Thermoelectric power generation

The thermoelectric power generation is based on the Seebeck effect – If heat is applied to a circuit at the junction of two different conductors, a current will be generated. Discovering the effect in 1821, Thomas Johann Seebeck observed that the magnitude of the voltage generated was proportional to the temperature difference and depended on the type of conducting material, but was unaffected by the temperature distribution along the conductors. Seebeck tested a wide range of materials, including the naturally found semiconductors ZnSb and PbS. The Seebeck coefficient (frequently measured in microvolts/K) is defined as the open circuit voltage produced between two points on a conductor when a uniform temperature difference of 1 K is applied between those points. The simplest TEG consists of a thermocouple consisting of n-type (materials with excess electrons) and p-type (materials with a deficit of electrons) elements connected electrically in series and thermally in parallel. Heat is input on one side and rejected from the other side, generating a voltage across the TE couple. The magnitude of the voltage produced is proportional to the temperature gradient.

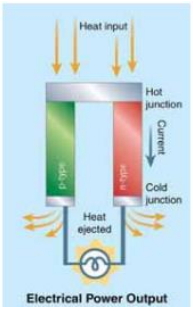

Figure 3; Simple illustration of TEG power generation [8]

When a thermoelectric couple is connected in series, the pair is placed between two objects at two different temperatures T_c and T_h (a heat sink and a heat source), it can produce Seebeck voltage V_S. In this case, only the Seebeck effect and heat conduction phenomena occur. If the electromotive force V_S is closed by a resistive load R_L then an electrical power P is generated and the thermoelectric module is utilizing all the described phenomena [24].

$$P = I^2 R_L = \left(\frac{V_s}{R_L + R_I}\right)^2 R_L = \left(\frac{\alpha(T_h - T_c)}{R_L + R_I}\right)^2 R_L \qquad (7)$$

Where; R_L is the internal resistance of the thermoelectric couples

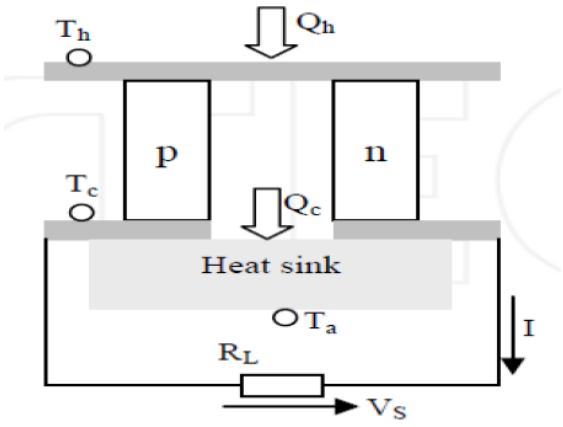

Figure 4: Power generation by a single thermocouple exposed to a temperature gradient[5]

The linear voltage-current characteristic and power output are shown in the figure below. The maximum power output is at half open circuit voltage and half short circuit current (as with all matched loads), the maximum power output is in the equation.

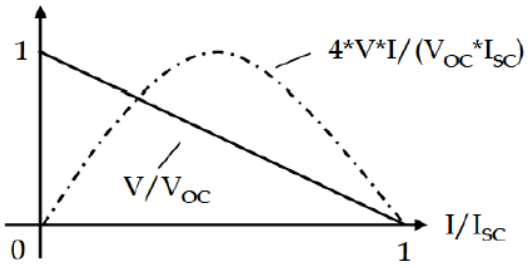

Figure 5: Voltage, current and power characteristics of the thermoelectric generator[17]

2.3.1 Thermoelectric Generators

Thermoelectric generators are solid-state devices with no moving parts, are silent, reliable, and scalable, making them ideal for small, distributed power generation, and energy harvesting. They can also be defined as heat engines in which charge carriers serve as the working fluid. The thermoelectric effects arise because charge carriers in metals and semiconductors are free to move much like gas molecules while carrying a charge as well as heat. [18] When a temperature gradient is applied to a material, the mobile charge carriers at the hot end diffuse to the cold end. The buildup of charge carriers results in a net charge (negative for electrons, e− and positive for holes, h+) at the cold end, producing an electrostatic voltage.[19] Equilibrium is thus reached between the chemical potential for diffusion and the electrostatic repulsion due to the build-up of charge. This property, the Seebeck effect, is the basis of thermoelectric power generation.

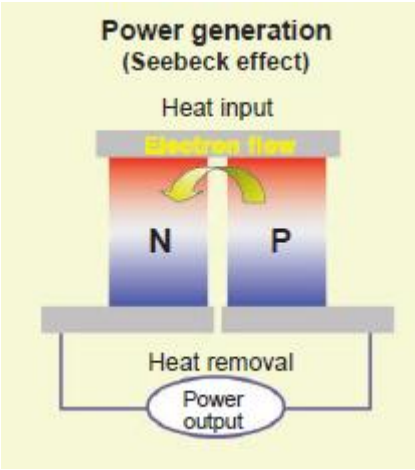

Figure 6: Power generation using Seebeck effect [19]

Thermoelectric devices contain many thermoelectric couples consisting of n-type and p-type thermoelectric elements connected thermally in parallel and electrically in series. Heavily doped semiconductors are the best thermoelectric materials. A thermoelectric generator utilizes heat flow across a temperature gradient to power an electric load through the external circuit. The temperature difference provides the voltage ($V = \alpha\Delta T$) from the Seebeck effect (Seebeck coefficient α), while the heat flow drives the electrical current, which therefore determines the power output. The rejected heat must be removed through a heat sink.

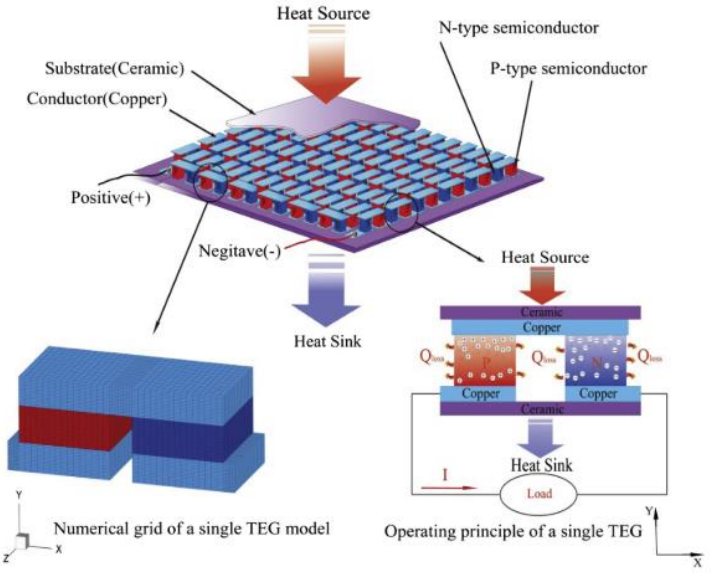

Figure 7: Illustration of TEG module [20]

2.3.2 Thermoelectric materials

All materials exhibit thermoelectric effects but the name 'thermoelectric materials' is used to describe the materials that are good at converting heat to electricity [21]. Thermoelectric materials are crucial in renewable energy conversion technologies to solve the global energy crisis. They have been proven to be suitable for high-end technological applications such as missiles and spacecraft. The thermoelectric performance of devices depends primarily on the type of materials used and their properties such as their Seebeck coefficient, electrical conductivity, thermal conductivity, and thermal stability. Classic inorganic materials have become important due to their enhanced thermoelectric responses compared with organic materials [8]. There exists a wide variety of different thermoelectric (TE) materials today some

of them have been known and used for decades, while others are a result of the more recent development of both understanding of the physics and more advanced production processes.

Thermoelectric materials can be categorized on many different levels, such as crystal structure, conversion efficiency, cost, and temperature range. The figure below shows the construction of a thermoelement. Modules are typically composed of around a hundred elements. Modules can be constructed as Peltier coolers or as high-temperature generators. Both of these use the same materials and can be used to produce power, but they differ in how the thermoelements are soldered to the conducting strip [13]. Since Seebeck's discovery, many materials have been considered useful to generate thermoelectricity. The first TEGs were based on electricity conductors and semiconductors, such as antimony, bismuth, copper, iron, lead, zinc, and different alloys, among others. Later, in the 20th century, many other thermoelectric materials (TM) were developed: ceramics, composites, etc.

Nevertheless, the updated semiconductors continue being basic TMs for the production of thermoelectric effects. It should be emphasized that all these materials were obtained empirically, through thousands of attempts based on the personal experience of a researcher. Therefore, the essential progress in the TMs area depends mainly on the advances in fundamental knowledge related to the nature of thermoelectric effects. A good thermoelectric material has a high Seebeck coefficient, high electric conductivity, and low thermal conductivity. When designing a TE material, there is always a tradeoff between keeping the electric conductivity high and the thermal conductivity low. The reason for this is that electrons are responsible for the transport of both electric current and heat. Heat can also be transported with lattice vibrations, so-called phonons, and lowering this contribution to the heat conductivity is of great importance when developing new materials.

Materials like glass have low thermal conductivity due to the unstructured way the material lattice is organized. Phonons are easily scattered, and the thermal conductivity due to lattice vibration is, thereby, minimal. In contrast, glass does not conduct electrons, so it is poor thermoelectric material. Good thermoelectric materials are crystalline materials that manage to scatter phonons without disrupting electrical conductivity, they should have phonon-scattering properties similar to glass but a crystal structure for conducting electrons[22]. These 'phonon-glass electron-crystal' properties are unusual, and there are no reliable theoretical models for

designing materials and predicting properties. The best thermoelectric materials known today are crystalline semiconducting materials, and several researchers are working on developing new and improving existing materials by means of, for example, nano-inclusions and partial substitution of the base material.

Bismuth telluride (Bi_2Te_3) is the most commonly used thermoelectric material, and it was first suggested as a TE material as early as 1954 [23]. Nevertheless, it remains today the best TE material for low-temperature conversion. Its thermoelectric properties strongly depend on carrier concentration, crystal size, and crystal orientation, so the material properties are different for Bi_2Te_3 from different manufacturers. Below are the properties of Bi_2Te_3;[24]

Table 2; Properties of Bismuth Telluride

Properties	
Chemical formula	Bi_2Te_3
Molar mass	800.76 g/mol
Appearance	Grey powder
Density	7.74 g/cm^3
Melting point	580 °C (1,076 °F; 853 K)

2.3.3 Performance of TE materials

The performance of TE materials is expressed through "figure-of-merit" denoted as ZT, a dimensionless value (constant) related to the efficiency of conversion of thermal energy to electric energy. Due to this, thermoelectric material properties are highly temperature dependent and there are multiple challenges in choosing the right material, since not all the properties vary linearly with temperature[25]. The thermoelectric figure of merit of the materials (ZT) depends on the Seebeck coefficient (α), absolute temperature (T), electrical resistivity (ρ), and thermal conductivity (κ) of the material: [26]

$$ZT = \frac{\alpha^2 T}{\rho k} \qquad (8)$$

The maximum efficiency of a thermoelectric device is determined by its figure of merit (ZT), which is an average of the component materials' ZT values. One key advantage of thermoelectrics is their scalability to small sizes, making them the most appropriate thermal-to-electric technology for energy harvesting.

The performance of TEG systems can be enhanced by increasing TE material figure of merit ZT, maintaining a large enough temperature differential across the TE module through efficient heat transfer and providing efficient hot and cold-side heat transfer that produces high thermal flows through the system.

While ZT improvement is limited by advances in TE material development, the hot-side and cold-side heat exchangers supplying heat to and dissipating heat from the device, respectively, play a critical role in determining the efficiency of a TEG system. A 100°C reduction in temperature differential in a ZT around 2 modules can result in over a 20% loss in performance. Increasing hot-side heat exchanger performance, in particular, increases TEG system output dramatically and identifies the requirements that will create sufficient TEG power output to enable the commercial viability of TEG technology technically and economically.

2.3.4 State-of-the-art materials

The most used materials today are still based on formulas developed in the 1950s and '60s. These materials were basically found when alloying semiconducting materials with isomorphous elements or compounds. To increase the electrical conductivity and reduce the lattice thermal conductivity, they were also heavily doped. Since all the thermoelectric properties of the material are dependent on temperature, they are usually divided into three different groups: [10]

- ✓ Low temperature below 200°C,
- ✓ Medium temperature between 200°C and 600°C
- ✓ High temperature above 600°C

Low temperature, < 200°C

The most common materials found in this temperature range are Bi_2Te_3 and Sb_2Te_3 solid solutions [44]. The mixing of these two compounds will introduce some variations in the mass

on the anionic lattice position in the crystal, leading to phonon scattering and thus decreased thermal conductivity. The best bismuth telluride-based materials used today have ZT values up to 1.5. Bismuth telluride melts at 580 °C [24] according to the reaction

$$Bi_2Te_3(s) \rightarrow 2BiTe(g) + 1/2Te2(g)$$

which limits the use up to approximately 500 °C material temperature.

Medium temperature, 200 – 600°C

The group IV-tellurides, PbTe, GeTe, and SeTe, are the most common materials in this temperature range. Both n and p-type materials can be made. The most used p-type is also called TAGS, short for (GeTe)0.85(AgSbTe2)0.15, with a ZT of up to 1.2. For n-type materials, the typical ZT is a bit below 1, but high ZT values of 2.2 at 915K have been reached by using nano-structuring methods. Both additions of SrTe nanoparticles dispersed in the crystal and meso-structuring of the crystal grains using powder processing techniques were used to achieve these high ZT values [22].

High temperature, > 600°C

At high temperatures, the most frequently used TE-materials are Silicon-germanium alloys. These have successfully been used for several long-term space missions such as Voyager 1 and 2. Still, they have very high thermal conductivity because of the diamond structure, which imposes a limitation on the maximum ZT value. So far, there has been no success in getting ZT values more than 1. Because of this limitation on efficiency (especially on the lower side of the temperature range), in addition to complicated production processes and the relatively expensive raw materials, which are not adequate for terrestrial applications such as waste heat recovery.

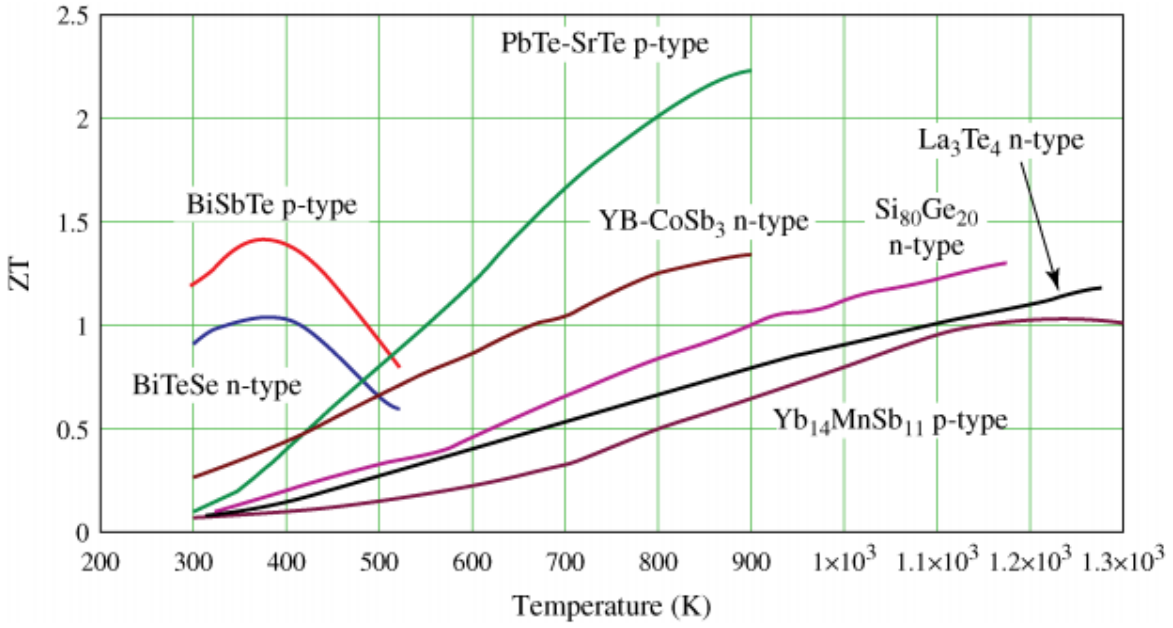

Figure 8: Figure of merit ZT of different thermoelectric materials performing a function of temperature [27]

Different thermoelectric materials have different values of the figure of merit which limit their use to applications with a specific temperature range. The figure above shows that for lower temperatures (200 to 400 K) bismuth telluride (Bi_2Te_3) is preferred while for temperatures between 600 and 800 K the material lead telluride (PbTe) is recommended.

Achieving the required level of hot-side heat exchange performance is a significant engineering challenge requiring new heat exchanger materials, designs and concepts that at the same time do not add greatly to capital and operating costs. The new heat exchanger materials/surfaces ought to provide heat exchanger performance two to five times greater than the best commonly available technologies. Adding to the challenge of hot-side exchanger design is the fact that most waste heat recovery systems have components that can foul and corrode heat exchange surfaces, thereby degrading TEG performance. Also, an increase in TE material performance is only important if an increase in hot-side heat transfer performance is simultaneously achieved. This again indicates the critical importance of hot-side heat exchange mechanism in the overall system design and performance [8].

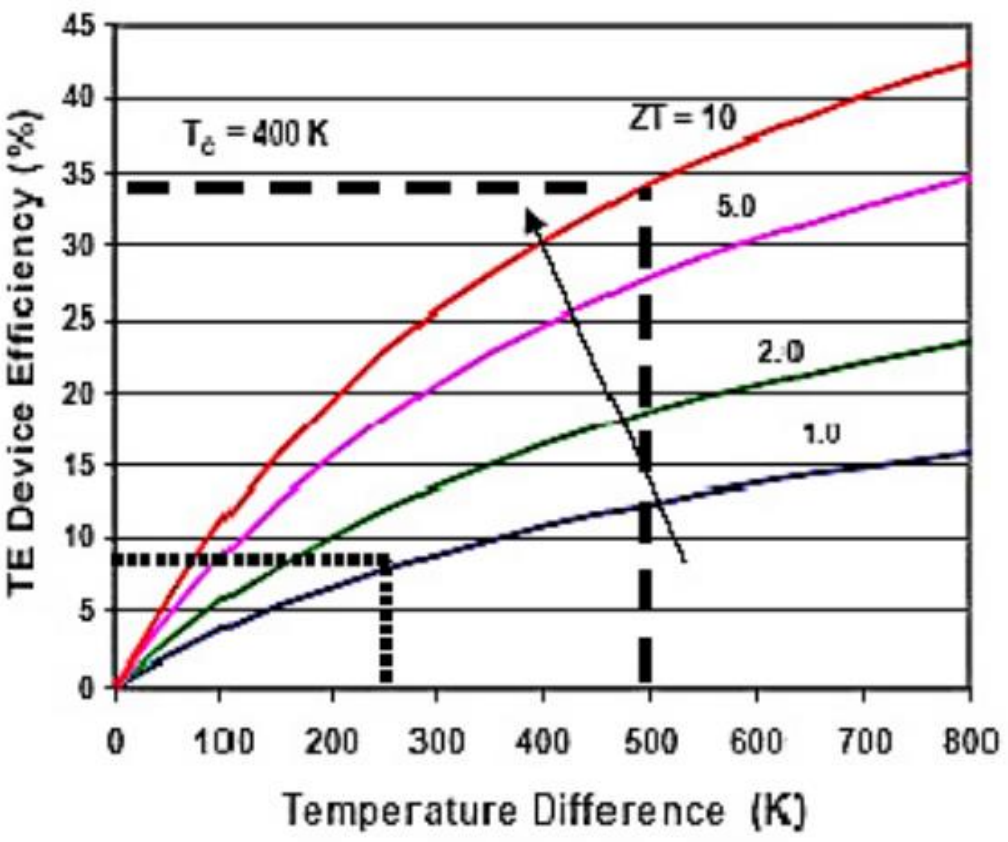

Figure 9: Efficiency, Temperature difference and ZT [4,7]

Table 3: Thermoelectric materials with different properties [28]

Material type	**Chemical composition**	**Temp-range**	**Thermoelectric properties (ZT)**	**Stability and durability**
Bismuth Telluride	Bi_2Te_3, Sb_2Te_3, Bi_2Se_3	-100 – 250°C	S: 100 - 250 µV/K σ: 100 - 1000 S/m ρ: 1 - 2 W/m·K ZT: ~1	Stable in air up to 300°C
Group 4 Tellurides	PbTe, GeTe, SiTe	200-600°C	ZT: ~ 1 - 1.2	n-type stable p-type very unstable at higher T
Silicon Germanium alloys	SiGe	600–1000°C	ZT: 0.8 - 1.2	High purity materials, mono and multi-crystal growth

Skutterudites	MX3 M = **Co**, Fe, Ni X = **Sb**, As Fillers: **In, Ce**	300-700°C	n-type: 1 - 1.8 p-type: 0.8 - 1.2	Oxidation above 380°C, sublimation of Sb above 550°C
Mg2BIV solid solutions	**Mg_2**(**Si-Sn**-Ge)	200-500°C	S: 100 - 250 µV/K σ: 1000 - 3000 S/cm ρ: 1 - 2.5 W/m·K ZT: ~1	Decomposes and oxidizes easily above 400-500°C needs protection
Silicides	**MnSi1,72** (HMS), $FeSi_2$, $CrSi_2$, CoSi, Ru_2Si_3	300-700°C	ZT HMS: ~0.8 ZT CrSi2: ~0.3 ZT FeSi2: ~0.4	Generally, very stable in whole temperature range, little to no oxidation
Clathrates	AxByC46-y A=Na, K, Rb B=Al, Ga, In C=Si, Ge, Sn	300-700°C	ZT >1 high potential	Powder metallurgical, Crystal growth
Half-Heussler compounds	ABX A=Mg, Zr, Ti, Hf B=Ag, Ni X=As, Sn	300-700°C	ZT: 1 - 1.5	Oxidation above 300-400°C [70]
Oxides	**Na_xCoO_2**, Ca-Co-O, $SrTiO_3$, ZnO	400-1000°C	ZT: ~0.3	Very stable at high temperature. No oxidation.

Table 4: Materials, modules specification, and performance of some of the TEGs fabricated and tested

Materials	Module specifications	TEG performance	Ref.
Fe-based compound	—	—	[29]
BiTe	P_{max} ~35 W (at $\Delta T = 300°C$) η_{max}. 4.5%	~125 W at 112.6 km/h speed	[30]
BiTe	5.3 × 5.3 cm Pmodule-13 W	1.0 kW	[31]
B and P doped Si_2Ge	20 × 20 cm P_{max}:1.2 W (at $\Delta T = 563$ K)	35.6 W	[32]
BiTe	6.2 × 6.2 × 0.5 cm (at $\Delta T = 563$ K)	42.3 W	[33]
Segmented Skutterudites and Bi_2Te_3 and commercial Bi_2Te_3 modules	Mod. Size:0.24 cm^2 P_{max}~18 W (at ΔT = 560°C) η_{mod}.-6–8%	266 W at 60 km/h driving in 2 L engine.	[34]
Bi_2Te_3/Sb_2Te_3	$P_{nominal}$: 7 W (at ΔT of 175°C)	44 W using 12 modules	[35]
Bi_2Te_3	0.4 × 0.4 cm	75 W	[36]
Bi_2Te_3	4 × 4 × 0.42 cm	350 W (using 12 modules)	[37]
Skutterudites	—	700 W (steady state) 450 W (US06 driving cycle)	[38]
Half Heusler	5.26 W/cm^2 (under $\Delta T = 500°C$)	1 kW	[39]

2.4 Design of a Thermoelectric Energy Harvester

Energy harvesting systems, because of their natural chemical-potential gradients, are best designed for a particular environment and are typically not easy to control to a one-size-fits-all solution. This is in contrast to batteries where the chemical potential gradient is known, stable, and well-regulated as it is an integral part of the power source. Thus, a battery can supply similar voltage and power in many different environments, but the power output of an energy harvester could vary by orders of magnitude depending on its location, use and the source of the energy being harvested.

Viable energy harvesting systems need to outperform a battery solution in terms of energy density, power density, and/or cost. Typically, the niche for energy harvesting is in long-lived applications where energy density is critical and routine maintenance is not an option. A likely scenario for use of an energy harvester is as a means of recharging a battery. In this case, the battery supplies high power (mW or W) during a short period of time, while the majority of the time the energy harvester trickles charges the battery (μW). While heat is a form of energy, the useful work content of heat is limited by the Carnot factor,

$$\eta Carnot = \frac{\Delta T}{T_h} \qquad (9)$$

where $\Delta T = T_h - T_c$ is the temperature difference across the thermoelectric. This puts thermoelectric energy harvesting at a distinct disadvantage when compared with the other forms of energy harvesting that are not Carnot limited.

A TEG converts heat (Q) into electrical power (P) with efficiency η calculated from;

$$P = \eta Q \qquad \eta = \frac{P}{Q} \qquad (10)$$

The maximum efficiency of a TE converter depends heavily on the temperature difference ΔT_{TE} across the device. This is because the thermoelectric generator, just like other heat engines, cannot have an efficiency greater than that of a Carnot cycle.

$$\eta = \Delta T_{TE} \frac{\eta_r}{T_h} \qquad (11)$$

Here η_r is the reduced efficiency, the efficiency relative to the Carnot efficiency. While the exact TE materials' efficiency is complex [6], the constant properties approximation (Seebeck coefficient, electrical conductivity, and thermal conductivity independent of temperature) leads to a simple expression for efficiency:

$$\eta = \frac{\Delta T}{T_h} * \frac{\sqrt{1+ZT}-1}{\sqrt{1+ZT}+ {T_c}/{T_h}} \qquad (12)$$

Where ZT is the TE device figure of merit. The efficiency of a TEG increases almost linearly with temperature difference [24,25]. This TE conversion efficiency can be improved by maximizing the Seebeck coefficient and lowering electrical resistivity and thermal conductivity.[42] In energy harvesting applications, where the temperature difference ΔT is small, the efficiency is, to an approximation, directly proportional to the ΔT across the TE material. A good-quality TE material should have high electrical conductivity, high thermos-power, and low thermal conductivity. Since the first two are determined only by the electronic properties of the material, they are often combined into the quantity $PF = \alpha^2 s$ referred to as the 'power factor'. Conversely, the thermal conductivity $K = K_e + K_l$ in thermoelectrics is the sum of two contributions; electrons and holes transporting heat (K_e) and phonons traveling through the lattice (K_l). It then means that ZT can be maximized by maximizing the electrical conductivity and minimizing the thermal conductivity. However, there is a relationship between the two which is not linear; Wiedemann–Franz law for electrons that obey degenerate and non-degenerate statistics (K_B is the Boltzmann constant, and e is the electron charge):

$$K_e/\sigma = L_0 T \qquad (13)$$

$$L_O = (\pi^2/3)(K_B/e)^2$$

Increasing the electrical conductivity not only produces an increase in the electronic thermal conductivity but also decreases the thermo-power; optimizing ZT becomes a challenge. While the power factor can in some cases be increased by varying the concentration of charge carriers in the material, decreasing K and K_L is much more problematic, especially for K_L, which is determined by the structure, rigidity, atomic masses, and other characteristics of the lattice [42].

2.4.1 Thermoelectric generator represented as a thermal network

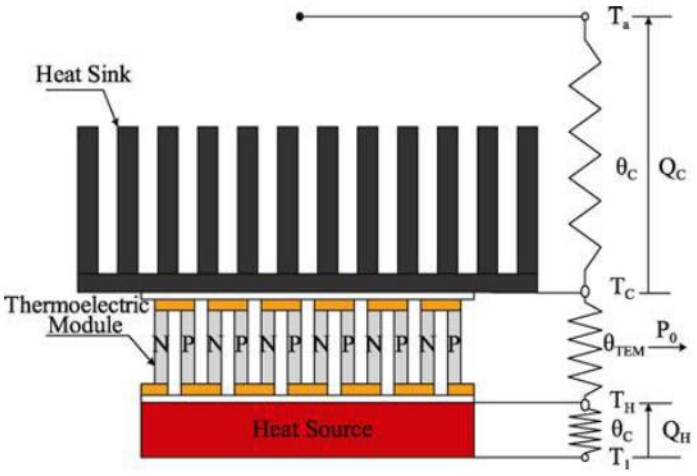

Figure 10: TEG device module thermal network [37]

It consists of thermal resistances Θ_H between the heat source and TE module, the thermal resistance of TEM Θ_{TE}, and thermal resistance Θ_C between the TEM and the heat sink [43].

Thermal resistances;

$$\Theta_H = \frac{T_1 - T_h}{Q_h} \ , \Theta_C = \frac{T_C - T_a}{Q_C} \qquad (14)$$

T_1 -Heat source temperature

T_a -Ambient temperature

T_H and T_C -TEG element temperatures

Q_h -Heat absorbed by TEG

Q_c -Heat emitted to the heat sink

Θ_H -Heat absorption intensity

Θ_C -Heat dissipation intensity; the smaller the Θ_C, the higher the heat dissipation

The total thermal resistance of N-couples

$$\Theta_{TEM} = \frac{\Theta_{TE}}{N} \qquad (15)$$

Where; Θ_{TE} is the thermal resistance of a single thermocouple and we neglect thermal transfer losses and contact resistances.

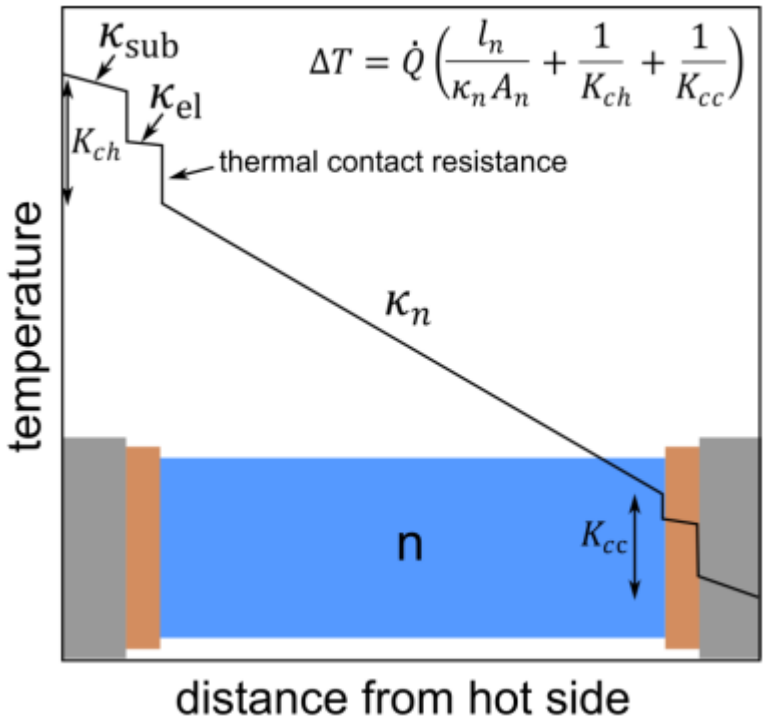

Figure 11; Typical temperature profile over a thermoelectric module [28]

Using Newton's law of heat transfer, when the system gets to a steady-state condition [44], using the thermal resistance equations, the energy balance equations become;

$$\dot{Q}_h = N\left(IT_h\alpha - \frac{1}{2}I^2R_{TE} + k(T_h - T_c)\right) = \frac{T_1 - T_h}{\Theta_h} \qquad (16)$$

$$\dot{Q}_c = N\left(IT_c\alpha - \frac{1}{2}I^2R_{TE} + k(T_h - T_c)\right) = \frac{T_c - T_a}{\Theta_c} \qquad (17)$$

Where; $R_{TE} = \frac{\rho_p l_p}{A_p} + \frac{\rho_n l_n}{A_n} + R_c$

R_c- Contact resistance

$$k = \frac{k_p A_p}{l_p} + \frac{k_n A_n}{l_n} \qquad (18)$$

Assuming that p- and n-type thermocouples are similar, $R_{TE} = \frac{\rho l}{A}$ (for $\rho = \rho_n + \rho_p$)

Also, thermo-conductivity of a material is given by;

$$K = \frac{kA}{l} = \frac{1}{\Theta}$$

$$K = K_p + K_n$$

For a TEG device, the total thermal conductivity is given by; [45]

$$\frac{1}{K_{TEG}} = \frac{2}{K_{Ceramic}} + \frac{1}{K_{Pellets}} \qquad (19)$$

Elaborating the equations above, the first terms represent the Peltier heat/power generated, the second, represent joule heating and have a factor of 0.5 since it is shared between the p- and n-type legs and the third terms represent the Fourier heat power transfer.

There is a difference between Q_h and Q_c which is the output power of the system. It may be expressed in electrical terms.

Using the first law of thermodynamics;

$$\dot{Q}_h - \dot{Q}_c = P_L = N(\alpha I_L(T_h - T_c) - I^2 R_{TE}) \qquad (20)$$

But also $P_L = V_L I$

For an external load resistance

$$\dot{Q} = NI^2 R_L \qquad (21)$$

Equating the two equations (20) and (21) gives;

$$P_L = NI^2 R_L = V_L I \qquad (22)$$

$$V_L = NIR_L = N(\alpha(T_h - T_c) - IR_{TE})$$

Maximum voltage occurs at open circuit; $I = 0$

$$V_{OC} = N\alpha(T_h - T_c) \qquad (23)$$

So, now finding the electrical current flowing, from the above equation;

$$I(R_L + R_{TE}) = \alpha(T_h - T_c)$$

$$I = \frac{\alpha(T_h - T_c)}{R_L + R_{TE}} \qquad (24)$$

Maximum current occurs at short circuit;

$$R_L = 0$$

$$I_{max} = \frac{\alpha(T_h - T_c)}{R_{TE}} \qquad (25)$$

Since current flows through all modules and is independent of thermocouples, the modules are connected serially electrically.

Putting the value of I in the energy equation of external load resistance;

$$\dot{Q} = P_L = N\frac{\alpha^2(T_h - T_c)^2}{(R_{TE} + R_L)^2}R_L$$

$$P_L = N\frac{\alpha^2(\Delta T)^2}{(R_{TE} + R_L)^2}R_L \qquad (26)$$

Maximum power is generated when internal resistance R_{TE} is on a matched load condition, i.e. $R_{TE} = R_L$. This gives P_{max} as;[46]

$$P_{max} = \frac{N\alpha^2(\Delta T)^2}{(2R_{TE})^2}R_{TE} = \frac{N\alpha^2(\Delta T)^2}{4R_{TE}} \qquad (27)$$

Originating from the dimensionless constant ZT (figure of merit), the efficiency of TEGs is quite low. ZT is around 1 and is temperature dependent also.

Conversion efficiency

This is given by a relationship between heat at the input junction and the delivered power. It is expressed as;

$$\eta_{conversion} = \frac{Power\ delivered}{Heat\ input\ at\ hot\ junction} = \frac{W_e}{Q_h} \qquad (28)$$

Thermodynamic efficiency

In the same trend, this is also given by a relationship between power supplied to load with heat absorbed at the hot junction.

$$\eta_{Thermo} = \frac{Power\ supplied\ to\ load}{Heat\ absorbed\ at\ hot\ junction} \qquad (29)$$

Power supplied to the load = Joule heating of the load resistor

$$P_{load} = I^2 R_L$$

$$peltier\ heat = \pi I = \alpha I T_h \qquad (30)$$

From Ohm's law, the current flowing through the circuit;

$$I = \frac{V}{R_{total}} = \frac{\alpha(T_h - T_c)}{R + R_L} \qquad (31)$$

Heat drawn from the junction is given by the Fourier term but there is also Joule heating from the generated current from the Seebeck voltage. Some generated heat also returns to the hot junction. [Assumption: half of the Joule heating is transported and half returned to the hot junction][47]

$$Q_h = Fourier - joule\ heating + half\ joule\ heating$$

$$Q_h = KA(T_h - T_c) - I^2R + \frac{1}{2}I^2R$$

$$Q_h = KA(T_h - T_c) - \frac{1}{2}I^2R \qquad (32)$$

If all power supplied to the load is only through Joule heating, efficiency can be got by combining the terms.

$$\eta = \frac{Power\ supplied\ to\ load}{Heat\ absorbed\ at\ hot\ junction} = \frac{Power\ supplied\ to\ load}{Peltier + Heat\ taken\ from\ hot\ junction(Q_h)}$$

$$\eta = \frac{I^2 R_L}{\alpha I T_h + KA(T_h - T_c) - \frac{1}{2}I^2R} \qquad (33)$$

From; $W = IV$

$$\frac{N\alpha^2 \Delta T^2}{R} \cdot \frac{R_L/R}{\left(1 + R_L/R\right)^2} = I \cdot \frac{N\alpha\Delta T}{\left(1 + R_L/R\right)} \left(\frac{R_L}{R}\right)$$

$$I = \frac{\alpha \Delta T}{R+R_L} \tag{34}$$

So, the efficiency becomes;

$$\eta = \frac{\left(\frac{\alpha \Delta T}{R+R_L}\right)^2 R_L}{\left(\frac{\alpha \Delta T}{R+R_L}\right) T_h + KA(T_h - T_c) - \frac{1}{2}\left(\frac{\alpha \Delta T}{R+R_L}\right)^2 R}$$

$$\eta = \frac{\left(1+\frac{T_c}{T_h}\right)\frac{R_L}{R}}{\left(1+\frac{R_L}{R}\right) - \frac{1}{2}\left(1-\frac{T_c}{T_h}\right) + \frac{\left(1+\frac{R_L}{R}\right)^2 \frac{T_c}{T_h}}{ZT_c}} \tag{35}$$

For maximum efficiency, we find the optimum values by getting the values of η after solving;

$$\frac{d\eta}{d\left(\frac{R_L}{R}\right)} = 0$$

But; $\frac{R_L}{R} = \sqrt{(1+ZT)}$ and $T = \frac{1}{2}(T_h + T_c)$

So; [48]

$$\eta_{max} = \left(1 - \frac{T_c}{T_h}\right) \frac{\sqrt{1+ZT}-1}{\sqrt{1+ZT}+\frac{T_c}{T_h}} \tag{36}$$

The TEG efficiency is also limited by the Carnot efficiency which is the highest efficiency that can be obtained. [49][50]

$$\eta_{carnot} = 1 - \frac{T_c}{T_h} \tag{37}$$

From this, maximum conversion η_{max} for a TEG can be estimated to be;

$$\eta_{max} = \eta_{carnot} \cdot \frac{\sqrt{1+ZT}-1}{\sqrt{1+ZT}+\frac{T_c}{T_h}} \tag{38}$$

$$\eta_{max} = \eta_{carnot} \cdot \eta_{rd}$$

Where; η_{rd} −Reduced device efficiency

From the equation above, ZT is the limiting factor. A better ZT material ought to be got or ways of improving ZTs of available materials sought for a better TEG efficiency.

Maximum power efficiency is obtained by letting R_L=R ($\frac{R_L}{R} = 1$)

$$\eta_{mp} = \frac{1-\frac{T_c}{T_h}}{2-\frac{1}{2}\left(1-\frac{T_c}{T_h}\right)+\frac{4\frac{T_c}{T_h}}{ZT_c}} \qquad (39)$$

Note; There are two thermal efficiencies: the maximum power efficiency η_{mp} and the maximum conversion efficiency η_{max}.

2.4.2 Thermoelectric device modeling

For a proper analysis, some aspects of the underlying complex phenomenon have to be known and by this, some assumptions ought to be made and also with simplifications.

Assumptions

- ✓ Assume transient heat loss and gain since brake temperature goes on gaining during the braking process and reducing after brakes are released.
- ✓ Heat losses due to radiation are neglected
- ✓ The gap between thermocouples is assumed to be perfectly isolated
- ✓ Axial heat conduction within thermocouples is also neglected
- ✓ Current flow in the thermocouples is assumed to be one dimensional, no current leakages

To calculate the total energy that can be harvested from a TEG module, an energy balance equation is used[51]. Energy balance equation for an infinitesimal element *dy* is given by;

$$\dot{Q} - \left(\dot{Q}_y + \frac{d\dot{Q}_y}{dy}dy\right) + \frac{I^2\rho}{A}dy = 0 \qquad (40)$$

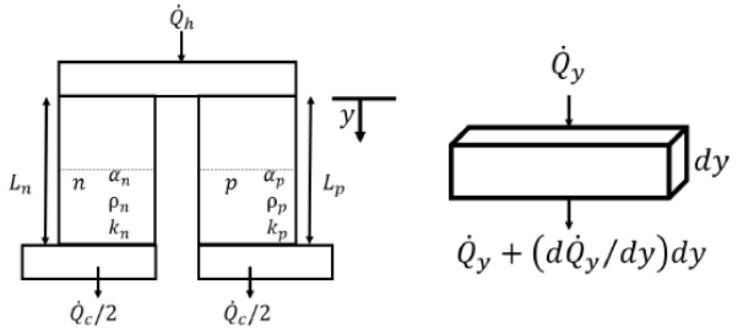

Figure 12: Heat flow rate in a single TE element [51]

The first part of the equation represents heat transfer across the hot surface (from which we are recovering the waste heat). The second term represents the joule heating effect associated with the release of heat due to the passage of current through the TE leg. Since this heating is throughout the element, half of it is in the n-type leg and the other half in the p-type leg. This insinuates that half flows towards one side as the other flows in the opposite direction.

Boundary conditions for the equation are;

$$T(y)|_{y=0} = T_h$$

$$T(y)|_{y=l} = T_c$$

Applying these conditions to the energy balance equation gives the temperature distribution across the thermocouple. As;

$$T(y) = \frac{I^2\rho y^2}{2A^2k} + \left(\frac{T_c - T_h}{l} + \frac{I^2\rho y^2}{2A^2k}\right)y + T_h \qquad (41)$$

So, the energy balances at either end; hot and cold are given by;

$$\dot{Q}_h = (\alpha_p - \alpha_n)T_h I + \left(-k_p A_p \frac{dT}{dy}|_{y=0} - k_n A_n \frac{dT}{dy}|_{y=0}\right) = 0 \qquad (42)$$

$$\dot{Q}_c = (\alpha_p - \alpha_n)T_c I + \left(-k_p A_p \frac{dT}{dy}|_{y=l} - k_n A_n \frac{dT}{dy}|_{y=l}\right) = 0 \qquad (43)$$

In these equations, the first terms account for the Peltier heat which sometimes is written as a function of Seebeck coefficient (ZT) and the second terms represent the Fourier law of thermal conduction at the boundaries

2.4.3 Contact resistances

Between two solid materials, the interface is never in perfect contact. Even if the surfaces look perfectly smooth, there will always be microscopic roughness on the surfaces that will form air-filled voids when the surfaces are pressed together. These voids decrease the surface area that is actually in contact, how much depends on surface roughness, the softness of the materials, and the contact pressure. Potential surface coatings, such as oxides or other impurities, might affect both the thermal and the electrical conductivity over an interface. The magnitude of the thermal contact resistance can be decreased by minimizing the area of the voids, either by smoothing or softening the surfaces or by increasing contact pressure. Another way to lower contact resistance is to fill the voids with a material with high conductivity. A thin layer of thermal grease or graphite is commonly used to fill the voids and enhance thermal contacts. Such material has far better thermal conductivity than air, but much lower than metals. A common method for lowering electrical contact resistance is to cover the surface with a soft, electrically conducting material that is resistant to oxidization. A technically beneficial but expensive choice of coating material is gold. The thickness of the gold layer is important, but if it is too thin, increases rather than decrease contact resistance. The most important contact resistances are the electrical resistances on both sides of thermoelectric pellets, and the thermal resistance between the connectors and the ceramic plates. There may also be thermal contact resistance between the pellets and the metal connectors. The locations of thermal and electrical contact resistances are highlighted below;

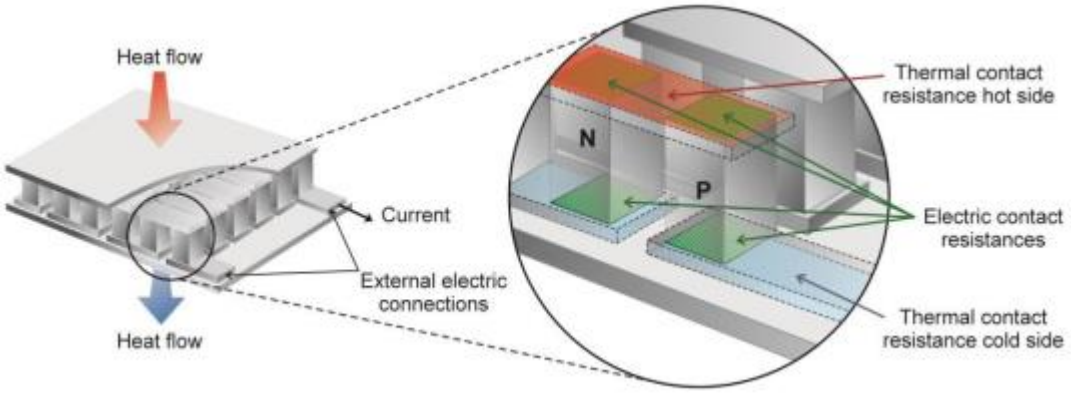

Figure 13: Contact resistances within a TE module [52]

2.5 Design of heat sink

Simon Ndiritu, [53] in a discussion on the internet said that minimizing thermal resistance is a faster means of drawing heat from any system by a heat sink. This is the principle that is applied in the design of heat exchangers in all systems and herein as well we apply it. By increasing the rate of loss of heat in the heat sink we facilitate this property. Heat sink parameters too ought to be optimized to minimize thermal resistance. These parameters include;

Fin thickness (size), spacing and shape; The flow of the coolant medium is greatly impacted by the arrangement of fins on a heat sink. Optimizing the configuration helps to reduce fluid flow resistance thus allowing more air to go through a heat sink. Its performance is also determined by the shape and design of its fins. Optimizing the shape and size of the fins helps to maximize the heat transfer density. Through modeling, the performance of different fin shapes and configurations can be evaluated.

Material; Heat sinks are designed using materials that have high thermal conductivity such as aluminum alloys and copper. Copper offers excellent thermal conductivity, antimicrobial resistance, biofouling resistance, corrosion resistance, and heat absorption. Its properties make it an excellent material for heat sinks but it is more expensive and denser than aluminum[54]. Diamond offers a high thermal conductivity that makes it a suitable material for thermal applications. Its lattice vibrations account for its outstanding thermal conductivity. Composite materials such as AlSiC, Dymalloy, and copper-tungsten pseudo-alloy are also commonly used in thermal applications

Thermal Interface Material; Surface defects, roughness, and gaps increase thermal contact resistance thereby reducing the effectiveness of a thermal solution. These defects increase the heat flow resistance by reducing the thermal contact area between an electronic component and its heat sink. Thermal resistance is reduced by increasing the interface pressure and decreasing the surface roughness. In most cases, there are limits to these resistance reduction methods. To overcome these limits, thermal interface materials are used. The electrical resistivity of a material, contact pressure, and size of the surface gaps should be considered when selecting a thermal interface material for a given thermal application

Profile and fin location; the kinds of fins are determined by the profile which determines how intimate the cooling fluid interacts with the heat sink to facilitate the heat transmission to the

cooling fluid. In the same way, the location of the fins affects the heat flux transmission as the more exposed the fins are the better the heat transfer.

2.5.1 Selecting the right heat sink

A good heat sink that can radiate heat into the ambient air fast is needed so as to have the desired temperature difference between the hot side and the cold side[55]. Considering the hot side temperature, the ambient temperature, the total resistance in the TEG module (thermal resistance of hot side heat sink, the thermal resistance of TEG and thermal resistance of cold side heat sink) we can choose the matching heat sink in the case.

Assuming 90% of the ΔT is lost across the module, we have then to select heat sinks that have a thermal resistance of at most 5% each of the TEG. This is caused by the overall ΔT being distributed across the three thermal resistances in proportion with their resistance values just like the voltage is distributed across a series of electrical resistance in an electrical circuit. Below is a figure that illustrates the thermal circuit of a TEG.

The heat sink has to be large enough to handle the transmitted heat. To effect faster cooling, there needs to be forced convection like a fan, but in our case, since the vehicle will be moving there is a created aerodynamic resistance and a simultaneous rotational movement of the disc, this on itself causes forced convection as the wind gets in contact with the wind and works as a fan with no power consumption. So, we will not need a fan to cool the heat sink.

2.6 Regenerative Braking

Regenerative braking is an inherent characteristic of dc shunt wound motors and does not require any change of connections. DC shunt motors are electrically stable also i.e., braking torque is independent of line voltage fluctuations. The dc series motors cannot be used readily for regenerative braking and some modification of shunt winding or separate excitation of the series field at low voltage is necessary to be employed to enable the motor to act as a generator. Inherently, a dc series generator has no stability of voltage, and therefore, an external means is required. A separate motor driven exciter has a separately excited field winding F_1 and also another field winding F_2 connected in the main motor circuit in such a way that the field created by it opposes the field created by separately excited field winding F_1 during regeneration[56].

The stabilising resistance R is employed to prevent current surges when the tram crosses from one section of the supply to another, and to compensate for variable line voltage.

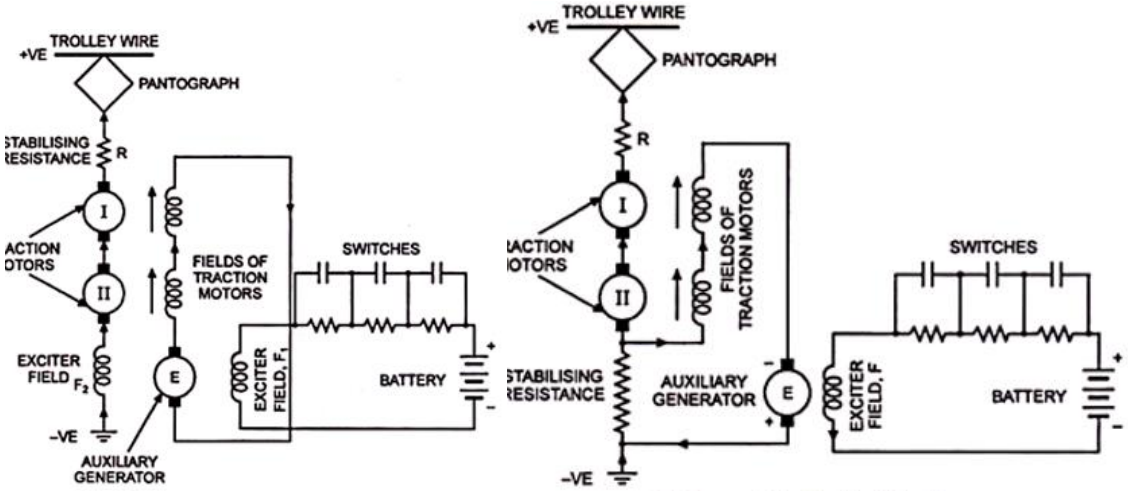

(a) Differentially Compounded Exciter *(b) Separately Excited Exciter*

In case the line voltage falls, regenerated current will tend to increase resulting in strengthening of field F_2 which will weaken the field F_1 and, therefore, reduction in emf generated by the exciter. Thus, the field of the traction motors will be weakened resulting in reduction of emfs generated by the traction motors operating as dc series generators. Hence, compensation for a decrease in the line voltage is automatically provided. Another arrangement has the exciter armature connected in the circuit of the field windings of traction motors and the stabilising resistance. The current through the stabilising resistance is the sum of the exciter current and the regenerated current. The voltage of the exciter circuit can be regulated by either varying its field strength or manipulating resistances in series with the armature. In case the line voltage falls the regenerated current will tend to increase resulting in increase in voltage drop across the stabilising resistance and, therefore, reduction in the voltage available in the exciter armature circuit causing a reduction in the excitation current of the traction motors operating as dc series generators. This reduces the emf's generated and thus compensation is provided automatically.

Regenerative braking is an inherent characteristic of an induction motor since an induction motor operates as an induction (non-synchronous) generator when run at speeds above synchronous speed and it feeds power back to the supply line. The machine, however, is not self-exciting as a generator and is required to be connected to a system supplied from

synchronous generators. This system supplies the excitation and determines the frequency at which the induction generator operates. Torque-speed characteristics of an induction machine are shown.

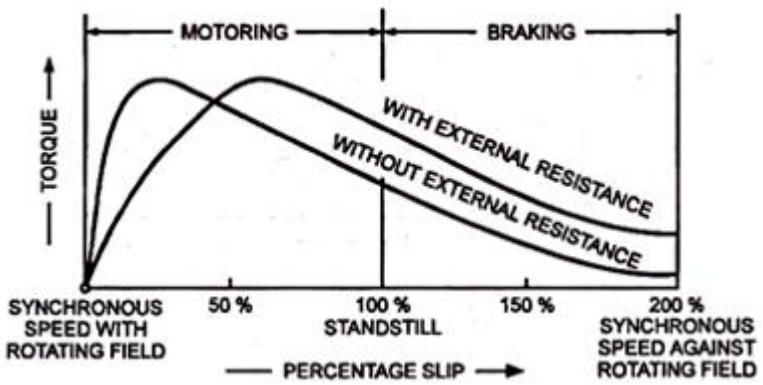

Figure 14: Torque-speed characteristic curve of an induction motor

From the torque-speed characteristics of an induction machine it is obvious that without any extra resistance in the rotor circuit, there is only a slight variation of speed with the torque whereas with the external resistance inserted in the rotor circuit speed increases for a particular braking torque. Thus, we see that with no extra resistance in the rotor circuit the speed during braking remains almost constant and independent of the gradient and the weight of the train. This is a great advantage with the induction motor when used for traction. But if increased speeds are necessary with light loads, these can be obtained by inserting external resistance in the rotor circuit. It returns about 20% of the total energy on certain railway run and saves a great deal of brake shoe wear.

Difficulties Encountered in Regenerative Braking:

Regenerative braking with ac series motors is more difficult than that with the dc series motor. The difficulties encountered are as follows:

During the regeneration period, the machine should not operate as a self-excited generator. Generally, high power factor is the main consideration in order to achieve a reasonable braking torque. Circuit for regeneration at high power factor usually suffers from self-excitation, and those which are inherently stable and free from self-excitation usually operate at a poor power

factor. For regenerative braking the regenerated power should have the same frequency as that of the main supply. This necessitates the energizing of the motor field winding from the ac mains. The regenerated current must be in phase opposition to the applied voltage and also the flux ϕ, so that power may be supplied back into the supply system. This arrangement below can provide the above conditions;

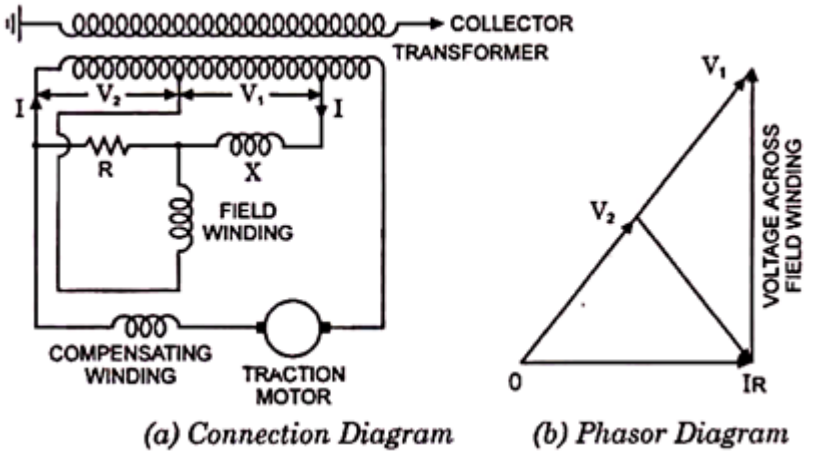

Figure 15: Regenerative braking with single phase AC series motor

In another satisfactory arrangement one of the traction motors is used as a generator to supply current to excite the fields of the remaining motors. As the speed of the locomotive falls, the voltage of the motors can be controlled by increasing the excitation current. This is accomplished by increasing the voltage on the exciting motor by employing another transformer tap. Further flexibility can be obtained by changing the tap from the generating motor.

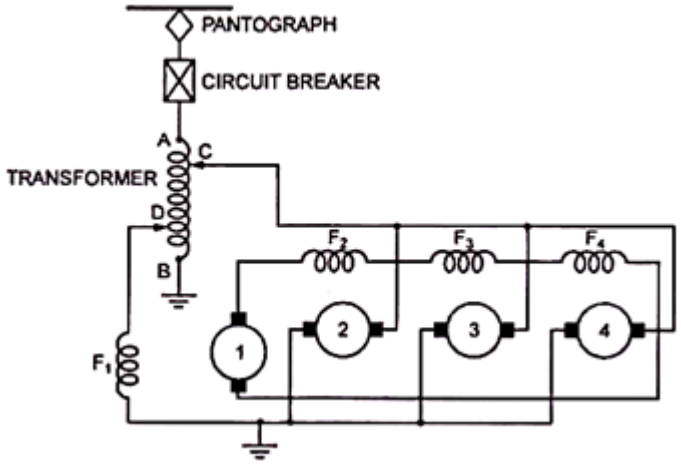

Figure 16: Connection diagram for regeneration with single phase AC series motor

Calculations of Energy Returned during Regeneration:

When the train is accelerated up to a certain speed, it acquires energy, known as kinetic energy, corresponding to that speed (KE = ½ mv^2). While coasting a part of this stored energy is utilised in propelling the train against frictional and other resistances to motion and, therefore, the speed falls. Under ideal conditions (no resistance to motion of the train) the speed of the train would have not decreased. Similarly, while the train is going down the gradient or moving on level track, the speed remaining the same or reduced, this stored energy can be converted into electrical energy and returned to the lines.

The amount of energy returned to the line depends upon:

- ✓ The initial and final speeds during regenerative braking
- ✓ The train resistance and gradient of the track also in case the train is moving down the gradient and
- ✓ Efficiency of the system.

Let the initial and final speeds of the train be V_1 and V_2 kmph respectively. The kinetic energy stored in the train at a speed of V_1 kmph

$$\mathrm{KE}_1 = \frac{1}{2}\frac{1000\mathrm{W_e}}{9.81}\left(\frac{1000\mathrm{V_1}}{3600}\right)^2 \textit{kg-m} \qquad (44)$$

$$KE_1 = \frac{1}{2}x1000x\frac{1000W_e}{9.81}\left(\frac{1000V_1}{3600}\right)^2 \text{N-m}$$

$$\mathrm{KE}_1 = 0.01072\mathrm{W_eV_1^2}\ \textit{watt-hours} \qquad (45)$$

Similarly, kinetic energy at speed V_2 is:

$$\mathrm{KE}_2 = 0.01072\mathrm{W_eV_2^2}\ \textit{watt-hours} \qquad (46)$$

Energy available during regeneration

$$\textit{Energy available} = 0.01072\ W_e\ (V_1^2 - V_2^2)\ \textit{watt-hours} \qquad (47)$$

Some of the energy is lost to overcome the resistance to motion and the losses in the traction system including traction motors.

Energy lost to overcome the resistance to motion

$$E_r = W\ x\ r\ x\ S\ x\ 1{,}000/3{,}600\ \textit{watt-hours} = 0.2778\ WrS\ \ \textit{watt-hours} \qquad (48)$$

where r is the specific resistance in newton/tonne.

While going down the gradient in the hilly track service, energy is supplied as tractive effort due to the gradient and energy is added up to the energy available during regeneration. Energy available due to motion down the gradient.

$$98.1GW \times S \times 1{,}000/3{,}600 = 27.25\ GSW \quad (49)$$

Hence total energy available during regeneration

$$E_R = [0.01072W_e\ (V_1^2 - V_2^2) + 27.25\ GSW - 0.2778\ WrS] \quad (50)$$

Taking η as the efficiency of the system, Energy returned to the line

$$Er_l = [0.01072W_t,\ (V_1^2 - V_2^2) + 27.25\ GSW - 0.2778WrS] \times \eta\ watt\text{-}hours \quad (51)$$

Advantages of Regenerative Braking:

- ✓ A part of energy is returned to the supply system, so energy consumption for the run is considerably (about 20 to 30 per cent) reduced thereby affecting a considerable saving in the operating cost.
- ✓ The wear of the brake shoes and wheels is reduced to a considerable extent. Therefore, their life is increased and replacement cost is reduced.
- ✓ Higher value of braking retardation is obtained so that the vehicle can be brought to rest quickly and running time is considerably reduced.
- ✓ Small amount of brake dust is produced when the mechanical brakes are applied.
- ✓ Higher speeds are possible while going down the gradients because the high braking retardation can be obtained with regenerative braking.
- ✓ Propulsion of heavier trains on gradients is possible without dividing them into sections with speed and safety.

Disadvantages of Regenerative Braking:

- ✓ Additional equipment is required for control of regeneration and for protection of equipment and machines, hence initial as well as maintenance cost is increased.

- ✓ The dc machines required in case of regenerative braking are of large size and cost more than those ordinarily employed, therefore, the weight of the locomotive and thus the required mechanical strength and cost increase.
- ✓ Owing to recuperated energy the operation of the substations becomes complicated and difficult.
- ✓ In case of substations employing mercury-arc rectifiers for conversion purpose, additional equipment is required either to deal with regenerated energy separately or to change one or more of the ordinary rectifiers over to inverted operation. No such difficulty is experienced in case of substations employing rotary convertors or motor-generator sets for converting purpose.
- ✓ Regenerative braking is employed down to a speed of 16 kmph, then rheostatic braking to about 6.5 kmph and then mechanical braking is required to bring the locomotive to rest.

In most of the cases, however, and especially with motor-coach trains the increased cost of the train equipment and the additional features required in order to obtain regenerative braking, combined with the increase in the maintenance cost of the electrical equipment, may entirely offset the economics in the energy consumption and the other items. For tramways, trolley buses, the regenerative braking is not recommended as it will unnecessarily increase the initial cost as well as increase the operating problems. Generally regenerative braking is desirable and necessary for the service lines having long gradients exceeding 0.6%.

3. CHAPTER THREE

3.0 Theoretical outline for designers and modeling

The conventional design of a power generating thermoelectric module is usually based on a set of formulae derived using a simple model in which the thermal and electrical contact resistance of the module are neglected. An expression is derived for the conversion efficiency which is independent of module geometry. Consequently, the design of the thermoelectric generator is guided solely by matching the load resistance to achieve either of the two limiting cases: maximum conversion efficiency or maximum power output. However, both power output and conversion efficiency of a thermoelectric module are dependent upon the thermo-element length for a given figure-of-merit, contact properties and temperature difference of operation. The optimum length necessary to obtain maximum power output differs from that of maximum conversion efficiency. Obviously, an appropriate thermo-element length for power generation will be a compromise between the requirements for maximum power output and maximum conversion efficiency. The module construction cost is closely related to the power output, while its conversion efficiency determines the running cost. The module geometry for power generation should then be optimized to minimize the cost of the generated electricity. In this project, an attempt is made to provide the necessary formulae and graphs to achieve an optimized module design.

3.1. Design

Design is a creative process by which new methods, devices, and techniques are developed to solve new or existing problems. Though many professions are concerned with creativity leading to new arrangements, structures, or artifacts, the design is an essential element in engineering education and practice. Due to increasing worldwide competition and the need to develop new, improved, and more efficient processes and techniques, a growing emphasis is being put on design.

3.1.1. Steps in the design process

The conceptual design yields the basic approach and the general features of the system. These form the basis of the subsequent quantitative design process. The starting or initial design is then specified in terms of the configuration of the system, the given quantities from the problem

statement, and an appropriate selection of the design variables. This initial selection of the design variables is based on information available from other similar designs, on current engineering practice, and on experience. Employing approximations and idealizations, a simplified model may then be developed for this initial design of the system so that its behavior and characteristics may be analyzed. Generally, the system behavior under a variety of conditions is investigated on the computer, by a process known as simulation, because of the complexity of the governing equations in typical thermal systems. An experimental or physical model may also be employed in some cases.

The outputs from the modeling and simulation effort allow the designer to evaluate the design with respect to the requirements and constraints given in the problem statement. If an acceptable design that satisfies these requirements and constraints is obtained, the process may be terminated or other designs may be sought with a view to improve or optimize the system. If an acceptable design is not obtained, the design is varied and the processes of modeling, simulation, and design evaluation repeated. These steps are carried out until a satisfactory design is obtained. Different strategies may be adopted to improve the efficiency of this iterative procedure. The figure below shows a typical overall design procedure, starting with the conceptual design, and indicating some of the steps mentioned here. Usually, the engineering design process focuses on the quantitative design aspects after the problem statement and the conceptual design have been obtained. Then, the design process starts with the initial design of the physical system and ends with the communication of the design to fabricate and assembly facilities involved in developing the system. The formulation of the design problem and conceptual design are precursors to this process and play a major role at various stages. Thus, the main steps that constitute the design and optimization process could be listed as:

1. Initial physical system
2. Modeling of the system
3. System simulation
4. Evaluation of different designs
5. Iteration and obtaining an acceptable design
6. Optimization of the system design
7. Automation and control

8. Communicating the final design

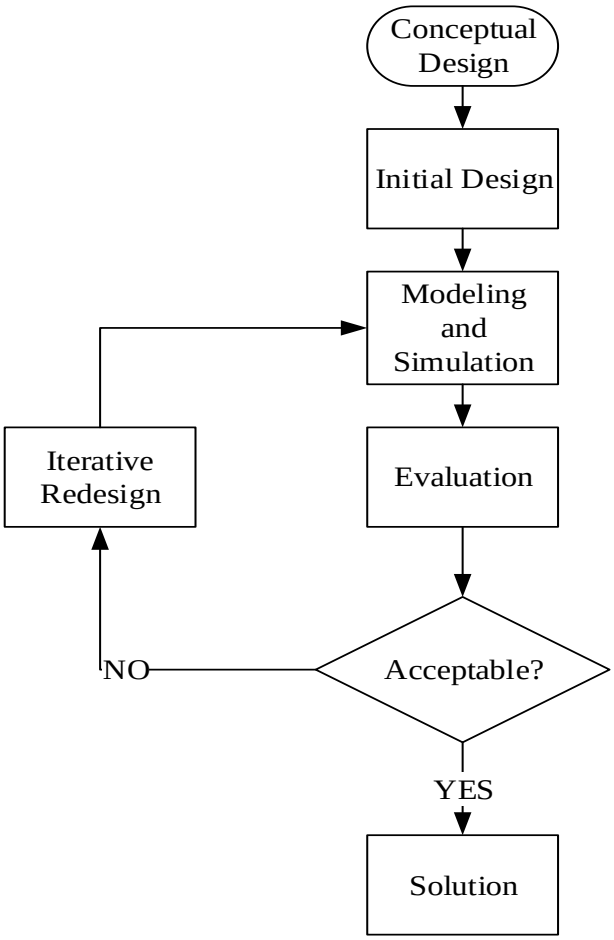

Figure 17: Iterative process to obtain an acceptable design

Three principal points considered during designing a thermoelectric generator:

1) *Specifications:* the operating temperatures T_C, T_H, and the required power output P (and or output voltage V or current I).

2) *Materials parameters:* the thermoelectric properties of thermo-element materials Z (α,ρ,γ), and the electrical and thermo-contact properties of the module.

3) *Design parameters:* the thermo-element length L, the cross-sectional area A and the number of thermocouples N.

4. CHAPTER FOUR

4.0 Methodology

4.1 Typical heat loss value calculation

These calculations were done in line with the data collected from an Ethiopian Railways Corporation subsidiary company Addis Ababa Light Rail Transit. With an average operational speed of the vehicles being 25 km/h, and an empty car weighing 64 tons, the calculations are done to establish the lowest possible energy that is lost to the environment during braking and later find out how much of this energy can be recuperated by the designed system of a thermoelectric generator.

4.1.1 Disc brake heat calculation

As earlier mentioned, during braking of a vehicle, all kinetic energy has to be lost so as for the vehicle to come to a halt. In the case of friction brakes, all kinetic energy is transformed into heat energy at the brake disc-pad interfaces. This is in line with the first law of thermodynamics which states that energy can neither be created nor destroyed but transformed from one form to another. The heat generated at the contacts causes a heat flux in the body and the bodies thermal energy increases. Below we show the heat energy calculation in the brake disc taking the case of the Addis Ababa light rail transit vehicles with the following basic vehicle data;[57]

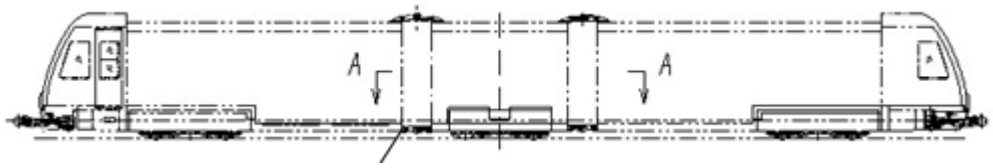

Figure 18: Car Scheme [57]

Number of bogies – 3

Vehicle mass – 64000 kg

Vehicle mass per bogie – 21333.333 kg

Average operational speed – 25 km/hr

Service brake deceleration rate – 1.1 m/s^2

Coefficient of braking between disc and pad – 0.5

Maximum applied pressure -100 bars

Effective brake pad area per disc – 240 cm^2

Assumptions made;

- ✓ Circulation is considered for all the braking torque involving all axles
- ✓ Brakes are applied on all the brake discs (8 in total) 1 per axle for the motor car bogies and 2 per axle for the trailer cars
- ✓ All heat is transmitted to the brake disc
- ✓ Heat flux is applied to both sides of the ventilated disc
- ✓ All kinetic energy is lost at the disc-pad contact no losses due to aerodynamic resistance or friction on the wheels
- ✓ Rail surfaces and decelerations; are uniform
- ✓ Thermal conductivity of the material is steady throughout the process and does not alter with an increase in thermal energy

Calculation

The tangential force between disc and pad

F_{TR} - Normal force between disc and pad

Coefficient of friction μ=0.5

Area of brake pad, A = 240 cm^2 = 0.024 m^2

$$Braking\ force\ applied, F_{BR} = \frac{P_{Cmax}}{2} A \qquad (52)$$

We use half of the maximum cylinder pressure as our pressure since it is divided for the two pads on either disc

Also;

$$F_{TR} = \mu F_{BR} \qquad (53)$$

$$F_{TR} = 0.5x\frac{100x10^5}{2}x0.024$$

$$F_{TR} = 60{,}000N = F_T$$

The tangential force between the pad and the disc is equal to the normal force because of the same applied force and material.

Brake torque

This is the torque that is possessed by the brake due to its momentum from the angular velocity.

$$Braking\ torque\ T_b = F_T R \qquad (54)$$

$$T_b = 60000x180x10^{-3}$$

$$T_b = 10{,}800\ Nm$$

Where; R is the disc radius

Braking distance

Using the Newtonian equations of motion, with a service-brake deceleration of 1.1m/s^2, initial velocity of 25km/hr = 6.944m/s (operational speed of the AALRT)

Using;

$$v^2 = u^2 + 2as$$

$$s = \frac{6.944}{2x1.1} = 21.9\ m$$

Braking time

This is the time the brakes are applied for, for an effective vehicle stopping. In the case of this study, this is the time during which the heat is generated at all the interfaces of the disc and pad.

Using;

$$s = ut + \frac{1}{2}at^2 \qquad (55)$$

$$u = 6.9444\ m/s, \qquad a = -1.1\ m/s^2, \quad s = 21.9\ m$$

$$21.9 = 6.944t - \frac{1}{2}x1.1t^2$$

$$0.55t^2 - 6.944t + 21.9 = 0$$

Solving the quadratic equation gives;

$$t_1 = 6.493\ s, \quad t_2 = 6.133\ s$$

Heat generated during braking

From the first law of thermodynamics, all the energy is converted into heat energy at the friction brakes.

$$E_v = Q_{br}$$

$$Q_{br} = \frac{1}{2}MV^2 + Mgsin\Theta \qquad (56)$$

$$Q_{br} = \frac{1}{2}x64000x6.944^2 + 64000x9.81xsin(0.905) = 1{,}552{,}928.82\ \text{J}$$

This is done for all the stations and an average used in this study.

	Station name	$\Theta(^0)$	Heat flux of vehicle	Heat flux per disc
1	Ayat 2	0.905°	2246715.527	280839.441
2	Ayat 1	0.818°	2098956.437	262369.555
3	Meri/CMC 2	0.917°	2098956.437	262369.555
4	CMC 1	2.767°	1647262.507	205907.813
6	Civil Service College	1.019°	1932493.664	241561.708
7	Sahlite Mhiret Church	0.79°	1969901.028	246237.629
8	Gurd Sholla	0.127°	2098956.437	262369.555
9	Megenagna	1.031°	2267289.578	283411.197
10	Lem Hotel	0.358°	2098956.437	262369.555
11	Mazoria	0.491°	2098956.437	262369.555
12	Chemical Corporation	1.247°	1862354.855	232794.357

13	Urael Church	1.394°	1871706.696	233963.337
14	Yordanose Hotel	0.849°	1960549.187	245068.648
15	Estifanos	0.155°	2098956.437	262369.555
16	Stadium	0.093°	2098956.437	262369.555
17	Le Gahar	0.458°	2098956.437	262369.555
18	Road Authority	0.102°	2098956.437	262369.555
19	Mexico Square	1.591°	1838975.252	229871.906
20	Lideta	1.247°	2465548.611	308193.576
21	Coca Cola	1.302°	2311243.231	288905.404
22	Tor Hailoch	0.504°	2098956.437	262369.555

Since the mass used is the whole mass of the vehicle, and all the 8 brake discs work concurrently, the heat energy is shared amongst them to give;

$$Q_D = \frac{Q_{br}}{number\ of\ brake\ discs}$$

$$Q_D = \frac{1.553x10^6}{8}$$

$$Q_D = 194.116x10^3\ J$$

Heat flux per disc is got by dividing the heat lost at every disc by the braking time;

$$F_D = \frac{194.116x10^3}{6.5x113.0974x10^{-3}} = 264.056x10^3\ W$$

$$A_b = 2\pi(r_1^2 - r_2^2) = 2\pi(180^2 - 120^2) = 113{,}097.4\ mm^2 = 113.0974x10^{-3}$$

For different stations on the track, the vehicle faces different conditions and so the braking force is not constant throughout. More heat flux is given off at stations that have a negative gradient and lower heat flux for those that have positive gradient due to the supporting $mgsin\Theta$ force and a resisting one in the positive gradient stations.

Using the equation below for the calculation of the heat flux;

$$F_{Total} = \frac{1}{2A_b t_b}(mv^2 \pm s_b mgsin\Theta)$$

Where;

m- mass of the vehicle, s_b- braking distance, t_b- braking time, A_b- effective braking area

Calculation of the flux given off per station during braking

Table 5: Stations on the east-west line of the AALRT with respective gradients and heat flux per disc during braking

	Station name	Gradient/slope	Station types	Heat flux per disc
1	Ayat 2	0.01580 [0.905°]	Ground [- down]	280839.441
2	Ayat 1	0.0143[0.818°]	Ground [level]	262369.555
3	Meri/CMC 2	0.0160[0.917°]	Ground [level]	262369.555
4	CMC 1	0.0483[2.767°]	Ground [+ up]	205907.813
6	Civil Service College	0.0178[1.019°]	Ground [- down]	241561.708
7	Sahlite Mhiret Church	0.0138[0.79°]	Ground [- down]	246237.629
8	Gurd Sholla	0.0022[0.127°]	Ground [- down]	262369.555
9	Megenagna	0.018[1.031°]	Underground [+ up]	283411.197
10	Lem Hotel	0.0063[0.358°]	Ground [- down]	262369.555
11	Mazoria	0.0086[0.491°]	Ground [Level]	262369.555
12	Chemical Corporation	0.0253[1.247°]	Elevated [+ up]	232794.357
13	Urael Church	0.0243[1.394°]	Ground [Level]	233963.337
14	Yordanose Hotel	0.0148[0.849°]	Ground [- down]	245068.648
15	Estifanos	0.0027[0.155°]	Ground [- down]	262369.555
16	Stadium	0.0o0016[0.093°]	Elevated [Level]	262369.555
17	Le Gahar	0.008[0.458°]	Elevated [+ up]	262369.555
18	Road Authority	0.0018[0.102°]	Ground [- down]	262369.555
19	Mexico Square	0.0278[1.591°]	Elevated [+ up]	229871.906
20	Lideta	0.0392[1.247°]	Elevated [- down]	308193.576
21	Coca Cola	0.0227[1.302°]	Ground [Level]	288905.404
22	Tor Hailoch	0.0088[0.504°]	Ground [- down]	262369.555

4.3 Size of the TEG legs and packing factor

When designing a TEG module, special attention ought to be given to the packing factor (fill factor) and the size of the leg as the design parameters. The size of the leg ω is the side length of the element, which is mostly a square element. It is obtained by;[58]

$$\omega = \frac{\sqrt{A}-\sqrt{N+2}\tau}{\sqrt{N+2}} \qquad (57)$$

In the same way, the packing factor (fill factor) ϕ is the ratio of the surface area of thermoelectric material (Nw^2) over the total surface area (A) of the module. The inverse of the packing factor is called thermal concentration factor. The packing factor is obtained by;

$$\phi = N\frac{A+(N+2)\tau^2-2\sqrt{A}\sqrt{N+2}\tau}{A(N+2)} \qquad (58)$$

By reducing the packing factor and the leg size, the overall device cost is reduced. But by reducing the leg size for a fixed packing factor, less material is used. The leg size cannot be reduced beyond an optimum since the temperature drops across the module decreases and thus decreasing power output. Since any change affects the cost of the device and the power output as well, an optimum geometry, packing factor and the leg size ought to be chosen to minimize the negative effects.

We now dive into the number of legs that can be filled in the available annular device to allow a good and optimum energy transfer with minimal thermal resistance. Choosing a leg size, ω of 2.5mm, and leg spacing, τ of 1mm;

The calculated annular area is;

$$Area\ of\ annulus = \pi(r_1^2 - r_0^2)$$

$$Area = \pi(180^2 - 110^2) = 63{,}774\ mm^2$$

Considering a sixth of the annular TEG device for study,

$$Area = \frac{1}{6}x63{,}774 = 10{,}629\ mm^2$$

Using equation (49);

$$\omega = \frac{\sqrt{A} - \sqrt{N+2}\tau}{\sqrt{N+2}}$$

$$2.5 = \frac{\sqrt{10629.1} - (\sqrt{N+2}\,)x1}{\sqrt{N+2}}$$

$$N = 865.7 \approx 866\ legs$$

So, calculating the packing factor using equation (50);

$$\phi = N\frac{A + (N+2)\tau^2 - 2\sqrt{A}\sqrt{N+2}\tau}{A(N+2)}$$

$$\phi = 866\,x\,\frac{10629.1 + (866+2)x1^2 - 2\sqrt{10629.1}\sqrt{866+2}\,x1}{10629.1(866+2)}$$

$$\phi = 0.509$$

Table 6: Leg sizes with the respective number of legs and packing factors

Leg size, ω (mm)	Area (mm^2)	space between legs, τ (mm)	Number of legs, N	Packing factor, Φ
1	10629.1	1	2655	0.249812
1.25	10629.1	1	2098	0.308348
1.5	10629.1	1	1699	0.359577
1.75	10629.1	1	1404	0.404382
2	10629.1	1	1179	0.443692
2.25	10629.1	1	1004	0.478337
2.5	10629.1	1	866	0.509028
2.75	10629.1	1	754	0.536355
3	10629.1	1	662	0.560807
3.25	10629.1	1	586	0.582788
3.5	10629.1	1	523	0.602633

4.6 Modeling and simulation

4.6.1 SolidWorks

Dassault Systemes (DS) SolidWorks Premium Computer Aided Drawing (CAD) software 2016 version was used to create a 3D computer model, which were then used to visualize the system components. SolidWorks is an excellent tool to visualize parts, put them into assemblies, and check if they fit together. Technical drawings, which are required for machine shop jobs, can be produced from a part model. Some machinery, such as CNC routers and 3D printers, can use the modeled part SolidWorks files directly to produce real parts, while other machinery, such as Plasma or laser cutters, may require the part models to be saved to a specific format. SolidWorks 3D part creation typically starts by creating a 2D sketch with lines, arcs, splines, points, etc.[59]. The sketch items have their dimensions defined together with relations such as tangency, parallelism, perpendicularity, and concentricity. The fully defined sketch is then used to extrude, revolve, sweep, or loft bosses or cuts. The resulting feature is then used to create sketches for subsequent bosses or cuts. Finally, 3D parts can be put into an assembly by creating mates, which define the tangency, parallelism, perpendicularity, and concentricity relations between planes, lines, arcs, and points similarly to the sketch relations. When constricted to a single degree of freedom, the parts can be moved relative to each other to visualize part movements in the real system. Drawings are created from a 3D part model by projecting its views onto a 2D sheet. Dimensions are then added to the projected views.

The brake-TEG model design is as shown below;

Here, the annular shaped TEG device has to be made in parts of segments to aid the installation of the sheet into the groove that was made to accommodate them. Since the connection in a TEG has to be in parallel thermally and in series electrically, by connecting the closest and lagging alone p-type leg to a lagging n-type leg in the next segment. With such a connection, the heat flows through all the components of the TEG device height-wise and current being generated flows through the legs to generated power from the device.

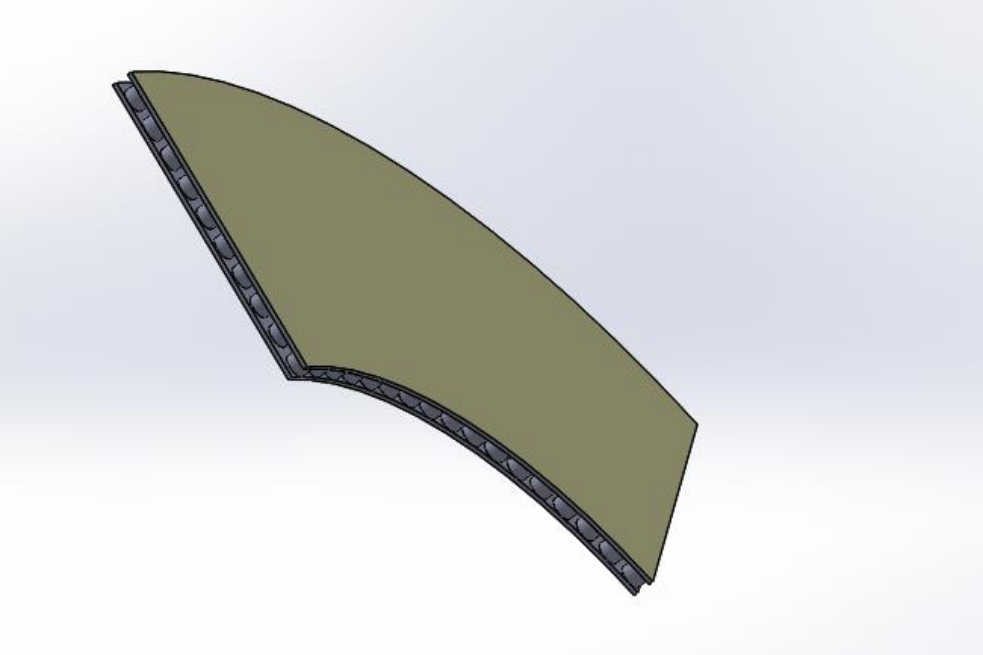

Figure 19: TEG module segment

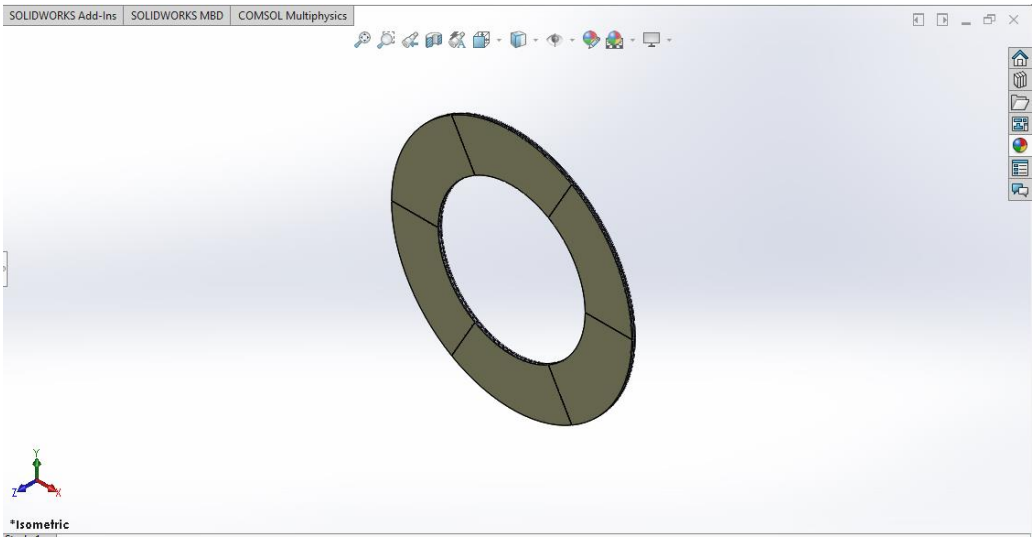

Figure 20: TEG module assembly

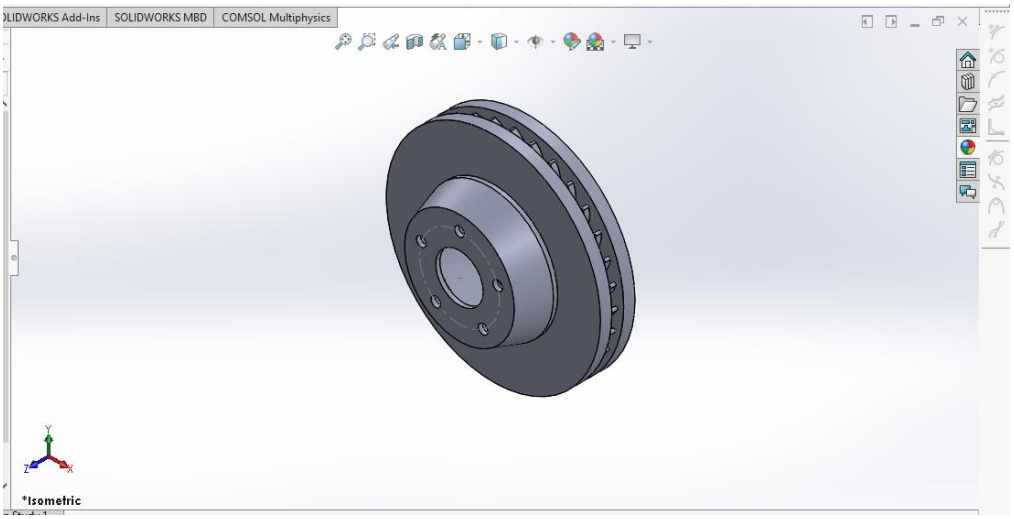

Figure 21: Brake disc (rotor) design modified

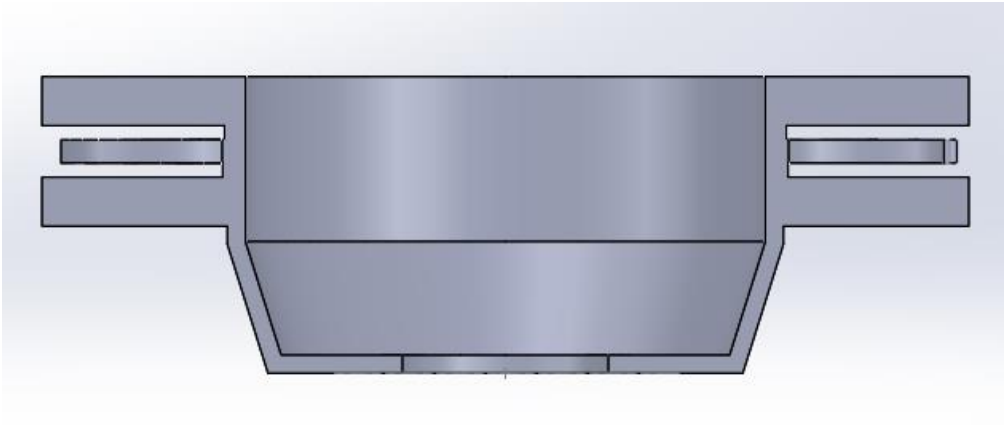

Figure 22: Modified brake disc section view

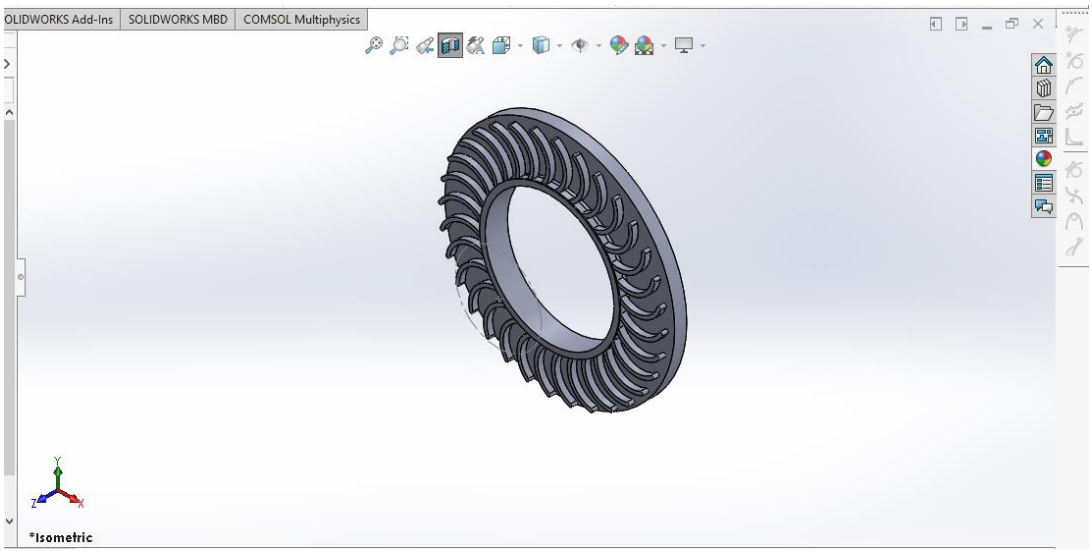

Figure 23: Brake disc section view showing fins (heat sink)

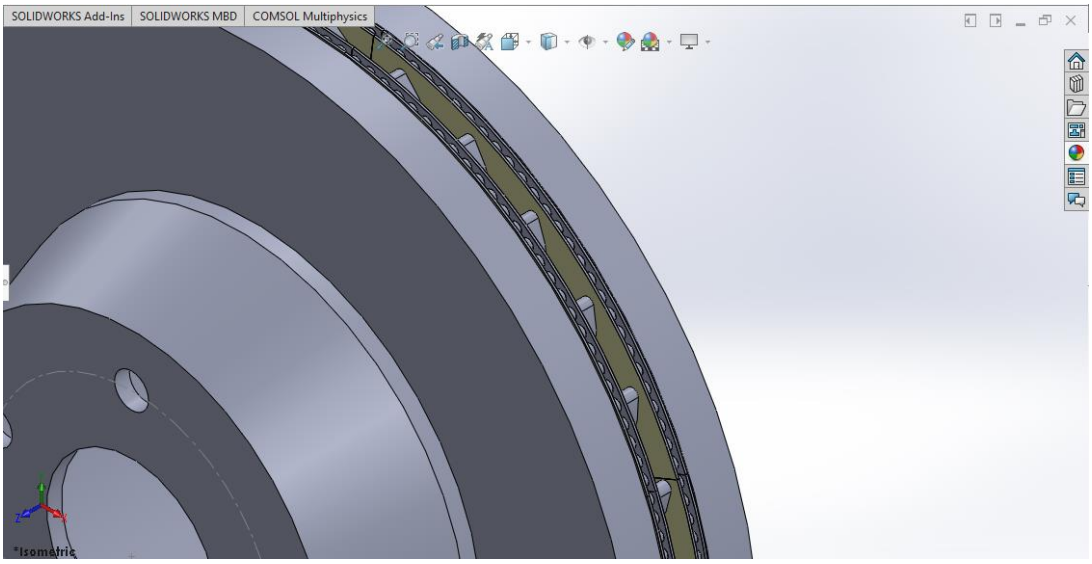

Figure 24: Close look at the assembly

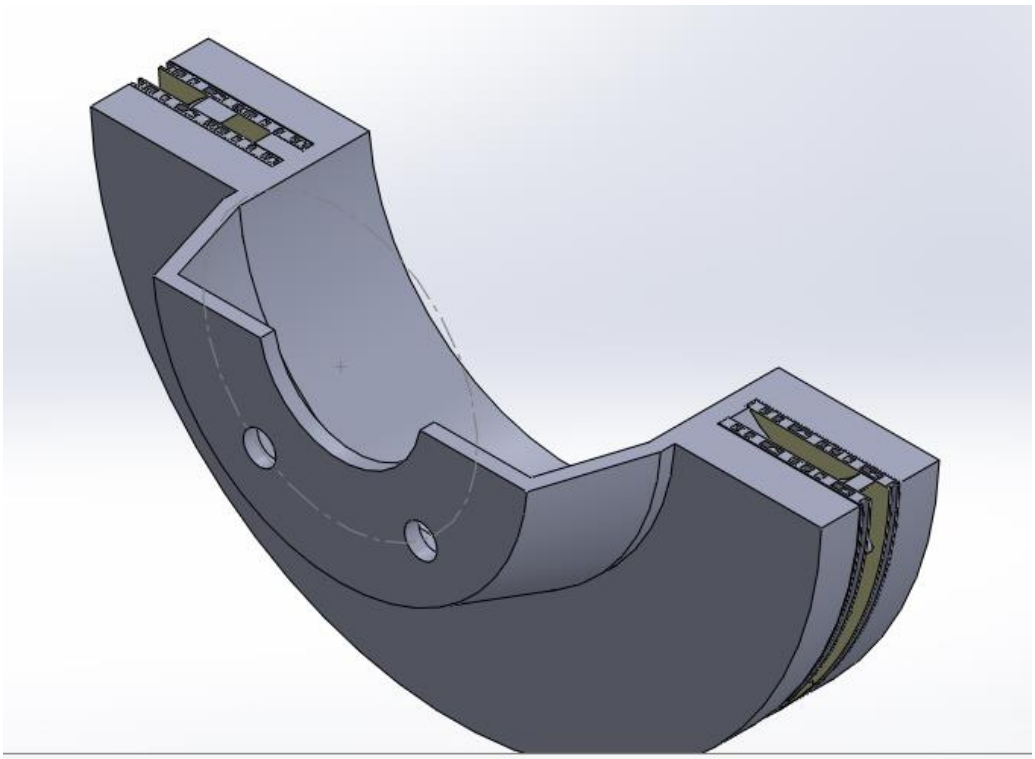

Figure 25: Sectioned disc TEG assembly to show details

4.6.2 Modeling and simulation using ANSYS

ANSYS Multiphysics software is a finite element analysis (FEM) software used to simulate engineering problems. The software creates simulated computer models of structures, electronics, or machine components to simulate strength, toughness, elasticity, temperature distribution, electromagnetism, fluid flow, and other attributes. ANSYS is used to determine how a product will function with different specifications, without building test products or conducting crash tests. Most Ansys simulations are performed using the Ansys Workbench software, which is one of the main products. Typically, ANSYS users break down larger structures into small components that are each modeled and tested individually. Finally, the Ansys software simulates and analyzes movement, fatigue, fractures, fluid flow, temperature distribution, electromagnetic efficiency, and other effects over time.

ANSYS simulation enables high-resolution modeling of thermoelectric devices also. Through this capability, users can determine the resulting temperature distribution, power, coefficient of

performance, and more when considering thermoelectric effects. A brief overview of the thermoelectric phenomena can be simulated.

ANSYS users have several software options to solve for thermoelectric cooling or generation using Mechanical, AIM, and IcePak. A Steady-State Thermal-Electric Conduction analysis in ANSYS Mechanical allows for a simultaneous solution of thermal and electric fields. This coupled-field capability models joule heating for resistive materials and contact electric conductance as well as Seebeck, Peltier, and Thomson effects for thermoelectricity. ANSYS AIM offers a quick and easy platform for designers to solve multiple physics. AIM features an intuitive graphical user interface and wizard-driven workflow. AIM includes direct current electric conduction analysis, so that current distribution, power loss and voltage drop of product designs can be determined. AIM's many options for multi-physics simulation include fully coupled thermoelectric–stress analysis, which allows power loss to be used as a heat source to compute temperatures and subsequent thermal deformation and stress of product designs. ANSYS IcePak is a vertical application for fluid-thermal analysis of electronics enclosures. IcePak offers a custom interface menu to build a thermoelectric module by specifying: orientation, dimensions, current, and materials (from a library).

In this case, for the brake disc heat simulation, we chose to use ANSYS workbench to do the simulation. Also, we choose to use ANSYS workbench (mechanical) to simulate the TEG for reasons of being conversant with the software and also being able to get all the required solutions from it.

Below are the values used in the simulations;

Table 7: Brake disc heat simulation input parameters

Disc material	Brake application time	Surface temperature
ASTM 40 Grey cast iron	6.5s	260 ^{0}C

Table 8: Brake disc material properties [60]

Grey cast iron ASTM 40				
Chemical composition: C=2.7-4%, Mn=0.8%, Si=1.8-3%, S=0.07% max, P=0.2% max				
Property	Value in metric unit		Value in US unit	
Density	7.06 *10^3-7.34	kg/m^3	441-458	lb/ft^3
Modulus of elasticity	124	GPa	18000	ksi
Thermal expansion (20 ºC)	$9.0*10^{-6}$	$ºC^{-1}$	$5.0*10^{-6}$	in/(in* ºF)
Specific heat capacity (25 ºC)	490	J/(kg*K)	0.117	BTU/(lb*ºF)
Thermal conductivity	53.3	W/(m*K)	370	$BTU*in/(hr*ft^2*ºF)$
Electric resistivity	$1.1*10^{-7}$	Ohm*m	$1.1*10^{-5}$	Ohm*cm
Tensile strength	276	MPa	40000	psi
Elongation	1	%	1	%
Shear strength	400	MPa	58000	psi
Compressive yield strength	Min. 827	MPa	Min.	psi
Fatigue strength	138	MPa	20000	psi
Hardness (Brinell)	180-302	HB	180-302	HB
Wear resistance	Low			
Corrosion resistance	Low			
Weldability	Low			
Machinability	Good			
Castability	High			

Table 9: Material properties of materials used in the simulation[61]

P-type semiconductor	Thermal Conductivity	1.5 W m^-1 C^-1
	Seebeck Coefficient	1.79e-004 V C^-1
	Resistivity	1.64e-005 ohm m
N-type semiconductor	Thermal Conductivity	1.5 W m^-1 C^-1
	Seebeck Coefficient	-1.87e-004 V C^-1
	Resistivity	1.64e-005 ohm m
Copper alloy	Density	8300 kg m^-3
	Coefficient of Thermal Expansion	1.8e-005 C^-1
	Specific Heat	385 J kg^-1 C^-1
	Thermal Conductivity	401 W m^-1 C^-1

Table 10: Parameters used in the first simulation

Type	Temperature		Voltage		Convection
Magnitude	160. °C (ramped)	22. °C (ramped)	0.1 V (ramped)	0. V (ramped)	1.e-006 W/m²·°C (ramped) at 22 °C

Table 11: Properties of Germanium Telluride

P-type semiconductor	Thermal Conductivity	1.2 W m^-1 C^-1
	Seebeck Coefficient	2.0e-004 V C^-1
	Resistivity	6e-005 ohm m
N-type semiconductor	Thermal Conductivity	1.2 W m^-1 C^-1
	Seebeck Coefficient	-2.0e-004 V C^-1
	Resistivity	6e-005 ohm m

5. CHAPTER FIVE

5.0 Results and analysis

This chapter shows the results attained from the design and the simulation and elaborating with explanations of the reasons for the results. The effects of increasing different parameters (including TE leg size, voltage, current) to the power generated and point of failure of TE material while in operation. It also holds a section where the power generated (harvested) by the TEG is compared to the energy lost to the atmosphere during braking and a percentage recovery calculated.

5.1 Brake disc heat simulation

As per the Addis Ababa LRT document, [57] the brake disc which weighs about 25 kg is made up of ASTM gray cast iron material. The friction plates of the discs get into contact with brake pads (sintered material) with a brake force to allow speed reduction. The speed reduction comes about by converting the kinetic energy of the vehicle at that instant into heat energy as per the first law of thermodynamics. The friction which causes heat energy concurrently causes the temperature to build up in the brake disc. Kumella [13] carried out a study that confirmed that the maximum temperature got by the brake disc during the braking of the vehicles of AALRT was 265 ^{0}C after a braking distance of 22 m in 6.5 seconds. Using this temperature 265 ^{0}C as an input on the friction plate surface, a transient thermal heat simulation was done in ANSYS workbench as shown below;

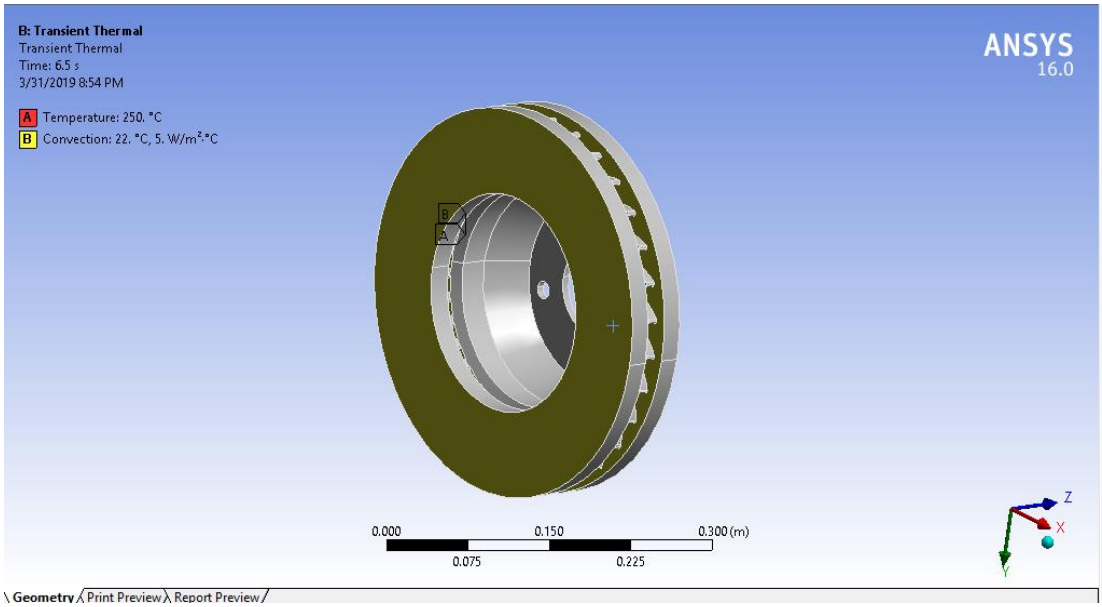

Figure 26: Brake heat simulation inputs

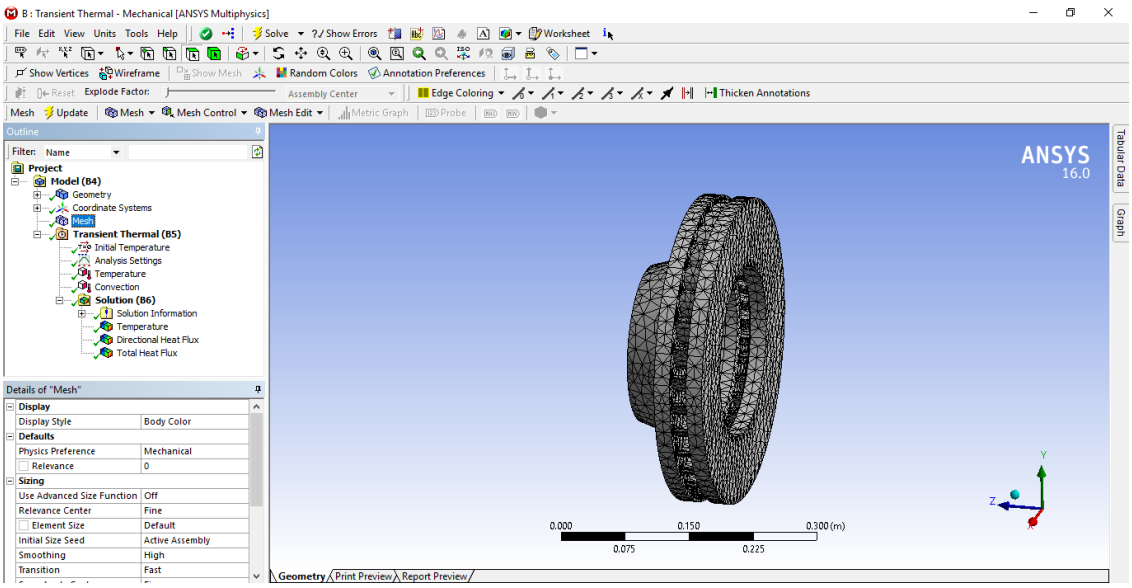

Figure 27: Meshed disc

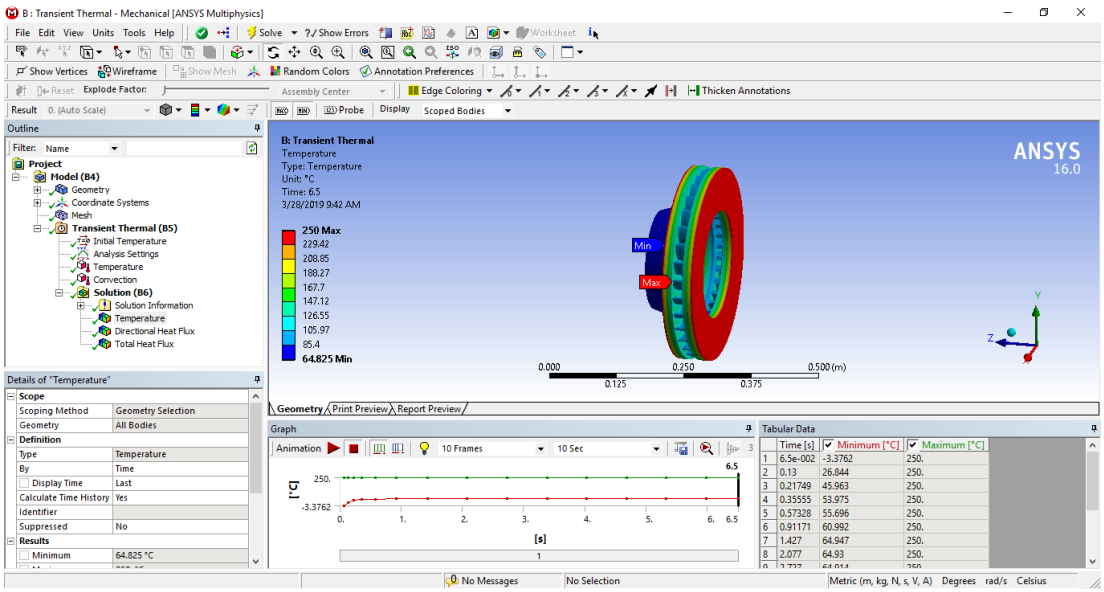

Figure 28: Temperature results from simulation

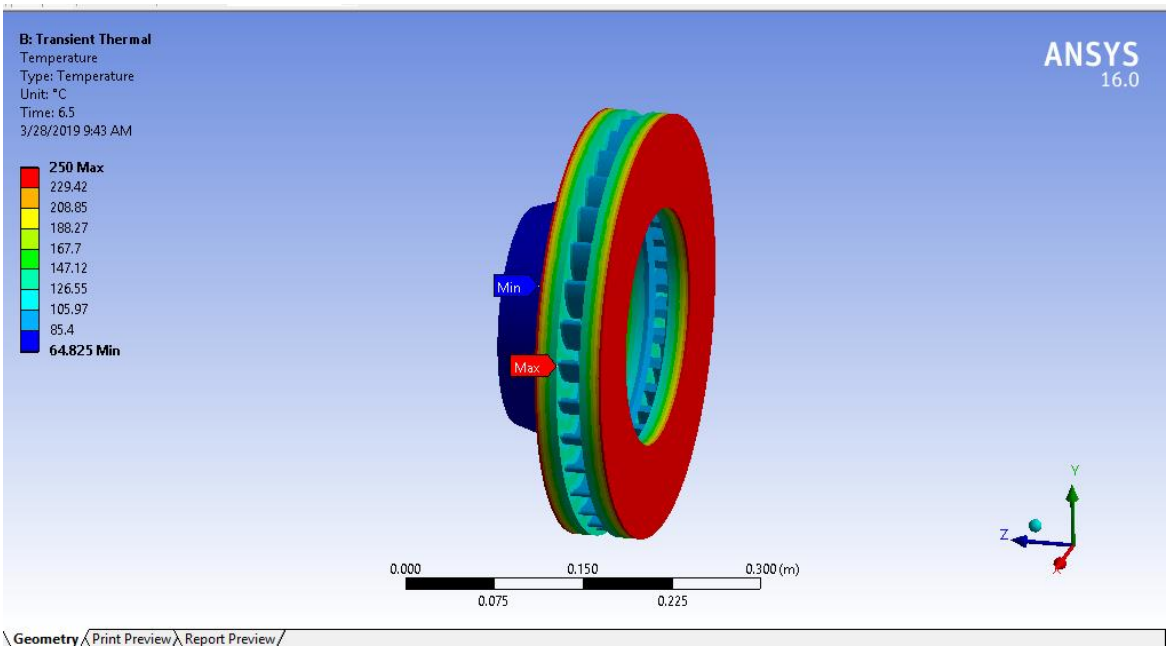

Figure 29: Inside temperature of friction plate at 167 ^{0}C

The results above verify that there can be some energy harvested from the brake disc friction plate component due to the high enough temperature (167 ^{0}C) on the inside of the friction plates. For this matter, there needs to be space for the TEG devices between the friction plates and the

cooling fins. A small modification on the brake disc was made and a second design was made with the required space; large enough to carry the 5mm TEG leg height. The hot junction side was put in contact with the hot surface and the cold junction put in contact with the cooling fins to aid in the quick drawing of heat from the system.

5.2 Simulation of the simplified brake disc

After the simulation of the disc, another similar simulation on the simplified disc was carried out to check for the inner friction plate temperature in the design. It was carried out and below are the processes;

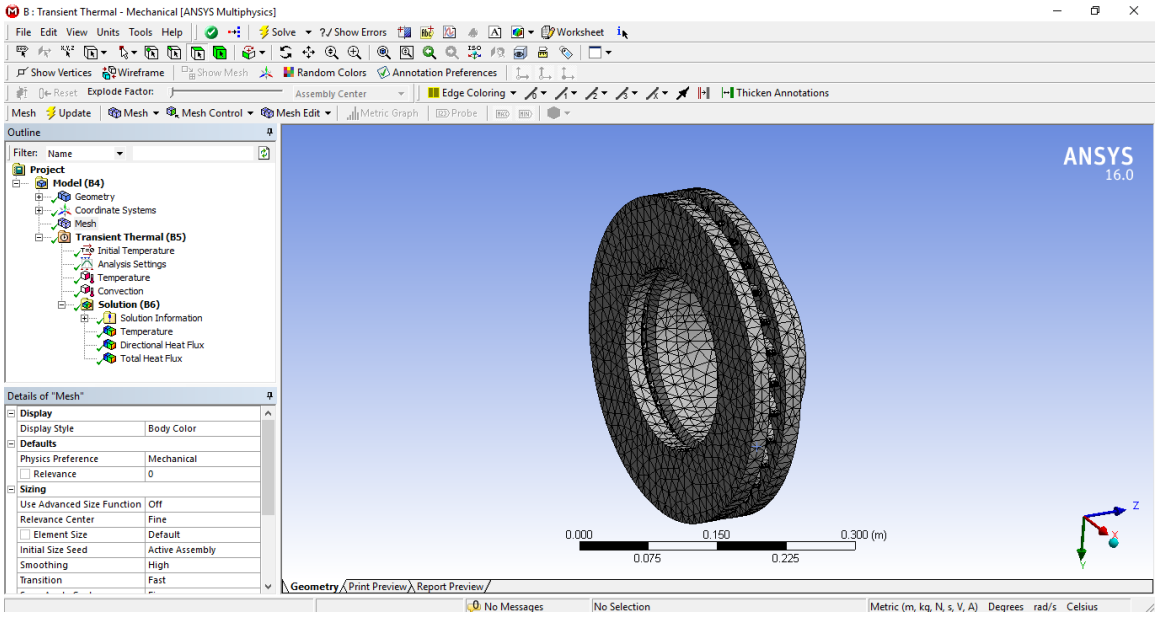

Figure 30: Simplified brake disc with mesh

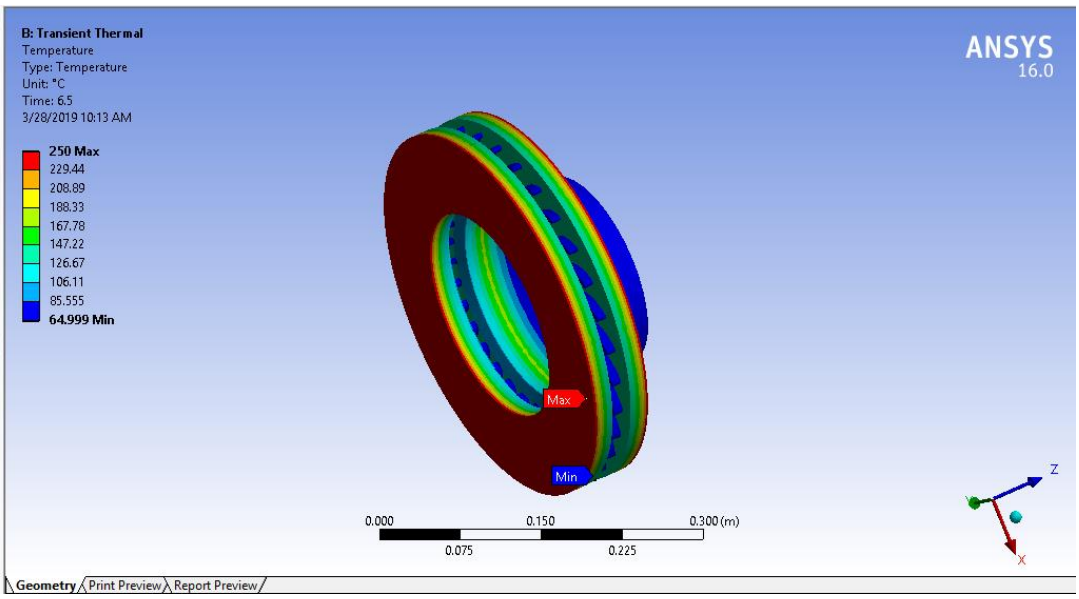

Figure 31: Temperature results of modified disc

From the simulation, the friction plate inside temperature which also doubles as the TEG hot junction input temperature was found to be 167 ^{0}C. This temperature is high enough to be used as an input in a TEG. Since the temperature is in the range of low heat, bismuth telluride was chosen to be used as the TE material in the device. The cooling fins which are always in touch with the ambient work as the cold end junction end, to be able to cause a temperature difference across the device.

5.3 Repeated braking simulation

During operation of the train, there is braking that occurs at every station. The process of braking causes the brake disc to heat up, temperature increases and then after it has come to a halt, the disc cools. This process continues for each and every station in a trip. From the concept of repeated braking, heat simulations were done in ANSYS workbench mechanical to find out how the brake disc temperature builds up every after a braking session. The heat flux was an input for the simulation that ran for a braking time of 6.5 S, whereas on the other side, cooling occurs by convection both during braking and after braking, although after braking, it is entirely cooling by convection. The simulation produced results that were plotted in the figure below to show the heating and cooling of the brake disc throughout the line. From the results got, an average temperature for the disc throughout the trip is calculated and found to be 261.5 ^{0}C

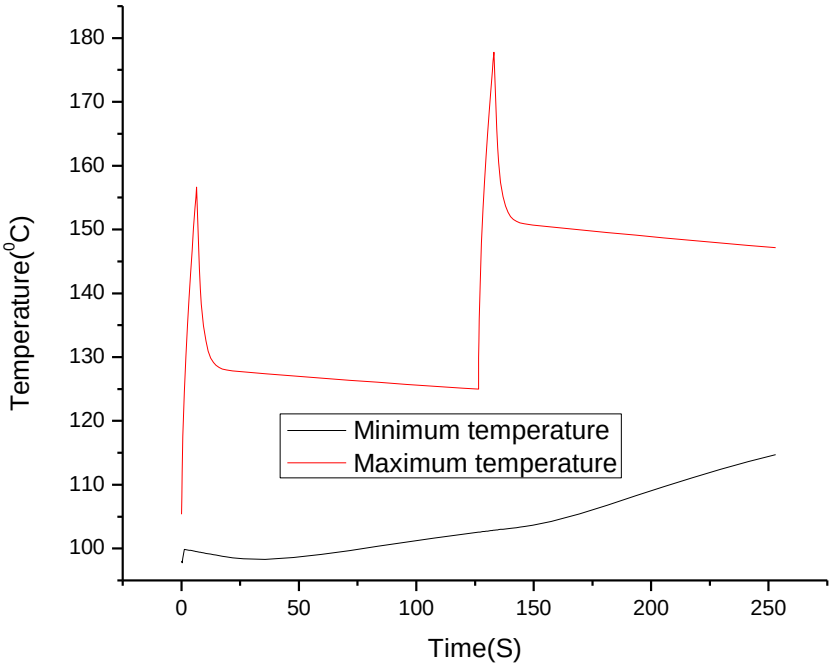

Figure 32: The heating and cooling for the first two stations

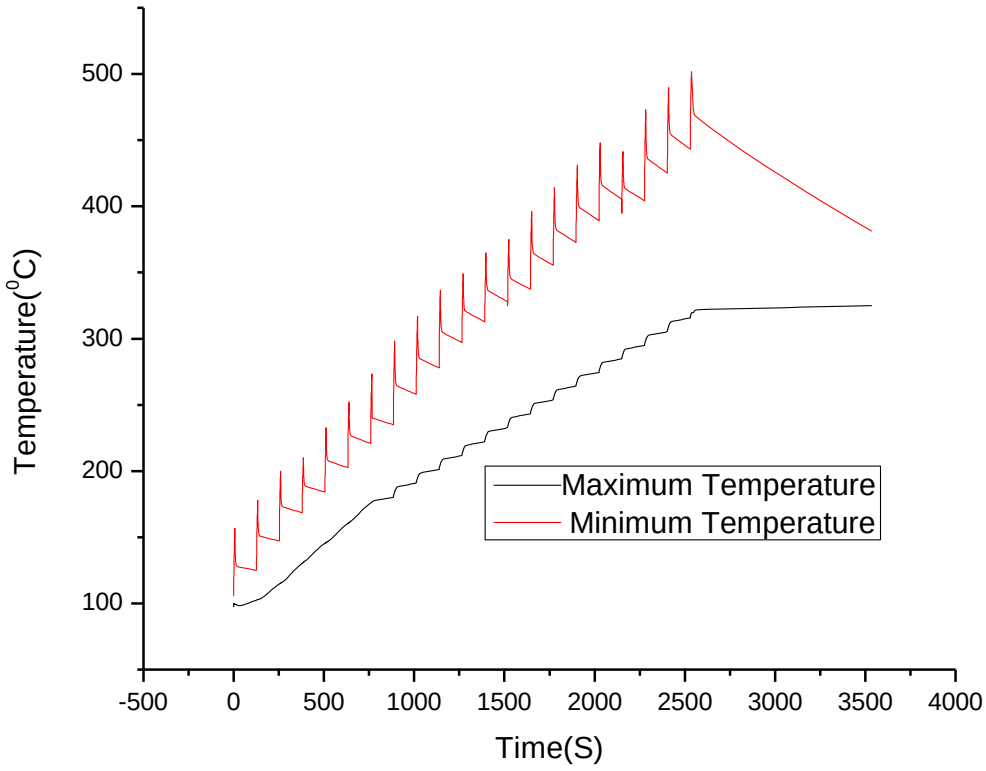

Figure 33: Graph of temperature of the brake disc vs time during the travel of the train along a line

5.4 Simulation of the Thermoelectric legs

The thermoelectric simulation was done in ANSYS workbench mechanical with a single pair of legs (p-type and n-type leg). We use a single pair of legs since the whole system is a repetitive one with the same unit multiple times. This means that just a single pair can be used in the simulation and later calculations done to see the overall output. The material properties and model used are shown below;

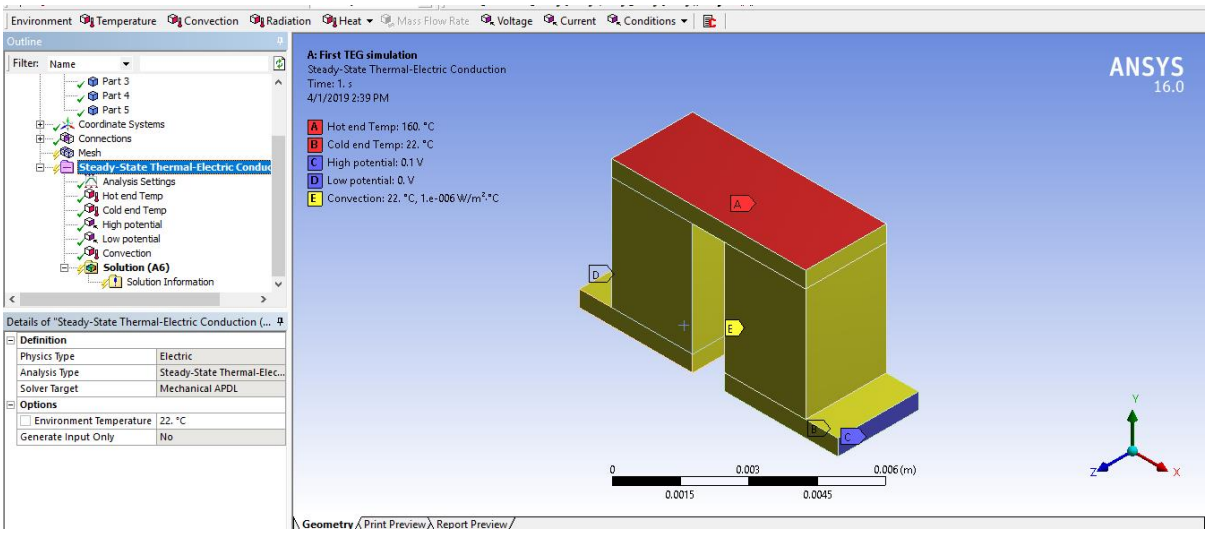

Figure 34: TEG pair of leg with some input parameters and boundary conditions

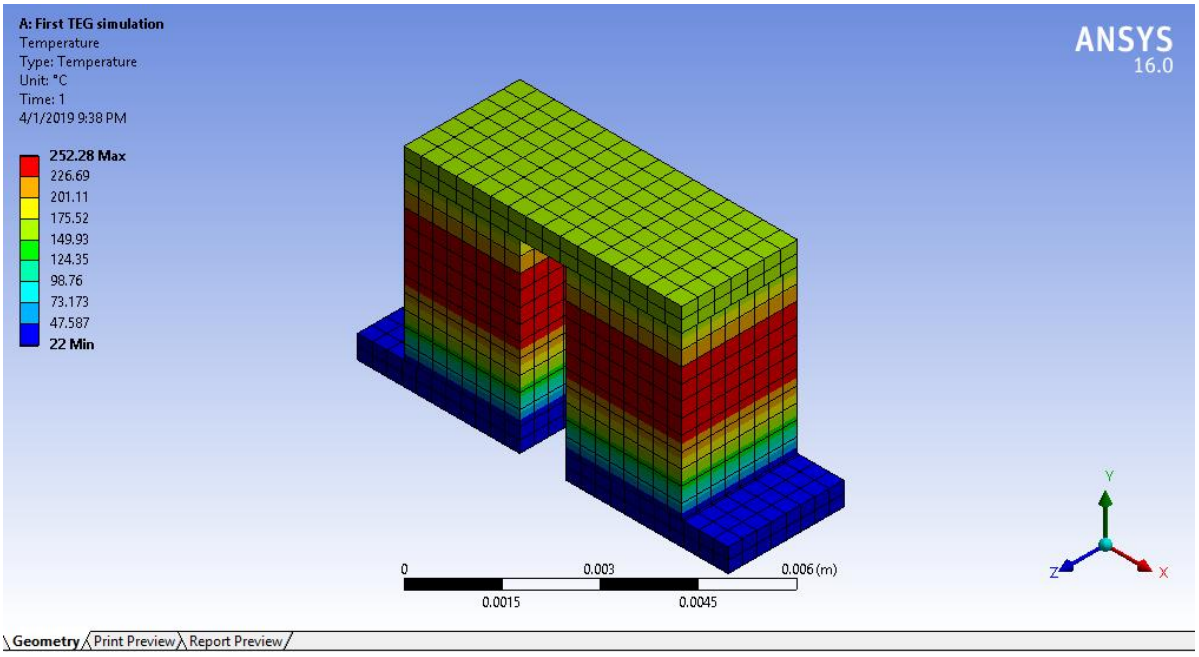

Figure 35: The temperature contours result from the simulation

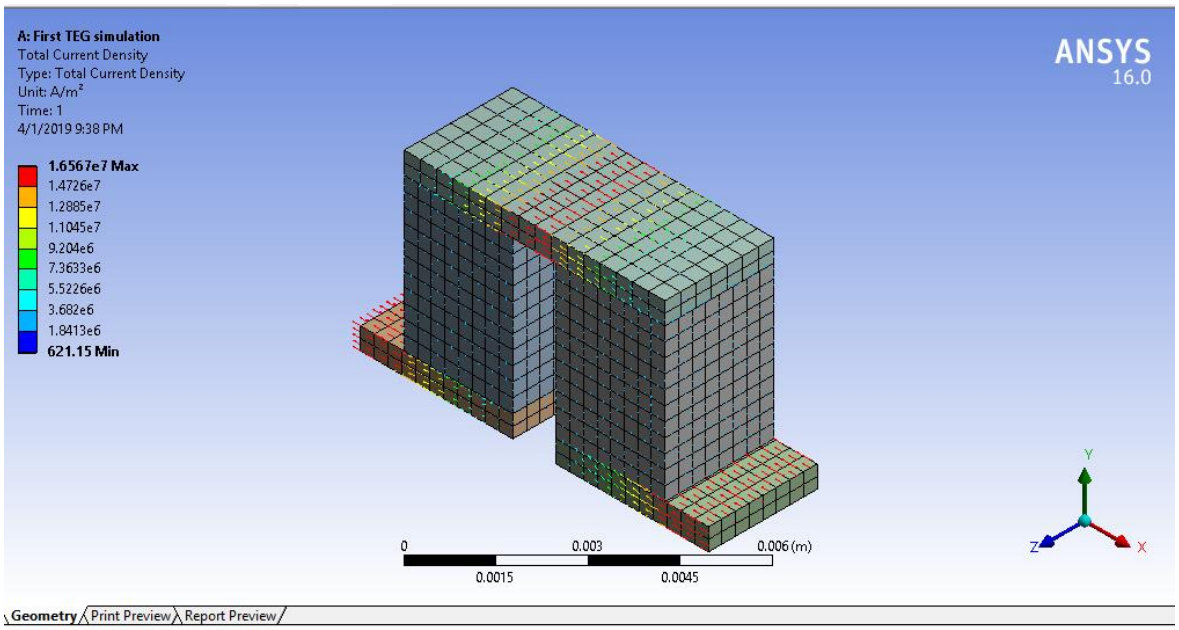

Figure 36: TEG current density

To obtain the right range of voltage to use for the simulations, a random range from 0.08-1 V was used and an observation made to that effect. A few aspects of the properties of the TE material, the power generated, the heat absorbed and others were keenly observed and some points were drawn. Below is a sample of the TEG pair legs simulation with the mentioned voltage range.

Table 12: Parameter changes with a change in voltage

Voltage (V)	Current (A)	Power generated (W)	Heat absorbed at the hot junction (W)	Maximum Temperature of TE (^{0}C)
0.08	1.5988	0.127904	0.46142	160
0.09	2.14	0.1926	0.55692	160
0.1	2.6812	0.26812	0.27702	160
0.2	8.0931	1.61862	1.1485	160.12
0.3	13.505	4.0515	3.0861	184.66
0.4	18.917	7.5668	5.5657	254.28
0.5	24.329	12.1645	8.5875	349.53
0.6	29.74	17.844	12.152	474.19
0.7	35.152	24.6064	16.259	623.83
0.8	40.564	32.4512	20.91	798.42
0.9	41.3784	37.24056	26.103	999.07
1	51.3784	51.3784	31.841	1225.4

From the graph above, it is observed that current flowing increases with an increase in voltage and so does the power generated. The heat absorbed at the hot junction and the maximum temperature in the TEG also increase with an increase in voltage. Since the power generated by the TEG must be a portion of the heats absorbed at the hot junction, we see more power generated than there actually is in a real sense which is an anomaly. This happens because of the temperature that builds up in the TE material and thus increases the current flowing since current flow increases with temperature as the electron mobility increases. So, the power generation that is our main concern here is only viable for values of power generated lower than the heat absorbed at hot junction. On the other hand, the TE material temperature also increases in the process. The increase in temperature of the TE material is a limiting factor too since there is a temperature at which the material loses its properties and later disintegrates [24] rendering the device useless.

So, having considered all these aspects, a decision was taken to run the simulations with voltages that are lower than 1.5 V because these showed values of temperature that could not increase the temperature of the device (which damages it and also causes need for more cooling in the device) and close values of power generated and heat absorbed at hot junction. This verifies what was mentioned by Twaha et al [62] that TEG pairs operate effectively at low voltages.

With the chosen voltage values, simulations were run and the detailed values are attached as appendices. Below, some of the results are presented with explanations given for some phenomena observed.

It is observed from the plotted I-V graph that current increases with increase in voltage. They are directly proportional in the power generation as mentioned by Jaegle [63].

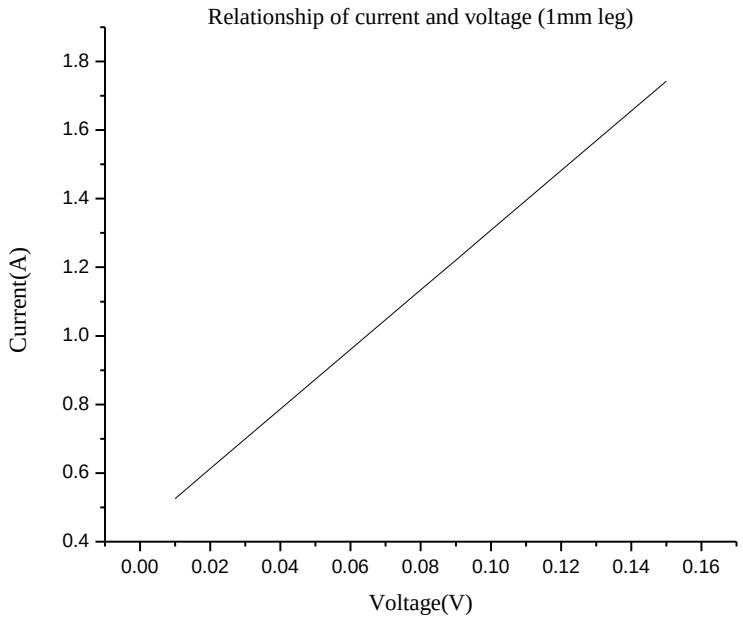

Figure 37: Relationship of current with the change in voltage

The current increases linearly with the voltage as seen in the graph. Similarly, the power generated increases with current, since $power = current\ X\ voltage$.

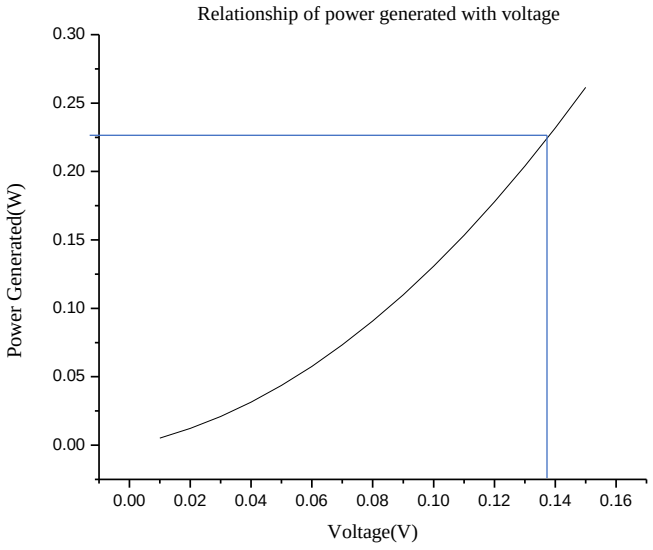

Figure 38: Relationship of the power generated with change in the voltage

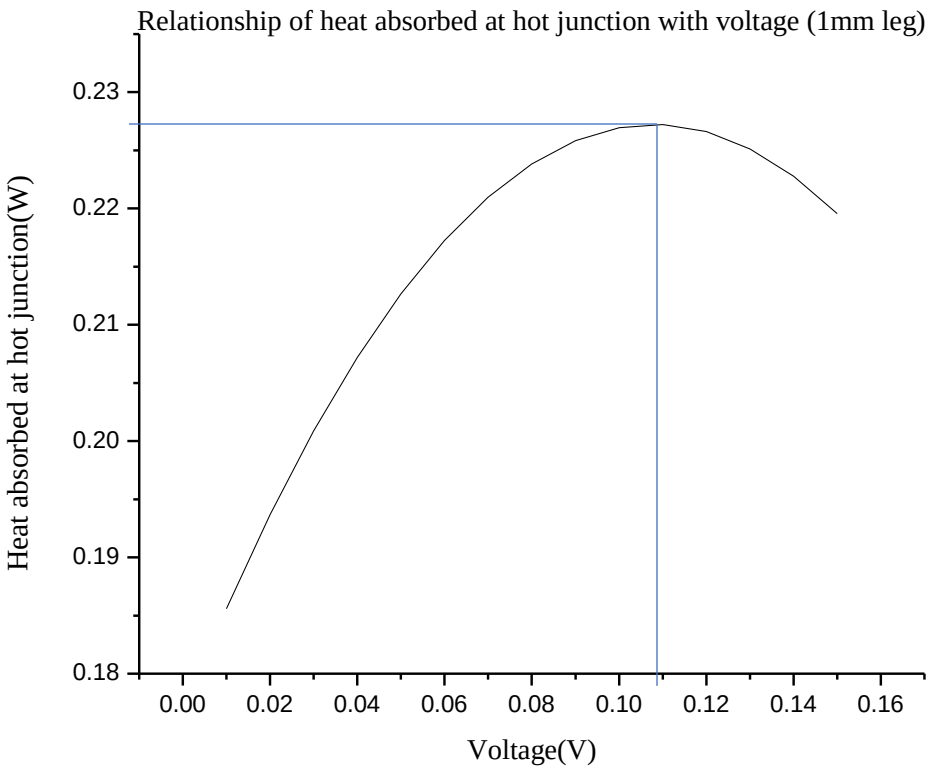

Figure 39: Relationship of heat absorbed at the hot junction with the change in voltage

From the plotted graph, the heat absorbed at the hot junction increases exponentially with an increase in input voltage across the TEG pair and then reduces after hitting a maximum value. Heat absorbed at the hot junction is the heat that is available to run the TEG for power generation. It also is the limiting factor on how much energy can be generated from a TEG since it cannot be created nor destroyed. The maximum heat absorbed from the graph is 0.227 W per TEG leg and this happens at voltage of 0.109 V.

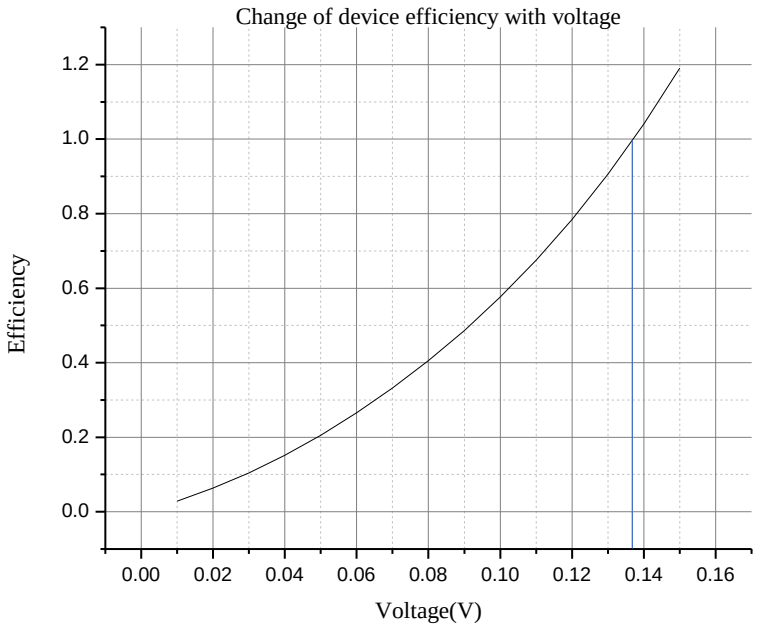

Figure 40: Change of device efficiency with voltage

The figure illustrates that the device efficiency increases with increase in voltage. The more the voltage the more the capacity of the electrons to carry the heat across the device. The highest efficiency is achieved at a point where the efficiency is 1. This occurs at a voltage of 0.137 V.

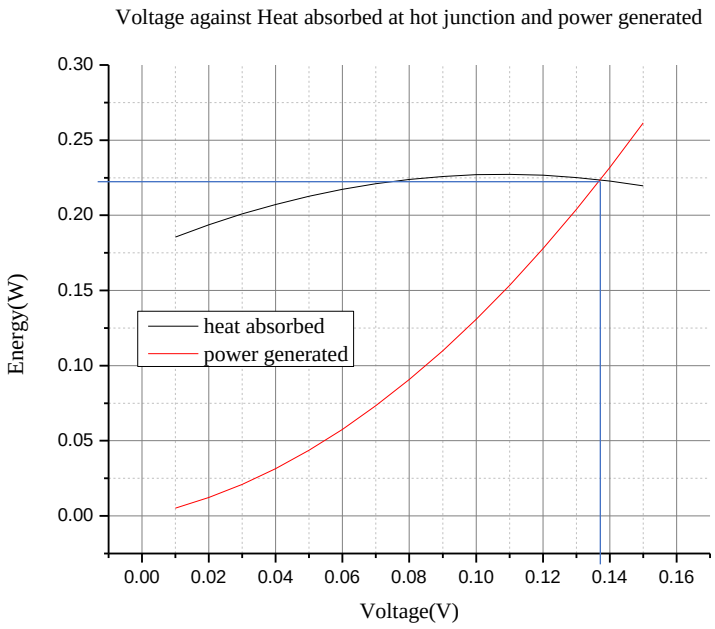

Figure 41: Heat absorbed, power generated by TEG changes with voltage

The maximum energy that can be generated is the heat absorbed at the hot junction as explained in figure (31). This curve increases from a minimum value up to a maximum and then reduces as the voltage increases. Likewise, the power that is generated increases with voltage as shown in the plot. The maximum power that can be generated is achieved when the two curves intersect. The intersection happens at a 0.137 V point which has a power generated and heat absorbed at 0.223655 W for a 1mm TEG leg. This is evidenced in all the cases of different TEG leg sizes. So, the maximum power that can be generated in all cases is at that same value.

In this study, we use the 0.13 V as our input voltage, since it is the value that gives an efficiency closest to 1 from the simulation data herein.

Table 13: Size of leg with 0.13 V input with responding power generated

Size of the leg, ω (mm)	Voltage (V)	Current (A)	Heat absorbed (W)	Power generated (W)	Number of legs, N	Power in the sector (W)
1	0.13	1.569	0.22513	0.20397	2654	270.6682
1.25	0.13	2.4503	0.35187	0.318539	2098	334.1474
1.5	0.13	3.5265	0.50661	0.458445	1698	389.2198
1.75	0.13	4.797	0.68881	0.62361	1404	437.7742
2	0.13	6.2615	0.9003	0.813995	1178	479.4431
2.25	0.13	7.9191	1.1392	1.029483	1004	516.8005
2.5	0.13	9.7661	1.4043	1.269593	866	549.7338
2.75	0.13	11.802	1.6986	1.53426	754	578.416
3	0.13	14.032	2.0205	1.82416	662	603.797
3.25	0.13	16.458	2.3698	2.13954	586	626.8852
3.5	0.13	19.08	2.7469	2.4804	522	647.3844
5	0.13	38.636	5.5853	5.02268	292	733.3113

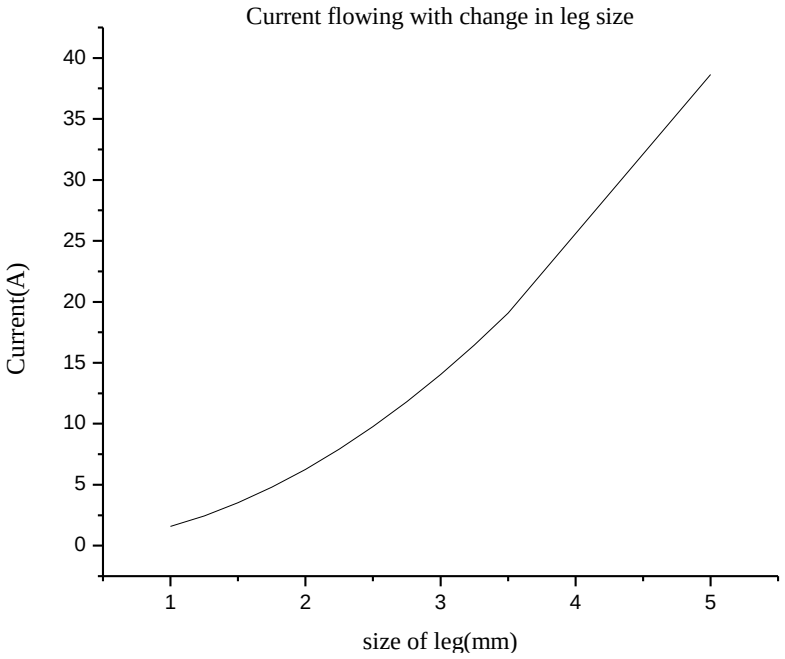

Figure 42: Relationship between current flowing with a change in the size of the leg

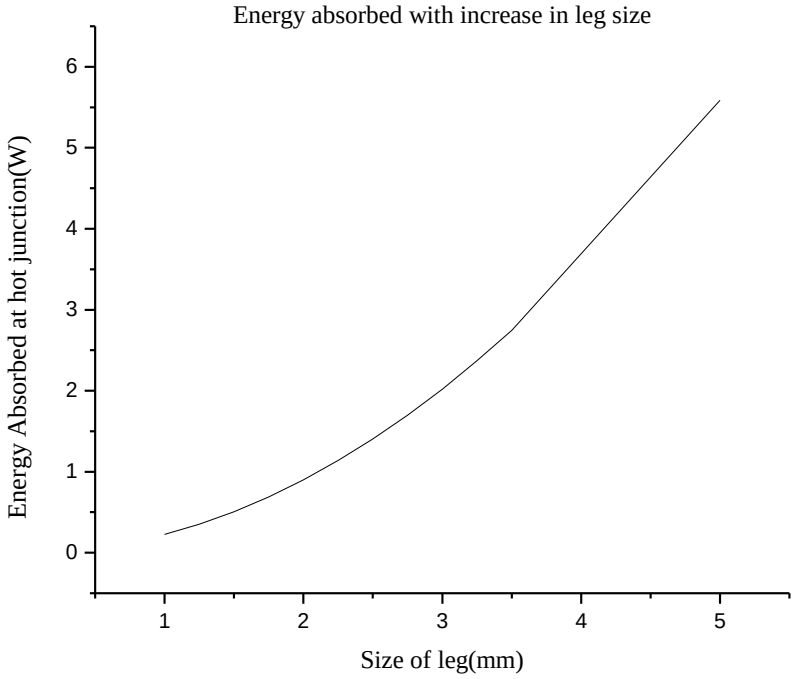

Figure 43: Relationship of heat absorbed with the change in the size of the leg

From figures (34) and (35), relationship of the size of the leg influence on current flowing and heat absorbed at the hot junction are illustrated respectively. From the plots, it shows that the bigger the size of the leg, the bigger the current that flows (in line with Ohm's law) and the more the heat absorbed at the hot junction. Since the amount of heat absorbed is a limiting

factor for the power that can be generated, (also power generated is got by the product between current flowing and voltage across the device), there ought to be more heat absorbed so as to allow for more power generated. This can be realised by increasing the size of the leg, the bigger the size of the leg, the more the power generated.

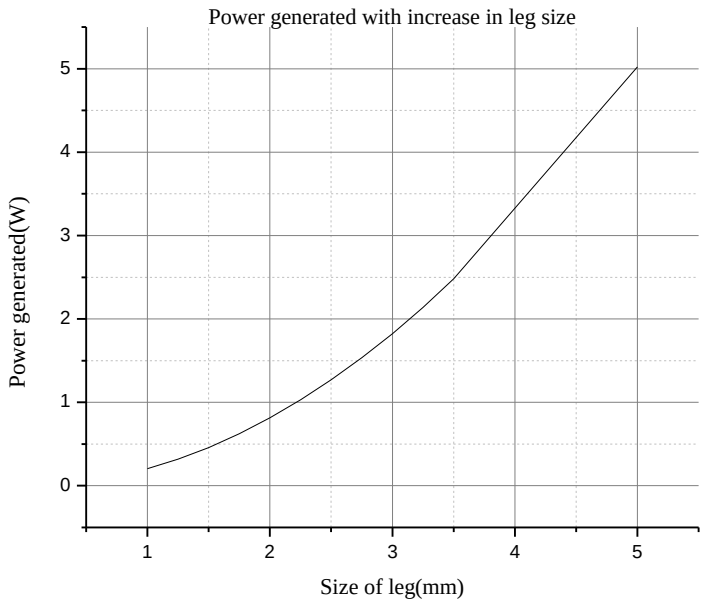

Figure 44: Relationship of power generated with the size of the leg

As explained from the above figures (34) and (35), power generated increases with the size of the leg. In figure (36), the point is further illustrated in relation to the concept of area covered by the legs. With a known fill factor (which explains how much area is covered by TE material) the number of legs in that particular area can be calculated and the power generated per area is got also. This one is got by multiplying the current flowing through the legs times the voltage across each leg times the number of legs (since they are serially connected, the voltages build up as the leg numbers increase).

Simulation results of GeTe

GeTe was chosen for this simulation due to its ability to hold the temperature and its recovery at this temperature. It has a high ZT in this temperature range, so it will be able to perform the job. Just like the other simulations, this too was done in ANSY workbench mechanical in the thermal electric section. Since it has already been confirmed that the 3.5mm leg TEG gives off enough power with a good packing factor, it is the only one that was simulated and the results are as follows;

Table 14: GeTe TEG simulation with the 261.5 ^{0}C temperature input

Voltage (V)	Current (A)	Heat absorbed at hot junction
0.01	10.217	3.8691
0.02	11.085	3.9669
0.03	11.953	4.0603
0.04	12.821	4.1451
0.05	13.690	4.2212
0.06	14.558	4.2887
0.07	15.426	4.3474
0.08	16.294	4.3975
0.09	17.162	4.4389
0.10	18.030	4.4716
0.11	18.899	4.4956
0.12	19.767	4.511
0.13	20.635	4.5176
0.14	21.503	4.5156
0.15	22.371	4.505

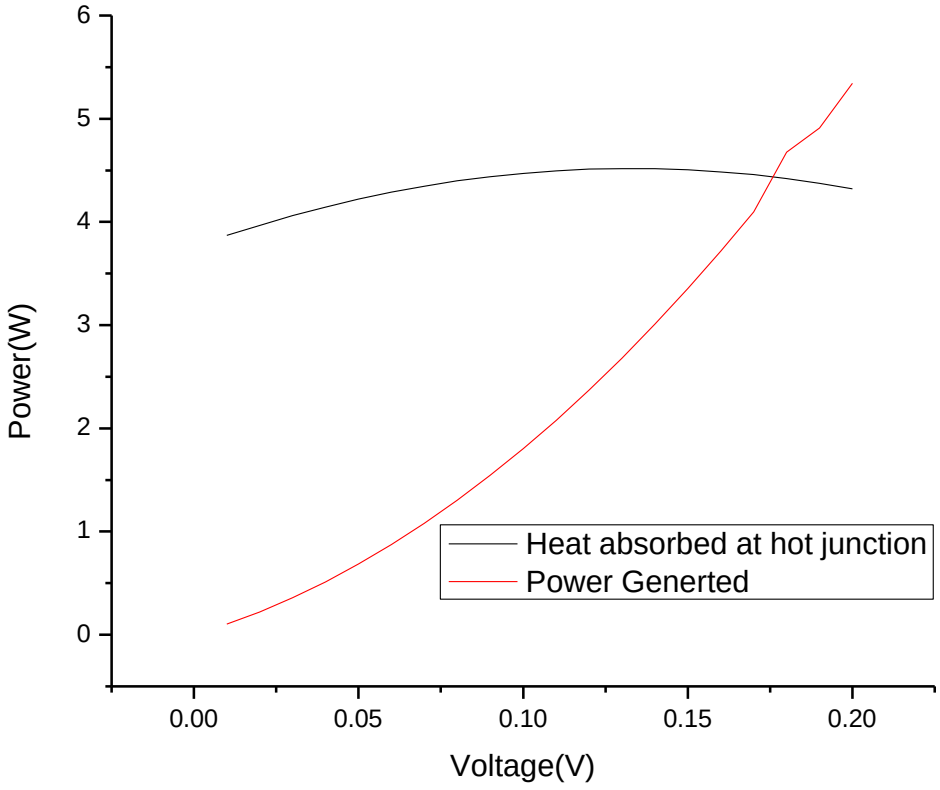

Figure 45: Heat absorbed and Power generated with voltage for a 3.5mm GeTe device

5.4 Energy harvested

From the results above, the voltage value of 0.13V is the highest value that produces a great amount of power closest to the maximum possible extractable energy (close to the intersection of Heat absorbed and Power generated). Even though the relationship of packing factor and power generated is positively proportional, we cannot choose a packing factor of 1 since the TE material is expensive and we have to take care of the cost per watt of power generated. So as stated by Montecucco [45], the best packing factor lies between 0.45-0.65, hence we choose the packing factor of 0.603 which is for a leg size of 3.5mm

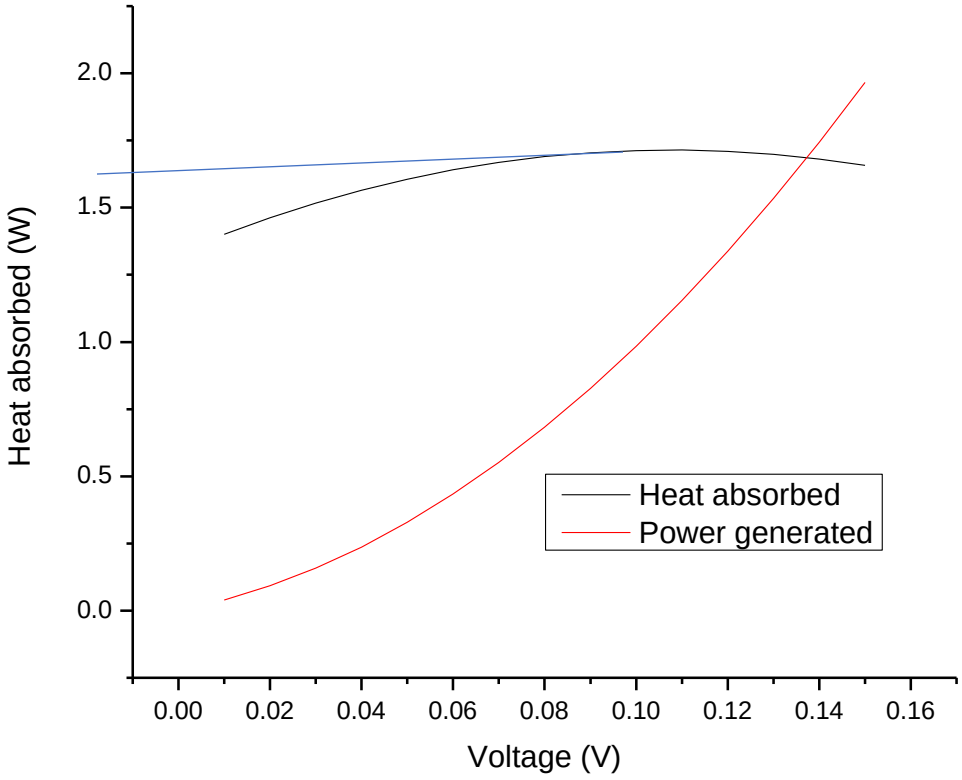

Figure 46: A plot of heat absorbed and power generated with voltage for a 3.5 mm leg TEG

From the figure 40, we show the power generated and heat absorbed at the hot junction for the chosen leg size of 3.5 mm. Where the plots intersect is our optimal point and it is at a voltage of 0.1375 V and a power of 1.6935 W. The maximum heat absorbed at thot junction is 1.7 W which is just almost equal to 1.6935 W that is at the intersection.

Calculations

Number of TEG legs N = 522

Size of TEG leg ω = 3.5 mm

Voltage across TEG legs V = 0.13 V

Current flowing through TEG device I = 19.08 A

Heat absorbed at the hot junction = 2.7469 W

The power generated by TEG pair P = 2.4804 W

The power generated in the sector of TEG = 647.3844 W

The conversion efficiency of the TEG pair

$$\eta_{Thermodynamic} = \frac{Power\ delivered}{Heat\ absorbed\ at\ hot\ junction} = \frac{W_e}{Q_h}$$

$$\eta_{Thermodynamic} = \frac{2.4804}{2.7469} = 0.903$$

$$\eta_{Thermodynamic} = 90.3\%$$

The power generated in full TEG

$$P_{teg} = power\ generated\ in\ TEG\ sector * 6$$

$$P_{teg} = 647.3844 * 6 = 3{,}884.3064\ W$$

Power generated per disc

$$P_D = P_{teg} * 2 = 7{,}768.6128\ W$$

Total power generated per vehicle

$$P_{total} = P_D * 8 = 62{,}148.89\ W$$

$$F_D = 264.056x10^3\ W$$

Percentage of energy recovered (simulation)

$$\eta_{Conversion} = \frac{P_D}{F_D} = \frac{7{,}768.6128}{264.056x10^3} = 0.0294$$

$$\eta_{Recovery} = 2.94\%$$

5.5 Mathematical model

The efficiency of a TEG is based on the material that the generator is made up of; the operating temperatures of the device and heat exchangers too. In this study, we chose Bismuth Telluride as the TE material. Below are the parameters used in the model and the efficiency got from the mathematical model.

$$Z = \frac{\alpha^2 \sigma}{K}$$

$$Z = \frac{(1.79 * 10^{-4})^2 * 1.1 * 10^5}{1.5} = 2.35 * 10^{-3}$$

$$T_c = 22\ ^0C = 295.13\ K$$

$$T_H = 160\ ^0C = 433.13K$$

Using the equation below, we calculate the TEG maximum power efficiency;

$$\eta_{mp} = \frac{1 - \frac{T_c}{T_h}}{2 - \frac{1}{2}\left(1 - \frac{T_c}{T_h}\right) + \frac{4\frac{T_c}{T_h}}{ZT_c}}$$

$$\eta_{mp} = \frac{1 - \frac{295.13}{433.13}}{2 - \frac{1}{2}\left(1 - \frac{295.13}{433.13}\right) + \frac{4 * \frac{295.13}{433.13}}{2.35 * 10^{-3} * 295.13}}$$

$$\eta_{mp} = 0.0419 = 4.19\%$$

So, the efficiency of the device is given as;

$$\eta_{TEG} = \eta_{mp} x \eta_{Thermodynamic}$$

$$\eta_{TEG} = 0.0419 x 0.903 = 0.0378$$

$$\eta_{TEG} = 3.78\%$$

The efficiencies got in both cases; by simulation and by the mathematical model are really close, 2.94% and 3.78% respectively. There is a difference in the efficiencies all emanating from the fact that the mathematical model does not account for the energy that is lost to the

environment by convection as it assumes that all the heat energy on the hot end is transferred to the cold end fully without any loss. The simulation too doesn't give the actual results since the results are an estimate just close to the right value. In relation to figure (9), [4,7] the graph shows the range of efficiencies and different temperature gradient with different ZT. In this case, the temperature difference we have is 140 K which lies in the 0-200 bracket and material ZT is 1. The efficiency of such a case is about 5% which is close to the efficiency attained in this thesis.

5.6 Energy harvested

Since in actual operation, the temperature is not constant, repeated braking simulations were done and the temperature observed how it increases after every single braking. The average temperature of the disc throughout the trip was found to be 261.5 ^{0}C. This temperature happens to be out of range of the previously used bismuth telluride, and falls in the range where germanium telluride works best, so germanium telluride was used in the TEG simulations. GeTe, a material with a high ZT value and gives a good TEG recovery efficiency. In order to find out how much energy is harvested, the same calculation as in the previous case were done and the solution is as follows;

Calculations

Number of TEG legs N = 522

Size of TEG leg ω = 3.5 mm

Voltage across TEG legs V = 0.17 V

Current flowing through TEG device I = 24.107 A

Heat absorbed at the hot junction = 4.4576 W

The power generated by TEG pair P = 4.09819 W

The power generated in the sector of TEG = 1069.62 W

The conversion efficiency of the TEG pair

$$\eta_{Thermodynamic} = \frac{Power\ delivered}{Heat\ absorbed\ at\ hot\ junction} = \frac{W_e}{Q_h}$$

$$\eta_{Thermodynamic} = \frac{4.09819}{4.4576} = 0.9194$$

$$\eta_{Thermodynamic} = 91.94\%$$

The power generated in full TEG

$$P_{teg} = power\ generated\ in\ TEG\ sector * 6$$

$$P_{teg} = 1069.62\ * 6 = 6{,}417.72\ W$$

Power generated per disc

$$P_D = \ P_{teg} * 2 = 12{,}835.44\ W$$

Total power generated per vehicle

$$P_{total} = P_D * 8 = 102.683.52\ kW$$

Average Q_D =258116.693W per braking process per disc

Percentage of energy recovered (simulation)

$$\eta_{Conversion} = \frac{P_D}{Q_D} = \frac{12{,}835.44}{258116.693} = 0.05$$

$$\eta_{Recovery} = 5.0\%$$

With the gradient of the track considered, a high brake disc temperature is achieved, more power is generated from the TEG device but the efficiency lowers. The lowering of the efficiency is due to the fact that the rate of heat loss by convection increases with the temperature of the body. Even though the efficiency has decreased, there is more power that we harvest from the second case.

Comparison with regenerative braking recovery

When this energy is compared to that energy that is recovered by regenerative braking, the following results are attained.

Using equation (53),

$Er_l = [0.01072W_t, (V_1^2 – V_2^2) + 27.25\ GSW – 0.2778WrS] \times \eta$

the possible energy to be recovered is calculated as follows

Since regeneration can only be used up to speeds of 16 km/hr, $V_1 = 25$ km/hr and $V_2 = 16$ km/hr

Average gradient of the track G = 0.21%

Braking distance S = 21.9 m

Weight of the vehicle W = 64000 x 9.81 = 627,840 N

Train resistance r = 4 kg/tonne

Efficiency $\eta = 0.85$

Calculation;

$$E_r = [0.01072 \times 64000 \times 9.81\ (25^2 – 16^2) + 27.25 \times 0.21 \times 21.9 \times 64000 \times 9.81 – 0.2778 \times 64000 \times 9.81 \times 4 \times 21.9] \times 0.85$$

$$E_r = (2.30379 + 78.6826 – 15.2787) \times 0.85$$

$$E_r = 55.85154 \times 10^6\ Wh$$

$$\text{Energy recovered per second} = E_r/3600 = 15.514 \times 10^3$$

Regenerative braking is quite a highly efficient energy harvesting method during braking, but in this case, it is not recommended due to its limitations. Since the operating velocity of the trains on the line is as low as 25 km/hr, there is not enough kinetic energy to harvest since regenerative braking can only be used up to 16 km/hr and then another kind of braking system kicks in. The gradient of the track too is a hinderance, since it is small. Regenerative braking works perfectly for track gradients of 0.6% and above.

6. CHAPTER SIX

6.0 Conclusions and Recommendations

This chapter is divided into two components, those achieved by this study, and those that are proposed to be done by other researchers in the future. Achievements summarize the study therein, while the future works propose what should be done as per the limitations of this study.

6.1 Conclusions

Waste heat from all kinds of industries, when not captured, is useless and contributes highly to global warming. There are a lot of methods to recover the waste heat generated but herein, research was made on the thermoelectric generator for waste heat recovery of brake heat energy in the railway sector; which is viewed as a renewable energy source since braking is an action that happens from time to time. Thermoelectric power generation is a way electrical potential is generated, by the presence of temperature difference and vice versa, and this result depends on material properties of thermocouples (TE legs) and their size.

After investigating the braking process of the AALRT vehicles, it was established that the maximum surface temperature of the friction plates was 260 ^{0}C and through simulation, the hot end temperature of the TEG was found to be 160 ^{0}C. Bismuth Telluride (Be_2Te_3) was chosen as the thermoelements materials. With repeated braking, the maximum surface temperature obtained was 510 ^{0}C and calculation of the average gave 261.5 ^{0}C which was used to choose another TE material was chosen which is germanium telluride (GeTe). The design was done, including the design and modeling of a thermoelectric generator, (using the repetitive pair units as a representation). A SOLIDWORKS 3D design of the brake disc, TEG device were done and heat simulations were done in ANSYS to find the TEG input temperature. Thermoelectric simulations were also done in ANSYS to check for the power output of the TEG. ANSYS mechanical was used because it aids in easy input and output value punching and retrieval respectively as well as input changes.

The study showed that more power is absorbed at the hot junction when the voltage across the TEG leg pair is increased and when the size of the TE legs are increased. As the amount of heat energy absorbed at the hot junction increases, it hits a maximum value and then reduces, so the maximum power that can be extracted is got where the maximum power curve intersects with

the voltage-current curve. The amount of energy is recovered from the simulation is $67.214\ kW$ per vehicle; which is 2.94% of the total energy lost at single braking per unit time. In the case of repeated braking, a massive amount of $102.683\ kW$ was recovered all emanating from the fact that there was more heat flux in this case and in turn caused a high temperature of the disc. This amount yielded in either case is capable of running many of the auxiliary equipment in the train, the lights, door operations, speaker and screens among others. So instead of using the direct power from the lines to run these auxiliary components, this harvested, recovered energy can be diverted to do this job, hence saving on power. With a vehicle with maximum payload, a lot more energy can be harvested. When the result was compared with a possible regenerative braking case, it was realised that regenerative braking gave off less power due to the low operational speed and the small gradient of the track.

6.2 Recommendations

In this master thesis, design and numerical model for a thermoelectric generator were developed and a preliminary set of parametric studies were performed on this device. Nevertheless, further studies ought to be done to refine this design in order to maximize the TEG power while minimizing the system size since the design herein is also limited.

Some suggestions are mentioned and briefly described as future directions for further studies on this design.

- The recovered energy is not stable since the heat that is used to generate power is also not constant. Due to this fact, the power being generated should be conditioned and a stabilizer used to give off a stable output. Since the auxiliary system devices that are meant to be powered by this power mostly use alternating current, the direct current produced has to be inverted so as to be useful. So, a system that stabilizes this power, conditions it and sized for the rail vehicle ought to be looked at to see the power used.
- The cold sink (heat exchanger) of this model should be studied further so that an efficient one be added to the device. For this, enhanced structures could be introduced instead of using simple disc vanes. Their influence on the electrical output power could be evaluated. Also, the pumping power for the coolant should be analyzed in future studies.

- The thermoelectric material improvement is itself a huge area of study. A deep material investigation would be out of the principal goal of this branch of study where this master thesis is inserted. Another idea which is suggested and explained next indirectly takes into account the thermoelectric material's performance. After getting an initial estimate for the temperature decrease along the TEG length, it is suggested to build thermoelectric modules with different materials. These thermoelectric modules made from different materials should then be distributed along the TEG length (like a sandwich) in order to assure that the material which they are made from is working at its maximum ZT value. Consequently, this would improve the performance of each thermoelectric module and increase the overall electrical output power of the TEG

After getting the first estimation for the additional parameters a deeper analysis should be performed. The proposed analysis is listed below;

  - The thermal and electrical contact resistance which were neglected in this work, need to be analyzed carefully, in order to account for the errors that arise from neglecting them.
  - The electrical system of the TEG needs to be analyzed in more detail. In this research area, it would be of most benefit to optimize the number of thermocouples per thermoelectric module. Additionally, the thermoelectric module's geometry should be analyzed in order to minimize the losses that arise from varying temperatures over the thermoelectric modules, which are caused by the temperature decrease along the TEG length.
- The heat exchangers' geometries which were done in this work also need to be studied and improved. After obtaining the first preliminary dimensions of the heat exchanger with this numerical TEG model, it is suggested to study and optimize their behavior through the use of 3D analyses, e.g. by using the software Fluent.
- Since the device is always in rotating motion and has current flowing, there will be a magnetic flux created in the vicinity, a study of the effect of this electromagnetic field on the power being supplied ought to be done to assess its impact.

References

[1] J.-P. Rodrigue, C. Comtois, and B. Slack, *The Geography of Transport Systems*, 3rd ed. 2013.

[2] John Donovan, "Energy harvesting and renewable energy sources | EE Times." [Online]. Available: https://www.eetimes.com/document.asp?doc_id=1279211#. [Accessed: 29-Apr-2019].

[3] S. C. Tzeng, T. M. Jeng, and Y. L. Lin, "Parametric study of heat-transfer design on the thermoelectric generator system," *Int. Commun. Heat Mass Transf.*, vol. 52, pp. 97–105, 2014.

[4] O. H. Ando Junior, A. L. O. Maran, and N. C. Henao, "A review of the development and applications of thermoelectric microgenerators for energy harvesting," *Renew. Sustain. Energy Rev.*, vol. 91, no. March, pp. 376–393, 2018.

[5] D. Sivaprahasam, S. Harish, S. Govindhan, and R. Gopalan, "Automotive Waste Heat Recovery by Thermoelectric Generator Technology," in *IntechOpen*, 2018.

[6] D. M. Rowe, *Thermoelectrics handbook : macro to nano*. CRC/Taylor & Francis, 2006.

[7] H. L. Talom and A. Beyene, "Heat recovery from automotive engine," *Appl. Therm. Eng.*, vol. 29, no. 2–3, pp. 439–444, 2009.

[8] T. Hendricks and W. T. Choate, "Engineering Scoping Study of Thermoelectric geneartor Systems for Industrial Waste Heat Recovery," no. November, 2006.

[9] D. Enescu, "Thermoelectric Energy Harvesting : Basic Principles and Applications," *Green Energy Adv.*, 2019.

[10] U. D. of Energy, "Waste Heat Recovery: Technology and Opportunities in U.S. Industry."

[11] S. Fecht, *Converting waste heat into electricity*, no. March. 2014, pp. 1–3.

[12] L. B. Kong, T. Li, H. H. Hng, F. Boey, T. Zhang, and S. Li, *Waste Energy Harvesting*, vol. 24. 2014.

[13] A. Kumella Eticha, “Analysis of the Performance of Disc Brake System of Addis Ababa Light Rail Transit Using Temperature and Coefficient of Friction as a Parameter,” *Int. J. Mech. Eng. Appl.*, vol. 4, no. 6, p. 205, 2016.

[14] Z. Wang, J. Han, X. Liu, Z. Li, Z. Yang, and E. Chen, “Temperature evolution of the train brake disc during high-speed braking,” *Adv. Mech. Eng.*, vol. 11, no. 1, p. 168781401881956, 2019.

[15] X. Wu, J. Zuo, and M. Wu, “Heat Simulation of High-speed Train’s Brake Disc Considering the Wind Speed of Disc Surface Influence on Convection Coefficient Xiaobiao Wu 1,” no. 1, pp. 145–149, 2012.

[16] L. C. Ding, A. Akbarzadeh, and L. Tan, “A review of power generation with thermoelectric system and its alternative with solar ponds,” *Renew. Sustain. Energy Rev.*, vol. 81, no. July 2017, pp. 799–812, 2018.

[17] A. Bitschi, “Modelling of thermoelectric devices for electric power generation,” no. 18441, p. 144, 2009.

[18] S. Xu *et al.*, “Patterned growth of vertically aligned ZnO nanowire arrays on inorganic substrates at low temperature without catalyst,” *J. Am. Chem. Soc.*, vol. 130, no. 45, pp. 14958–14959, 2008.

[19] L. E. Bell, “Cooling, Heating, Generating Power, and Recovering Waste Heat with Thermoelectric Systems,” *Science (80-.).*, vol. 321, no. 5895, pp. 1457–1461, 2008.

[20] Z. Niu *et al.*, “Elucidating modeling aspects of thermoelectric generator,” *Int. J. Heat Mass Transf.*, vol. 85, pp. 12–32, 2015.

[21] J.-W. Bos, *Thermoelectric materials: Efficiencies found in nanocomposites*, vol. 49. 2012.

[22] G. . Nolas, J. Sharp, and H. . Goldsmid, *Thermoelectrics Basic Principles and New Materials Developments*, vol. 153. 2001.

[23] H. J. Goldsmid and R. W. Douglas, “The use of semiconductors in thermoelectric refrigeration,” *Br. J. Appl. Phys.*, vol. 5, no. 11, pp. 386–390, 1954.

[24] W. M. Haynes, *Handbook of Chemistry and Physics Edition 95*. 2014.

[25] D. S. Patil, R. R. Arakerimath, and P. V. Walke, "Thermoelectric materials and heat exchangers for power generation – A review," *Renew. Sustain. Energy Rev.*, vol. 95, no. July, pp. 1–22, 2018.

[26] K. Gaurav and S. K. Pandey, "Efficiency calculation of thermoelectric generator using temperature dependent material's properties," no. March, 2016.

[27] S. Siouane, S. Jovanovic, and P. Poure, "A Novel Identification Method of Thermal Resistances of Thermoelectric Modules Combining Electrical Characterization Under Constant Temperature and Heat Flow Conditions," *Trans. Environ. Electr. Eng.*, vol. 1, no. 4, p. 44, 2016.

[28] G. Skomedal, *Thermal durability of novel thermoelectric materials for waste heat recovery*. 2016.

[29] U. Birkholz, E. Grob, U. Stohrer, and K. Voss, *Conversion of waste exhaust heat in automobile using FeSi2 thermoelements*. 1988.

[30] L.-D. Zhao *et al.*, "Ultralow thermal conductivity and high thermoelectric figure of merit in SnSe crystals," *Nature*, vol. 508, p. 373, Apr. 2014.

[31] J. C. Bass, N. B. Elsner, and F. A. Leavitt, "Performance of the 1 kW Thermoelectric Generator for Diesel Engines," in *The International Conference on Thermoelectrics, 1994, Kansas City, Kansas, USA*, 1994.

[32] K. Ikoma, M. Munekiyo, K. Furuya, M. Kobayashi, T. Izumi, and K. Shinohara, "Thermoelectric module and generator for gasoline engine vehicles," in *Seventeenth International Conference on Thermoelectrics. Proceedings ICT98 (Cat. No.98TH8365)*, 1998, pp. 464–467.

[33] J. G. Haidar and J. I. Ghojel, "Waste heat recovery from the exhaust of low-power diesel engine using thermoelectric generators," in *Proceedings ICT2001. 20 International Conference on Thermoelectrics (Cat. No.01TH8589)*, 2001, pp. 413–418.

[34] K. Matsubara, "Development of a high efficient thermoelectric stack for a waste

exhaust heat recovery of vehicles," in *Twenty-First International Conference on Thermoelectrics, 2002. Proceedings ICT '02.*, 2002, pp. 418–423.

[35] K. T. Wojciechowski, M. Schmidt, R. Zybala, and J. Merkisz, "Comparison of Waste Heat Recovery from the Exhaust of a Spark Ignition and a Diesel Engine," vol. 39, no. 9, pp. 2034–2038, 2010.

[36] S. Kim, S. Park, S. Kim, and S. Rhi, "A Thermoelectric Generator Using Engine Coolant for Light-Duty Internal Combustion Engine-Powered Vehicles," vol. 40, no. 5, pp. 812–816, 2011.

[37] S. Kim, B. Won, S. Rhi, S. Kim, J. Yoo, and J. Jang, "Thermoelectric Power Generation System for Future Hybrid Vehicles Using Hot Exhaust Gas," vol. 40, no. 5, pp. 778–779, 2011.

[38] D. Crane *et al.*, "TEG On-Vehicle Performance and Model Validation and What It Means for Further TEG Development," vol. 42, no. 7, pp. 1582–1583, 2013.

[39] Y. Zhang *et al.*, "High-temperature and high-power-density nanostructured thermoelectric generator for automotive waste heat recovery," *ENERGY Convers. Manag.*, vol. 105, pp. 946–950, 2015.

[40] S. Priya and D. Inman, *Energy Harvesting Technologies*. Springer, 2009.

[41] H. J. Goldsmid, "Bismuth telluride and its alloys as materials for thermoelectric generation," *Materials (Basel).*, vol. 7, no. 4, pp. 2577–2592, 2014.

[42] M. Hamid Elsheikh *et al.*, "A review on thermoelectric renewable energy: Principle parameters that affect their performance," *Renew. Sustain. Energy Rev.*, vol. 30, pp. 337–355, 2014.

[43] Z. G. Zhou, D. S. Zhu, H. X. Wu, and H. S. Zhang, "Modeling, experimental study on the heat transfer characteristics of thermoelectric generator," *J. Therm. Sci.*, vol. 22, no. 1, pp. 48–54, 2013.

[44] Z. Ouyang and D. Li, "Modelling of segmented high-performance thermoelectric generators with effects of thermal radiation, electrical and thermal contact resistances,"

Sci. Rep., vol. 6, no. March, pp. 1–12, 2016.

[45] A. Montecucco, J. Siviter, and A. R. Knox, "Constant heat characterisation and geometrical optimisation of thermoelectric generators," *Appl. Energy*, vol. 149, no. June, pp. 248–258, 2015.

[46] R. Ahiska and H. Mamur, "A review: Thermoelectric generators in renewable energy," *Int. J. Renew. Energy Res.*, vol. 4, no. 1, pp. 128–136, 2014.

[47] D. J. Paul, "Thermoelectric Energy Harvesting Douglas."

[48] C. L. Hapenciuc, T. Borca-Tasciuc, and I. N. Mihailescu, "The relationship between the thermoelectric generator efficiency and the device engineering figure of merit Z d,eng . The maximum efficiency η max," *AIP Adv.*, vol. 7, no. 4, 2017.

[49] B. Ismail and W. Ahmed, "Thermoelectric Power Generation Using Waste-Heat Energy as an Alternative Green Technology," *Recent Patents Electr. Eng.*, vol. 2, no. 1, pp. 27–39, 2010.

[50] H. Karamitaheri, "1.2 Device Efficiency," *Thermal and Thermoelectric Properties of Nanostructures*. [Online]. Available: http://www.iue.tuwien.ac.at/phd/karamitaheri/node10.html. [Accessed: 22-Apr-2019].

[51] S. Cristina and A. Vale, "Thermoelectric generator from space to automotive sector-model and design for commercial and heavy duty vehicles," no. November, 2015.

[52] O. Högblom, *Multiscale Simulation Methods for Thermoelectric Generators*. 2016.

[53] Simon Ndiritu, "6 Factors to Consider for a Better Heat Sink Design | SimScale Blog." [Online]. Available: https://www.simscale.com/blog/2016/10/key-factors-heat-sink-design/. [Accessed: 22-Feb-2019].

[54] J. H.Lienard, *A Heat Transfer Textbook*, Third. MIT, 2004.

[55] V. Siegel, "Heatsink Design and Selection: Material," *ABL Heatsinks*.

[56] Electrical Engineering, "Regenerative Braking: Difficulties and Advantages." [Online]. Available: http://www.engineeringenotes.com/electrical-engineering/electric-braking/regenerative-braking-difficulties-and-advantages-electrical-engineering/37168.

[Accessed: 30-Jun-2019].

[57] C. R. Vehicle, “Operation and Maintenance Manual for Addis Ababa Light Rail Vehicle.”

[58] T. Katkus, “Design and construction of high temperature thermoelectric power generator module characterisation system,” 1954.

[59] D. Solidwork Dassault Systemes, “What’s New Solidworks 2016,” 2016.

[60] “Grey cast iron ASTM 40 [SubsTech].” [Online]. Available: http://www.substech.com/dokuwiki/doku.php?id=grey_cast_iron_astm_40. [Accessed: 08-Apr-2019].

[61] H. Lee, *Thermoelectrics: Design and Materials*. 2017.

[62] S. Twaha, J. Zhu, Y. Yan, and B. Li, “A comprehensive review of thermoelectric technology: Materials, applications, modelling and performance improvement,” *Renew. Sustain. Energy Rev.*, vol. 65, pp. 698–726, 2016.

[63] M. Jaegle, “Multiphysics Simulation of Thermoelectric Systems - Modeling of Peltier-Cooling and Thermoelectric Generation,” *Multiphysics Simul. Thermoelectr. Syst. - Model. Peltier-Cooling Thermoelectr. Gener.*, no. 6, p. 7, 2008.

Appendices

Tables of results of simulation with an increase in leg size (also decrease in leg numbers)

Size of leg (mm)	Voltage (V)	Current (A)	Heat absorbed (W)	Power generated (W)
ω=1	0.01	0.52566	0.18559	0.005257
	0.02	0.6126	0.19368	0.012252
	0.03	0.69954	0.20089	0.020986
	0.04	0.78649	0.20717	0.03146
	0.05	0.87344	0.21264	0.043672
	0.06	0.96038	0.21724	0.057623
	0.07	1.0473	0.22098	0.073311
	0.08	1.1343	0.22384	0.090744
	0.09	1.2212	0.22584	0.109908
	0.1	1.3082	0.22696	0.13082
	0.11	1.3951	0.22722	0.153461
	0.12	1.482	0.22661	0.17784
	0.13	1.569	0.22513	0.20397
	0.14	1.6559	0.22278	0.231826
	0.15	1.7429	0.21957	0.261435
ω =1.25	0.01	0.82095	0.28994	0.00821
	0.02	0.95673	0.30257	0.019135
	0.03	1.0925	0.31384	0.032775
	0.04	1.2283	0.32376	0.049132
	0.05	1.3641	0.33231	0.068205
	0.06	1.4999	0.33951	0.089994
	0.07	1.6356	0.34535	0.114492
	0.08	1.7714	0.34983	0.141712
	0.09	1.9072	0.35296	0.171648
	0.1	2.043	0.35472	0.2043
	0.11	2.1787	0.35513	0.239657

	0.12	2.3145	0.35418	0.27774
	0.13	2.4503	0.35187	0.318539
	0.14	2.586	0.3482	0.36204
	0.15	2.7218	0.34318	0.40827
ω =1.5	0.01	1.1815	0.41744	0.011815
	0.02	1.3769	0.43562	0.027538
	0.03	1.5724	0.45184	0.047172
	0.04	1.7678	0.46612	0.070712
	0.05	1.9632	0.47843	0.09816
	0.06	2.1586	0.4888	0.129516
	0.07	2.354	0.4972	0.16478
	0.08	2.5494	0.50366	0.203952
	0.09	2.7448	0.50816	0.247032
	0.1	2.9403	0.5107	0.29403
	0.11	3.1357	0.51129	0.344927
	0.12	3.3311	0.50993	0.399732
	0.13	3.5265	0.50661	0.458445
	0.14	3.7219	0.50133	0.521066
	0.15	3.9173	0.4941	0.587595
ω =1.75	0.01	1.6071	0.56781	0.016071
	0.02	1.8729	0.59251	0.037458
	0.03	2.1388	0.61455	0.064164
	0.04	2.4046	0.63393	0.096184
	0.05	2.6704	0.65066	0.13352
	0.06	2.9362	0.66473	0.176172
	0.07	3.2021	0.67614	0.224147
	0.08	3.4679	0.68489	0.277432
	0.09	3.7337	0.69099	0.336033
	0.1	3.9995	0.69443	0.39995
	0.11	4.2654	0.69521	0.469194

	0.12	4.5312	0.69334	0.543744
	0.13	4.797	0.68881	0.62361
	0.14	5.0628	0.68162	0.708792
	0.15	5.3287	0.67178	0.799305
ω =2.0	0.01	2.0987	0.74182	0.020987
	0.02	2.4448	0.77411	0.048896
	0.03	2.7918	0.80298	0.083754
	0.04	3.1388	0.82828	0.125552
	0.05	3.4857	0.85017	0.174285
	0.06	3.8327	0.86858	0.229962
	0.07	4.1797	0.88352	0.292579
	0.08	4.5267	0.89499	0.362136
	0.09	4.8736	0.90299	0.438624
	0.1	5.2206	0.90752	0.52206
	0.11	5.5676	0.90859	0.612436
	0.12	5.9145	0.90618	0.70974
	0.13	6.2615	0.9003	0.813995
	0.14	6.6084	0.89095	0.925176
	0.15	6.9554	0.87813	1.04331
ω =2.25	0.01	2.6532	0.93886	0.026532
	0.02	3.092	0.97951	0.06184
	0.03	3.5309	1.016	0.105927
	0.04	3.9697	1.048	0.158788
	0.05	4.4085	1.0757	0.220425
	0.06	4.8474	1.099	0.290844
	0.07	5.2862	1.1179	0.370034
	0.08	5.725	1.1324	0.458
	0.09	6.1638	1.1426	0.554742
	0.1	6.6027	1.1483	0.66027
	0.11	7.0415	1.1497	0.774565

	0.12	7.4803	1.1466	0.897636
	0.13	7.9191	1.1392	1.029483
	0.14	8.3583	1.126	1.170162
	0.15	8.7972	1.1098	1.31958
ω =2.5	0.01	3.2718	1.1584	0.032718
	0.02	3.813	1.2088	0.07626
	0.03	4.3542	1.2538	0.130626
	0.04	4.8953	1.2934	0.195812
	0.05	5.4365	1.3276	0.271825
	0.06	5.9777	1.3563	0.358662
	0.07	6.5189	1.3797	0.456323
	0.08	7.06	1.3976	0.5648
	0.09	7.6012	1.4102	0.684108
	0.1	8.1424	1.4173	0.81424
	0.11	8.6837	1.4173	0.955207
	0.12	9.2249	1.4135	1.106988
	0.13	9.7661	1.4043	1.269593
	0.14	10.307	1.3897	1.44298
	0.15	10.848	1.3697	1.6272
ω =2.75	0.01	3.9539	1.4012	0.039539
	0.02	4.6079	1.4621	0.092158
	0.03	5.2619	1.5165	0.157857
	0.04	5.9159	1.5644	0.236636
	0.05	6.5699	1.6058	0.328495
	0.06	7.2239	1.6406	0.433434
	0.07	7.8779	1.6688	0.551453
	0.08	8.5319	1.6906	0.682552
	0.09	9.186	1.7037	0.82674
	0.1	9.84	1.7122	0.984
	0.11	10.494	1.7142	1.15434

	0.12	11.148	1.7097	1.33776
	0.13	11.802	1.6986	1.53426
	0.14	12.456	1.681	1.74384
	0.15	13.11	1.6568	1.9665
ω =3.0	0.01	4.701	1.9971	0.04701
	0.02	5.4786	1.7396	0.109572
	0.03	6.2562	1.8043	0.187686
	0.04	7.0338	1.8612	0.281352
	0.05	7.8114	1.9104	0.39057
	0.06	8.589	1.9518	0.51534
	0.07	9.3666	1.9831	0.655662
	0.08	10.144	2.0087	0.81152
	0.09	10.922	2.0266	0.98298
	0.1	11.699	2.0367	1.1699
	0.11	12.477	2.0391	1.37247
	0.12	13.255	2.0377	1.5906
	0.13	14.032	2.0205	1.82416
	0.14	14.81	1.9996	2.0734
	0.15	15.587	1.9709	2.33805
ω =3.25	0.01	5.5138	1.956	0.055138
	0.02	6.4258	2.041	0.128516
	0.03	7.3378	2.1169	0.220134
	0.04	8.2499	2.1837	0.329996
	0.05	9.1619	2.2413	0.458095
	0.06	10.074	2.2817	0.60444
	0.07	10.986	2.3262	0.76902
	0.08	11.898	2.3563	0.95184
	0.09	12.81	2.3772	1.1529
	0.1	13.722	2.389	1.3722
	0.11	14.634	2.3917	1.60974

	0.12	15.546	2.3853	1.86552
	0.13	16.458	2.3698	2.13954
	0.14	17.37	2.3451	2.4318
	0.15	18.282	2.3114	2.7423
ω =3.5	0.01	6.3919	2.2683	0.063919
	0.02	7.4492	2.3669	0.148984
	0.03	8.5065	2.4548	0.255195
	0.04	9.5637	2.5322	0.382548
	0.05	10.621	2.5958	0.53105
	0.06	11.679	2.6517	0.70074
	0.07	12.736	2.697	0.89152
	0.08	13.793	2.7318	1.10344
	0.09	14.85	2.756	1.3365
	0.1	15.908	2.7696	1.5908
	0.11	16.965	2.7726	1.86615
	0.12	18.022	2.765	2.16264
	0.13	19.08	2.7469	2.4804
	0.14	20.137	2.7183	2.81918
	0.15	21.194	2.679	3.1791
ω =5	0.01	12.944	4.6124	0.12944
	0.02	15.085	4.8112	0.3017
	0.03	17.226	4.9887	0.51678
	0.04	19.367	5.1447	0.77468
	0.05	21.508	5.2793	1.0754
	0.06	23.649	5.3925	1.41894
	0.07	25.79	5.4843	1.8053
	0.08	27.931	5.5546	2.23448
	0.09	30.072	5.6036	2.70648
	0.1	32.213	5.6311	3.2213
	0.11	34.354	5.6372	3.77894

	0.12	36.636	5.622	4.39632
	0.13	38.636	5.5853	5.02268
	0.14	40.777	5.5272	5.70878
	0.15	42.918	5.4477	6.4377

Annex 1: Results of repeated braking along the 21 stations of the line

Time [s]	Minimum [°C]	Maximum [°C]
6.50E-02	98.043	105.37
0.13	97.929	108.05
0.28499	97.765	111.94
0.63437	98.503	117.56
1.2844	99.881	124.6
1.9344	99.834	130.2
2.5844	99.787	135.03
3.2344	99.74	139.31
3.8844	99.695	143.18
4.5344	99.649	146.78
5.1844	99.604	150.18
5.8344	99.559	153.43
6.1672	99.536	155.05
6.5	99.513	156.65
1.2	99.431	143.87
1.6	99.404	140.71
2	99.377	138.29
2.8813	99.317	134.93
3.8847	99.25	132.53
4.9328	99.18	130.93
6.0084	99.108	129.87
7.1164	99.035	129.17
8.2751	98.959	128.7
9.5226	98.88	128.37
10.94	98.792	128.14
12.708	98.687	127.96
15.286	98.55	127.83
19.883	98.373	127.68
29.102	98.3	127.41
41.102	98.567	127.06
53.102	99.062	126.71
65.102	99.676	126.38
77.102	100.34	126.06
89.102	101	125.74
101.1	101.64	125.44
113.1	102.23	125.14
120	102.56	124.98
6.50E-02	102.56	129.92
0.13		132.43
0.28474	102.57	135.94
0.63292	102.59	141.22
1.2829	102.62	147.91
1.9329	102.65	153.13
2.5829	102.68	157.59
3.2329	102.71	161.55
3.8829	102.74	165.17
4.5329	102.77	168.54
5.1829	102.8	171.72
5.8329	102.83	174.76
6.1665	102.84	176.29
6.5	102.86	177.79
1.2	102.91	165.73
1.6	102.93	162.77
2	102.95	160.5
2.8817	102.99	157.37
3.8858	103.03	155.15
4.9355	103.08	153.67
6.0146	103.13	152.69
7.1303	103.17	152.03
8.3066	103.23	151.58
9.5952	103.28	151.26
11.114	103.35	151.04
13.161	103.45	150.87
16.63	103.64	150.7
24.465	104.22	150.4
36.465	105.42	149.96
48.465	106.8	149.53
60.465	108.25	149.1
72.465	109.69	148.69
84.465	111.08	148.29
96.465	112.39	147.9
108.46	113.61	147.52
120	114.69	147.16
6.50E-02	114.69	152.1
0.13	114.7	154.61
0.28466	114.71	158.11
0.63249	114.74	163.39
1.2825	114.8	170.07
1.9325	114.86	175.3
2.5825	114.92	179.74
3.2325	114.98	183.69
3.8825	115.03	187.32
4.5325	115.09	190.69

Time [s]	Minimum [°C]	Maximum [°C]
5.1825	115.15	193.87
5.8325	115.2	196.9
6.1662	115.23	198.43
6.5	115.26	199.93
1.2	115.37	187.75
1.6	115.4	184.81
2	115.44	182.57
2.8818	115.52	179.47
3.8863	115.6	177.25
4.9368	115.69	175.76
6.0177	115.79	174.77
7.1375	115.88	174.11
8.3231	115.98	173.65
9.6344	116.09	173.33
11.212	116.23	173.1
13.435	116.42	172.92
17.543	116.81	172.7
28.096	118.06	172.25
40.096	119.71	171.74
52.096	121.47	171.23
64.096	123.24	170.74
76.096	124.96	170.26
88.096	126.59	169.8
100.1	128.12	169.35
112.1	129.52	168.91
120	130.4	168.62
6.50E-02	130.4	172.46
0.13	130.41	174.43
0.28449	130.43	177.19
0.63151	130.47	181.33
1.2815	130.54	186.57
1.9315	130.61	190.67
2.5815	130.68	194.15
3.2315	130.75	197.25
3.8815	130.82	200.09
4.5315	130.89	202.74
5.1815	130.96	205.23

Time [s]	Minimum [°C]	Maximum [°C]
5.8315	131.03	207.6
6.1658	131.06	208.8
6.5	131.1	209.98
1.2	131.22	200.38
1.6	131.26	198.07
2	131.3	196.31
2.8821	131.4	193.86
3.8873	131.5	192.1
4.9393	131.6	190.92
6.0237	131.71	190.13
7.1516	131.83	189.59
8.3564	131.95	189.22
9.7151	132.08	188.97
11.421	132.25	188.76
14.055	132.52	188.58
19.871	133.15	188.3
31.871	134.65	187.76
43.871	136.26	187.22
55.871	137.91	186.7
67.871	139.52	186.19
79.871	141.06	185.68
91.871	142.49	185.2
103.87	143.82	184.72
115.87	145.03	184.25
120	145.43	184.09
6.50E-02	145.44	188.6
0.13		190.91
0.28453	145.46	194.16
0.63173	145.49	199.02
1.2817	145.56	205.16
1.9317	145.62	209.97
2.5817	145.68	214.06
3.2317	145.74	217.69
3.8817	145.8	221.03
4.5317	145.87	224.13
5.1817	145.93	227.06
5.8317	145.99	229.85

Time [s]	Minimum [°C]	Maximum [°C]
6.1659	146.02	231.25
6.5	146.05	232.63
1.2	146.16	221.39
1.6	146.2	218.68
2	146.23	216.62
2.882	146.31	213.75
3.8868	146.4	211.69
4.9382	146.5	210.31
6.021	146.59	209.38
7.1454	146.69	208.75
8.342	146.79	208.32
9.6804	146.91	208.02
11.331	147.06	207.79
13.785	147.28	207.59
18.828	147.77	207.31
30.828	149.21	206.71
42.828	150.82	206.12
54.828	152.5	205.53
66.828	154.17	204.96
78.828	155.76	204.41
90.828	157.27	203.86
102.83	158.65	203.33
114.83	159.92	202.81
120	160.45	202.59
6.50E-02	160.46	207.17
0.13		209.53
0.28449	160.48	212.85
0.63148	160.52	217.8
1.2815	160.58	224.06
1.9315	160.65	228.96
2.5815	160.71	233.13
3.2315	160.77	236.83
3.8815	160.84	240.24
4.5315	160.9	243.4
5.1815	160.97	246.38
5.8315	161.03	249.22
6.1657	161.06	250.65

Time [s]	Minimum [°C]	Maximum [°C]
6.5	161.09	252.06
1.2	161.21	240.59
1.6	161.25	237.82
2	161.28	235.72
2.882	161.37	232.79
3.887	161.46	230.69
4.9387	161.56	229.27
6.0223	161.66	228.33
7.1484	161.76	227.68
8.349	161.87	227.23
9.6973	161.99	226.92
11.375	162.15	226.68
13.919	162.38	226.47
19.351	162.94	226.15
31.351	164.43	225.5
43.351	166.09	224.85
55.351	167.81	224.22
67.351	169.51	223.6
79.351	171.14	222.99
91.351	172.66	222.4
103.35	174.07	221.82
115.35	175.36	221.25
120	175.84	221.03
6.50E-02	175.84	225.88
0.13	175.85	228.38
0.28447	175.86	231.91
0.63143	175.9	237.17
1.2814	175.96	243.81
1.9314	176.03	249.01
2.5814	176.09	253.42
3.2314	176.15	257.35
3.8814	176.22	260.96
4.5314	176.28	264.31
5.1814	176.34	267.47
5.8314	176.4	270.48
6.1657	176.44	272
6.5	176.47	273.49

Time [s]	Minimum [°C]	Maximum [°C]
1.2	239.62	239.99
2.4	239.36	239.95
6	238.62	239.82
16.8	236.44	239.41
28.8	234.11	238.93
40.8	231.87	238.43
52.8	229.74	237.92
64.8	227.71	237.4
76.8	225.79	236.88
88.8	223.98	236.36
100.8	222.27	235.83
112.8	220.65	235.31
120	219.71	234.99
6.50E-02	219.7	240.71
0.13	219.69	244.22
0.32039	219.67	249.5
0.7213	219.62	256.35
1.3713	219.53	263.91
2.0213	219.45	270.22
2.6713	219.36	275.53
3.3213	219.28	280.16
3.9713	219.2	284.34
4.6213	219.11	288.21
5.2713	219.03	291.85
5.9213	218.95	295.32
6.5	218.88	298.32
1.2	218.73	284.24
1.6	218.68	280.84
2	218.63	278.04
2.9041	218.51	273.75
3.9463	218.38	270.5
5.0403	218.25	268.45
6.1664	218.11	267.08
7.3301	217.97	266.13
8.5539	217.82	265.46
9.8867	217.67	264.97
11.439	217.49	264.58

Time [s]	Minimum [°C]	Maximum [°C]
13.488	217.26	264.26
16.862	216.91	263.97
24.513	216.32	263.48
36.513	215.84	262.76
48.513	215.69	262.05
60.513	215.74	261.34
72.513	215.9	260.65
84.513	216.1	259.97
96.513	216.31	259.3
108.51	216.51	258.64
120	216.67	258.01
6.50E-02	216.67	263.08
0.13	216.67	266.25
0.32022	216.67	271.27
0.72038	216.68	277.53
1.3704	216.69	284.73
2.0204	216.7	290.69
2.6704	216.7	295.61
3.3204	216.71	299.88
3.9704	216.72	303.75
4.6204	216.73	307.32
5.2704	216.74	310.69
5.9204	216.75	313.9
6.5	216.75	316.67
1.2	216.77	303.65
1.6		300.49
2	216.78	297.89
2.9044	216.79	293.9
3.9472	216.8	290.88
5.0428	216.81	288.79
6.1723	216.83	287.47
7.3439	216.84	286.58
8.586	216.86	285.94
9.9632	216.87	285.46
11.631	216.9	285.12
14.025	216.93	284.86
18.694	217.05	284.5

Time [s]	Minimum [°C]	Maximum [°C]
30.694	217.68	283.67
42.694	218.56	282.86
54.694	219.59	282.06
66.694	220.68	281.27
78.694	221.75	280.5
90.694	222.78	279.74
102.69	223.74	278.99
114.69	224.61	278.25
120	224.97	277.92
6.50E-02	224.98	282.74
0.13		285.9
0.32014	224.99	291.17
0.71996	225.02	297.42
1.37	225.07	304.63
2.02	225.11	310.59
2.67	225.15	315.5
3.32	225.2	319.77
3.97	225.24	323.63
4.62	225.28	327.21
5.27	225.33	330.57
5.92	225.37	333.78
6.5	225.41	336.55
1.2	225.48	323.52
1.6	225.51	320.35
2	225.54	317.75
2.9045	225.59	313.76
3.9477	225.66	310.72
5.0442	225.73	308.63
6.1756	225.8	307.24
7.3517	225.87	306.34
8.6043	225.94	305.69
10.007	226.03	305.23
11.744	226.14	304.9
14.36	226.3	304.6
19.969	226.71	304.16
31.969	227.87	303.27
43.969	229.23	302.38

Time [s]	Minimum [°C]	Maximum [°C]
55.969	230.69	301.51
67.969	232.16	300.66
79.969	233.59	299.82
91.969	234.93	299
103.97	236.17	298.19
115.97	237.29	297.38
120	237.66	297.12
6.50E-02	237.66	301.32
0.13	237.67	304.18
0.31996	237.69	308.86
0.71902	237.72	314.38
1.369	237.78	320.79
2.019	237.84	326.07
2.669	237.9	330.42
3.319	237.95	334.21
3.969	238.01	337.64
4.619	238.07	340.8
5.269	238.12	343.78
5.919	238.18	346.62
6.5	238.23	349.08
1.2	238.33	337.45
1.6	238.36	334.64
2	238.4	332.32
2.9048	238.47	328.76
3.9487	238.56	326.05
5.0466	238.65	324.18
6.1815	238.74	322.93
7.3656	238.84	322.12
8.6372	238.94	321.52
10.088	239.05	321.13
11.958	239.2	320.82
15.035	239.45	320.49
22.894	240.18	319.88
34.894	241.51	318.94
46.894	242.96	318.02
58.894	244.46	317.12
70.894	245.93	316.23

Time [s]	Minimum [°C]	Maximum [°C]
82.894	247.33	315.36
94.894	248.63	314.49
106.89	249.82	313.64
113.45	250.43	313.18
120	251.01	312.72
6.50E-02	251.02	316.94
0.13		319.81
0.31992	251.04	324.52
0.71878	251.07	330.07
1.3688	251.13	336.51
2.0188	251.19	341.82
2.6688	251.24	346.19
3.3188	251.3	350
3.9688	251.35	353.44
4.6188	251.41	356.62
5.2688	251.46	359.61
5.9188	251.52	362.47
6.5	251.57	364.94
1.2	251.66	353.22
1.6	251.7	350.39
2	251.73	348.06
2.9048	251.8	344.48
3.9489	251.89	341.75
5.0472	251.97	339.86
6.1828	252.06	338.63
7.3686	252.15	337.81
8.6445	252.25	337.21
10.106	252.37	336.8
12.009	252.51	336.49
15.202	252.77	336.14
23.703	253.55	335.45
35.703	254.85	334.47
47.703	256.28	333.51
59.703	257.75	332.57
71.703	259.19	331.63
83.703	260.55	330.72
95.703	261.82	329.82

Time [s]	Minimum [°C]	Maximum [°C]
107.7	262.97	328.92
113.85	263.53	328.47
120	264.05	328.02
6.50E-02	318.19	325.12
0.13	317.55	328.14
0.32089	317.1	332.75
0.72447	317.69	338.63
1.3745	319.03	345.16
2.0245	319.2	350.63
2.6745	319.03	355.22
3.3245	318.86	359.22
3.9745	318.69	362.83
4.6245	318.5	366.17
5.2745	318.31	369.31
5.9245	318.12	372.31
6.5	317.96	374.88
1.2	317.62	362.62
1.6	317.5	359.65
2	317.39	357.22
2.9041	317.13	353.47
3.9465	316.84	350.65
5.0413	316.53	348.86
6.1696	316.22	347.66
7.3396	315.89	346.81
8.5801	315.55	346.21
9.9579	315.18	345.75
11.639	314.72	345.37
14.114	314.06	345.07
19.339	312.74	344.62
31.339	310.19	343.71
43.339	308.06	342.83
55.339	306.25	341.96
67.339	304.67	341.11
79.339	303.26	340.27
91.339	301.96	339.43
103.34	300.75	338.6
115.34	299.61	337.78

Time [s]	Minimum [°C]	Maximum [°C]
120	299.17	337.46
6.50E-02	299.16	342.51
0.13		345.68
0.32002	299.14	350.63
0.71931	299.1	356.9
1.3693	299.04	364.11
2.0193	298.98	370.08
2.6693	298.92	374.99
3.3193	298.86	379.26
3.9693	298.8	383.12
4.6193	298.74	386.7
5.2693	298.68	390.06
5.9193	298.62	393.26
6.5	298.57	396.03
1.2	298.46	382.83
1.6	298.43	379.65
2	298.39	377.05
2.9045	298.31	373.04
3.9478	298.21	369.99
5.0443	298.12	368.09
6.1759	298.02	366.8
7.3526	297.91	365.88
8.6069	297.8	365.22
10.015	297.68	364.71
11.767	297.54	364.31
14.441	297.33	363.98
20.381	296.95	363.43
32.381	296.59	362.42
44.381	296.53	361.43
56.381	296.66	360.45
68.381	296.9	359.48
80.381	297.17	358.53
92.381	297.44	357.59
104.38	297.67	356.65
112.19	297.8	356.05
120	297.92	355.46
6.50E-02	297.92	360.3

Time [s]	Minimum [°C]	Maximum [°C]
0.13	297.92	363.46
0.31992	297.92	368.67
0.7188	297.93	374.92
1.3688	297.94	382.13
2.0188	297.95	388.09
2.6688	297.95	393
3.3188	297.96	397.27
3.9688	297.97	401.13
4.6188	297.98	404.7
5.2688	297.99	408.05
5.9188	298	411.26
6.5	298	414.03
1.2	298.02	400.84
1.6		397.66
2	298.03	395.05
2.9047	298.04	391.03
3.9485	298.05	387.97
5.0462	298.06	385.93
6.1805	298.07	384.62
7.3633	298.08	383.7
8.6321	298.1	383.03
10.076	298.11	382.5
11.929	298.14	382.16
14.946	298.18	381.79
22.563	298.42	381.08
34.563	299.09	379.99
46.563	299.97	378.92
58.563	300.96	377.86
70.563	301.96	376.82
82.563	302.94	375.8
94.563	303.84	374.78
106.56	304.66	373.78
113.28	305.09	373.22
120	305.48	372.67
6.50E-02	305.49	377.39
0.13		380.61
0.31986	305.5	385.88

Time [s]	Minimum [°C]	Maximum [°C]
0.71844	305.53	392.12
1.3684	305.56	399.34
2.0184	305.6	405.29
2.6684	305.64	410.2
3.3184	305.67	414.47
3.9684	305.71	418.33
4.6184	305.75	421.89
5.2684	305.78	425.25
5.9184	305.82	428.45
6.5	305.85	431.22
1.2	305.92	418.02
1.6	305.94	414.84
2	305.96	412.23
2.9049	306.01	408.2
3.949	306.06	405.14
5.0476	306.12	403.04
6.1837	306.18	401.72
7.371	306.24	400.79
8.6502	306.3	400.11
10.121	306.38	399.61
12.049	306.47	399.26
15.344	306.65	398.84

Time [s]	Minimum [°C]	Maximum [°C]
24.456	307.3	397.97
36.456	308.4	396.82
48.456	309.66	395.69
60.456	310.98	394.58
72.456	312.29	393.48
84.456	313.52	392.4
96.456	314.66	391.33
108.46	315.7	390.28
120	316.58	389.27
6.50E-02	316.58	393.99
0.13	316.59	397.21
0.3198	316.6	402.48
0.71815	316.63	408.71
1.3681	316.68	415.94
2.0181	316.73	421.89
2.6681	316.78	426.79
3.3181	316.83	431.06
3.9681	316.88	434.92
4.6181	316.92	438.48
5.2681	316.97	441.83
5.9181	317.02	445.03
6.5	317.06	447.8

Time [s]	Minimum [°C]	Maximum [°C]
1.2	317.14	434.58
1.6	317.17	431.4
2	317.2	428.78
2.905	317.26	424.75
3.9494	317.33	421.68
5.0485	317.41	419.56
6.1861	317.48	418.24
7.3766	317.56	417.31
8.6637	317.65	416.61
10.154	317.74	416.13
12.141	317.88	415.77
15.66	318.12	415.32
26.086	319.03	414.28
38.086	320.31	413.08
50.086	321.71	411.9
62.086	323.15	410.74
74.086	324.56	409.6
86.086	325.88	408.47
98.086	327.09	407.36
110.09	328.19	406.25

Annex 2: TEG module drawing

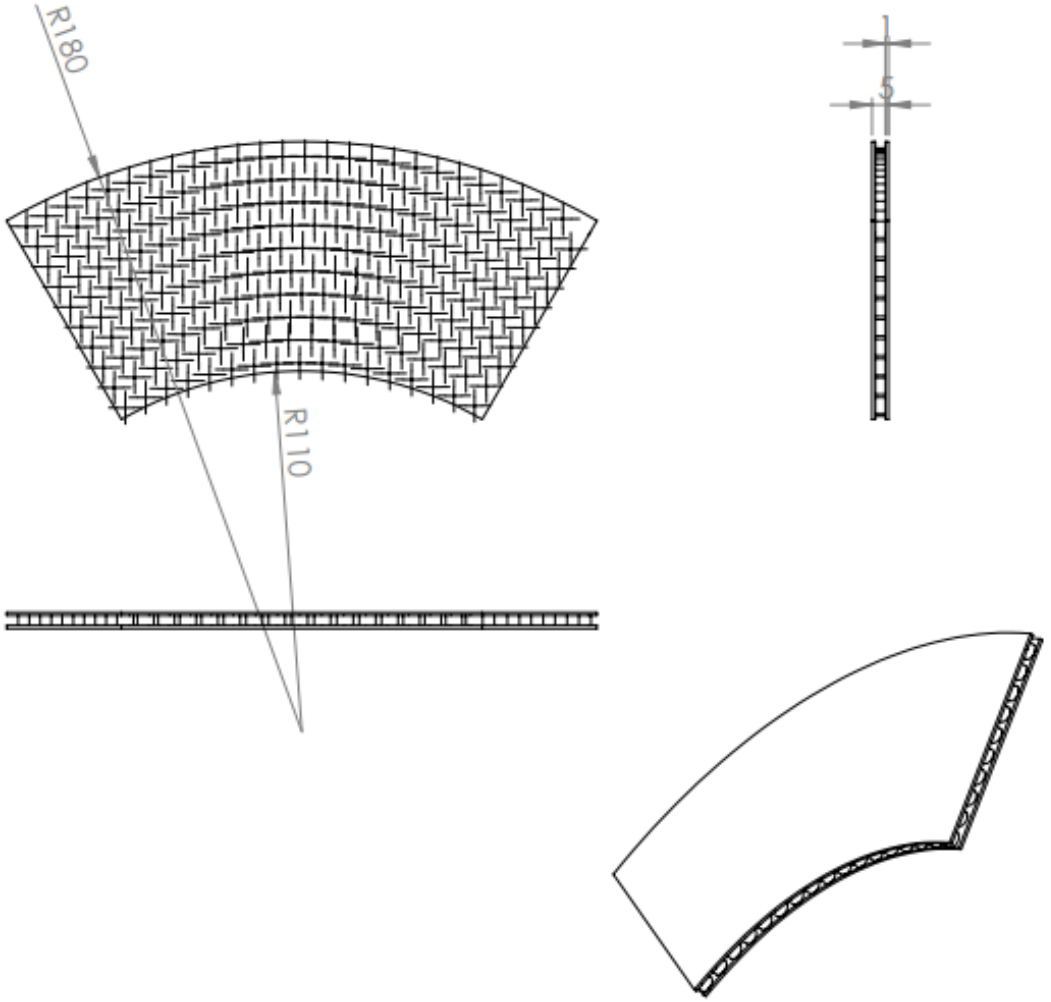

Annex 3: TEG module assembly

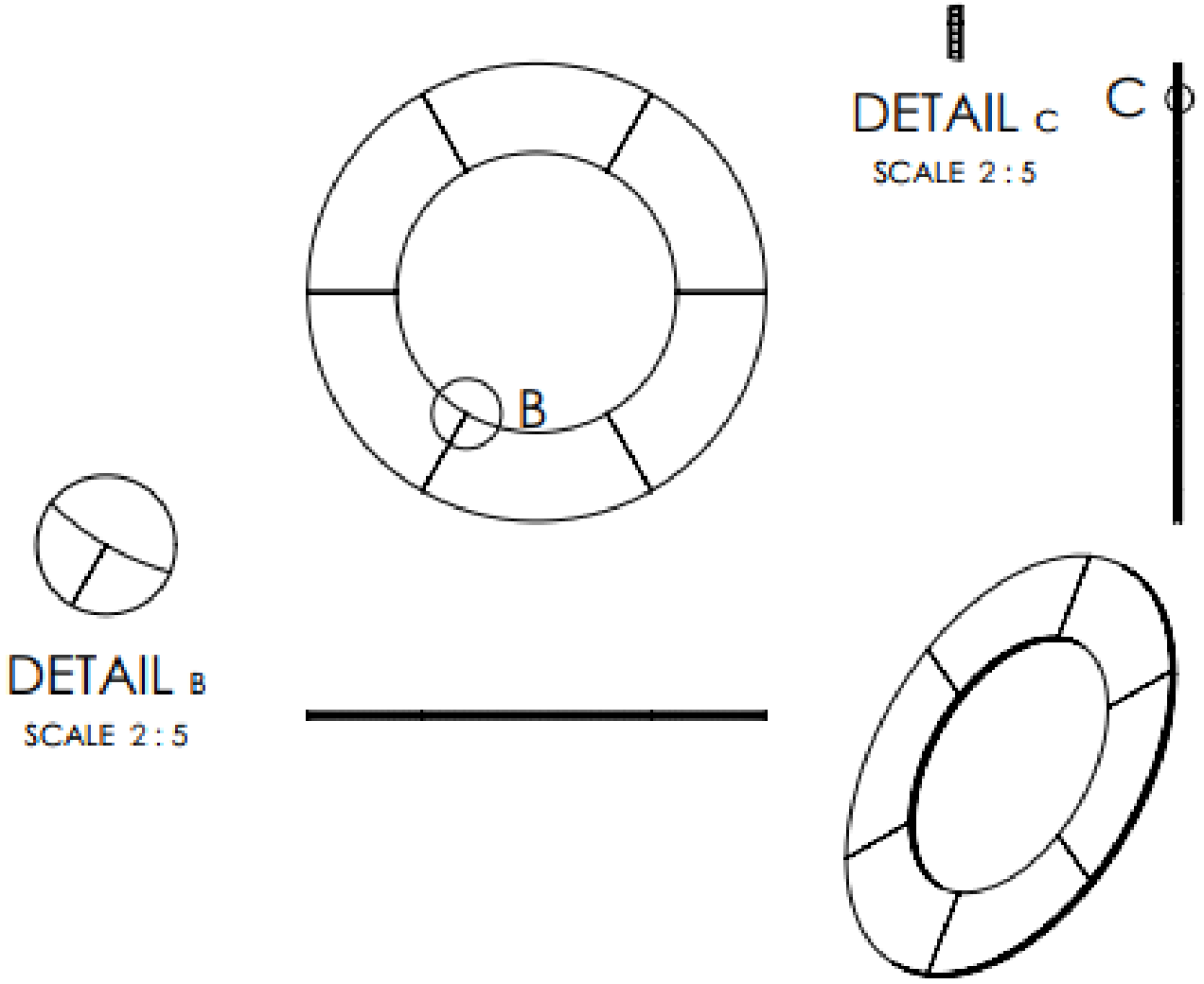

Annex 4: Modified Disc to accommodate TEG devices

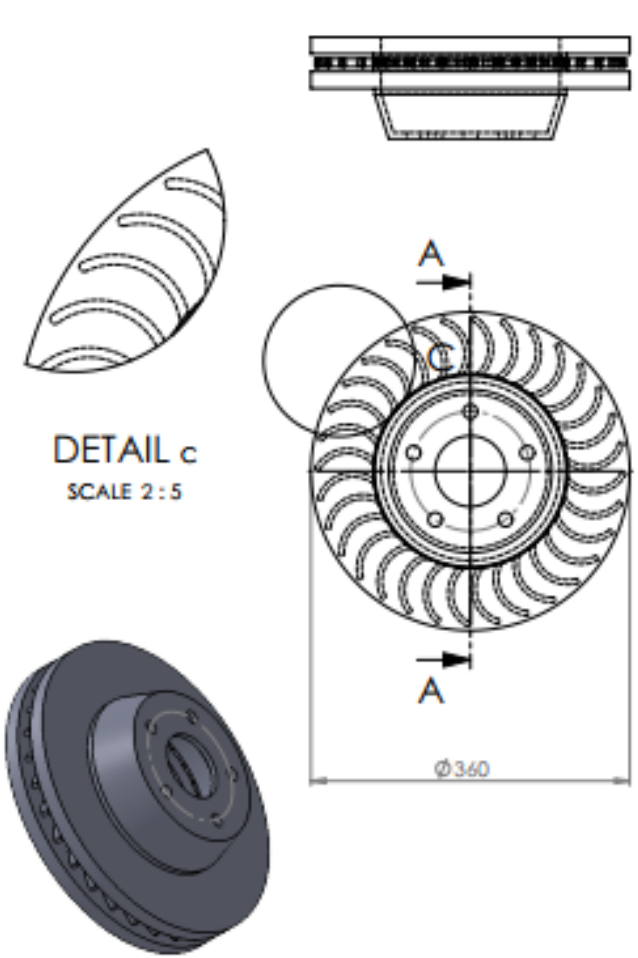

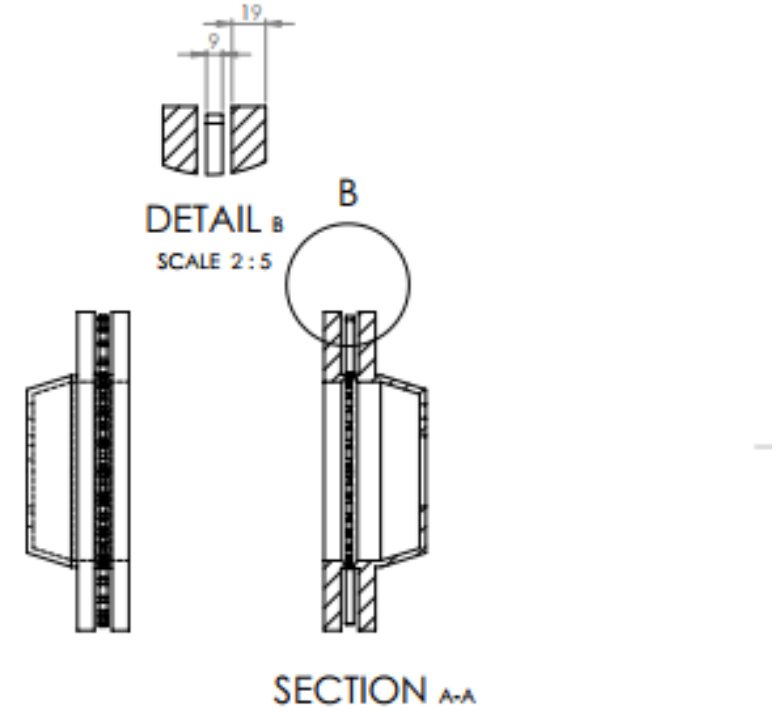

Annex 5: AALRT brake disc simplified for the study

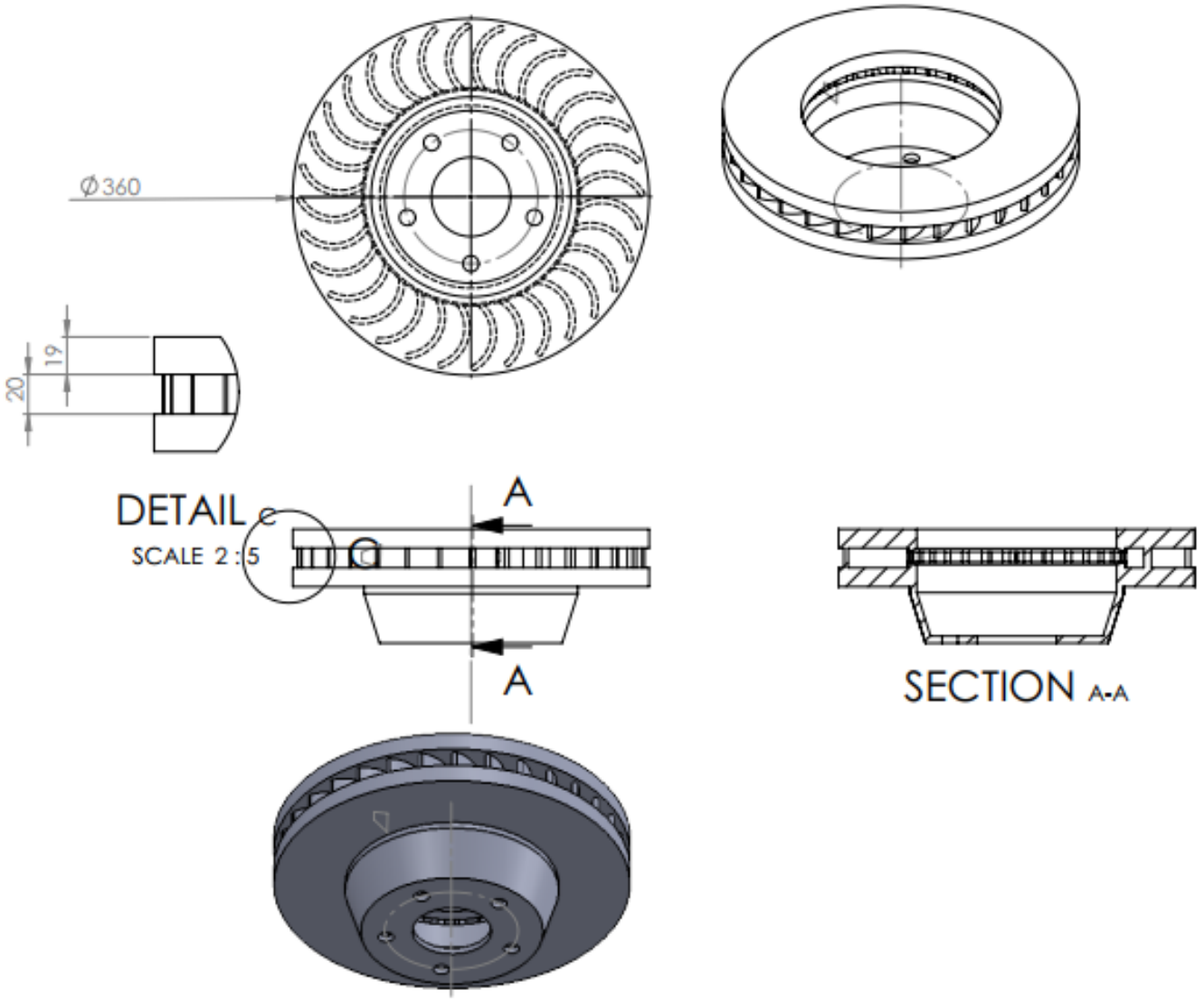

Annex 6: AALRT vehicle brake disc detail drawing [57]